

2020

New Autonomous Hydrogen Bus: H2-60

Team C



(s) – Alexander Acaster

Vehicle Concept Definition and Design:

Design Report

04/03/2020

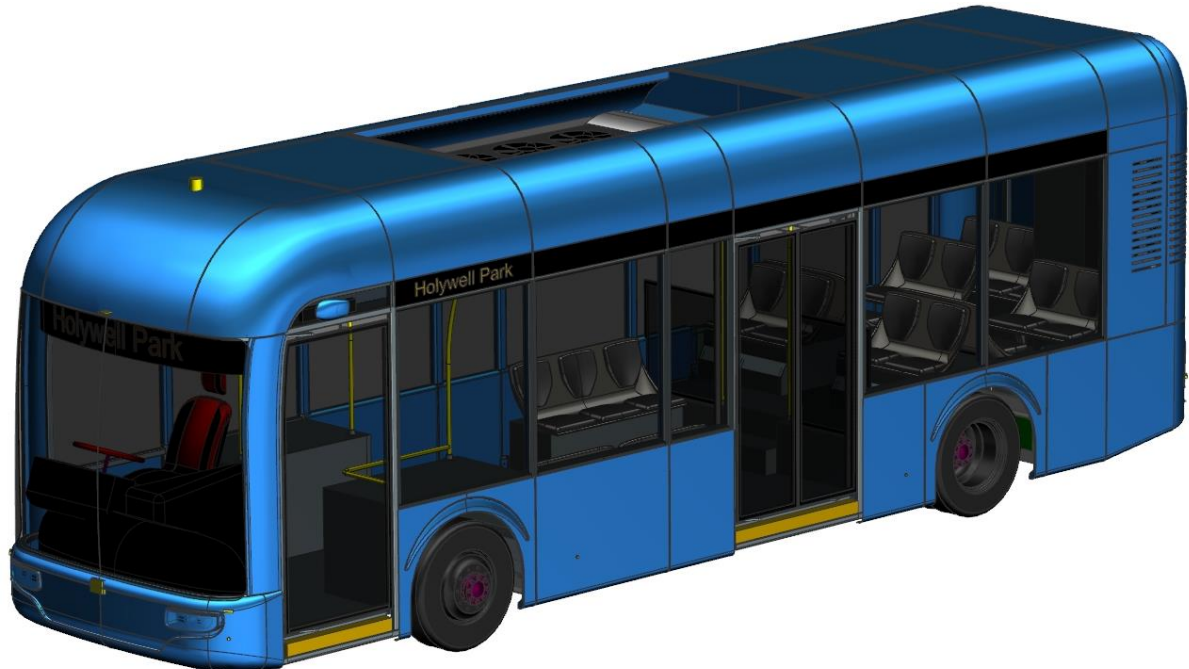
Report Contents

Section No.	Team Member	Responsibility	Page Numbers
1	Alex Acaster B622081	Team Leader: Vehicle Objectives, Target Performance, Vehicle Specification Overview and Team Progression	2-26
2	Erlend Strutt-Hofstad B614287	Body & Styling, Passenger Compartment, HVAC & Thermal Management	27-51
3	Hugo Burston B719796	Suspension, Braking, Wheel and Tyres	52-76
4	Adam Lofthouse B623365	Powertrain: Motors, Batteries, Fuel Cell System	77-100
5	Paul Theodosie B716787	Autonomy, Ramp and Door Systems	101-125
6	Clayton Hunt B724884	Chassis, Crash Protection and Flooring	126-147

Vehicle Concept Definition and Design: Design Report

Section 1

Team Leader: Vehicle Objectives, Target Performance, Vehicle Specification Overview and Team Progression



Alex Acaster - B622081

Number of Pages: 25
Number of Words: 2037

Contents

1.1 Project Specification.....	4
1.1.1 Cost and Volume.....	4
1.1.2 Vehicle Objectives Review and Performance	5
1.1.3 Hydrogen Review	7
Hydrogen Requirements	7
Hydrogen Cost and Weight Comparison	7
1.2 Vehicle Requirement Review and Performance	8
1.2.1 Legislative Performance	8
1.2.2 Market Research Alliance	9
1.2.3 Competitive Position	10
1.2.4 Example Business Deployment and Performance	11
1.2.5 Vehicle Selling Points Performance.....	11
1.2.6 Vehicle Specification Targets Review and Performance	12
1.3 Complete Vehicle Packaging and Illustrations.....	13
1.3.1 CAD Illustrative Views.....	13
1.3.2 Dimensioned Technical Drawings.....	15
1.4 Weight Distribution and Vehicle Load Cases.....	16
1.4.1 Overall Distribution.....	16
1.4.2 Passenger Distribution and Loading	17
Approximation of Bus at Full Capacity	17
Approximation of All Passengers Entering/ Exiting	18
1.4.3 Unified Loading Cases for Team Member Use.....	19
1.5 Vehicle Design Conclusions and Team Performance	19
1.5.1 Overall Vehicle Conclusions and Success Review.....	19
1.5.2 Lessons Learned.....	20
1.5.3 Team Performance Review	21
Appendix	22
Appendix A	22
Appendix B – Market Research Results	23
Appendix C – Project Planning – Gantt chart	24
Appendix D – Example Meeting Minutes	25
References	26

1.1 Project Specification

This report outlines the key design decisions taken by team members in order to meet criteria defined at the Concept stage and provide a successful new shuttle bus design, named the H2-60. The H2-60 aims to please customers and consumers and the performance of this is detailed in this first section of the report. Further sections detail how the bus design performs in terms of design area targets which are aligned with overall vehicle objectives.

1.1.1 Cost and Volume

To estimate the overall success of this project it is useful to compare the project and manufacturing costs to the expected sales volume and hence revenue. Table 1A summarises the estimated costs of production combined from all sections of this reports, also summarised in Appendix A. This cost estimation does not account for any amenities, employees, premises, licenses or equipment so the likely cost would be at least 2x the cost highlighted in Table 1A - £475250 per bus.

Table 1A – Vehicle Cost Summary

Cost Type/ Bus	Value
Raw Materials and Purchased Items	£195476
Estimated Production Total Cost	£42149
Total	£237625

Comparing the data to estimated revenue per vehicle, assumed to be £900,000 [1], the plot shown in Figure 1A can be determined to consider how many units are required to break even with a £10 million pound investment for start-up, using the production price of £475250 per bus. [2]. Number of units to break even is 23. Achievable within 1-2 years.

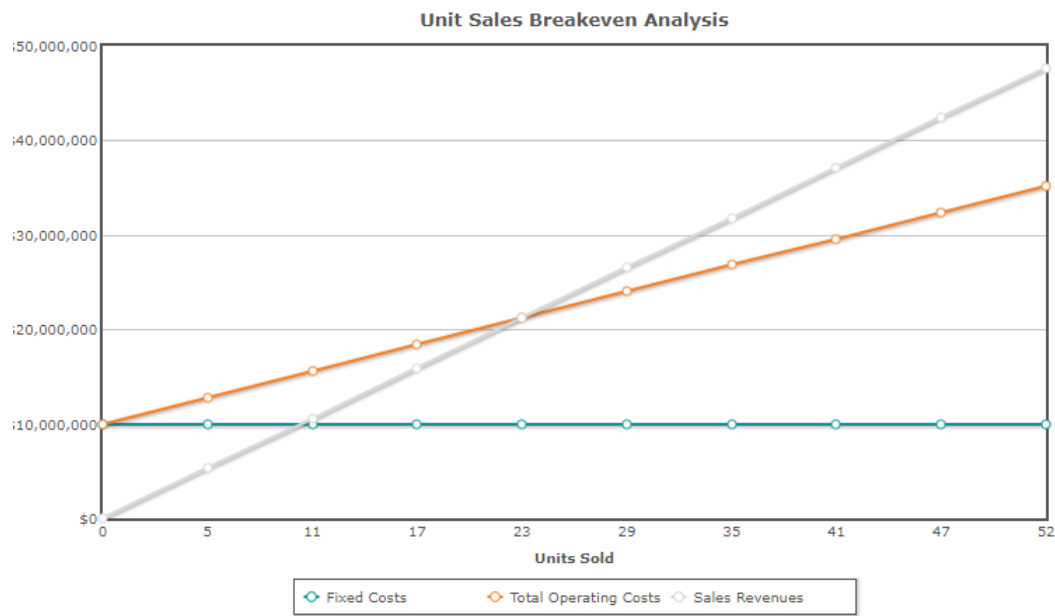


Figure 1A – Break Even Analysis

1.1.2 Vehicle Objectives Review and Performance

This section reviews the objectives outlined in the Concept Report, with some objectives refined and clarified, these are shown in Table 1B.

Table 1B: List of Updated Vehicle Objectives

Category	Code	Description
Form	FO1	Class leader in future technology, attractive and functional design
	FO2	Have vehicle shape and dimensions to what consumers expect and require
Function	FU1	Class leader in ability to be reliable and on time
	FU2	Inspire the modern way of transport through being an intelligent electrified vehicle
User Requirements	US1	Class leader in passenger comfort
	US2	Improve efficiency loading/unloading of passengers
	US3	Facilitate disabled passengers/wheelchair users, with accessible doors and ramp system
	US4	Easy contactless payment (either student card or debit)
	US5	Excel in safety to all stakeholders with new technology
Performance Requirements	PE1	To excel in performance on an EU shuttle bus route. This will be explored and targeted appropriately in this report.
	PE2	To be able to last a full day's service including management of waste energy. This will be explored and targeted appropriately in this report.
	PE3	To be competitive to competition buses and technology and not be restricted by the technology in any way, e.g. ability to charge in cold conditions, <i>or the technology resulting in a less optimized and efficient service</i>
Environmental Impact	EI1	To minimize any waste of energy e.g. not carry any excess weight
	EI2	To not emit any damaging pollutants or material, CO ₂ , NOx.
	EI3	To reduce noise of existing bus systems
Cost	CO1	Ensure it is a viable and cost-effective option to appropriate competition
Manufacturing	MA1	Be of a sensible architecture to be easily manufactured
	MA2	Designed to make any repairs easy

Table 1C considers each of these objectives and describes how each of these are attained by design solutions within this report. Since these objectives were adhered to throughout the design process, most of these objectives have been met. The limit to the success of some of these objectives would require more research time to consider. Such as CO1, while the fundamental cost is considered in Section 1.1.1, a more detailed financial estimation of material cost and production costs especially would need to be carried out along with the estimation of business costs such as employees, assets and utilities.

Table 1C: Descriptions of how each objective is achieved

Category	Code	Objective Obtained By:	Relevant Section:
Form	FO1	<ul style="list-style-type: none"> • Use of Hydrogen hybrid technology for propulsion, with a range above any other benchmarked vehicle • LED lighting and modern design specification create an exciting but functional design 	4.2.2
	FO2	<ul style="list-style-type: none"> • The dimensions are benchmarked against competition buses • A seating/sanding layout that is what consumers want 	2 1.2.3 1.2.2
Function	FU1	<ul style="list-style-type: none"> • New and sophisticated automation features introduced to streamline a bus service, no current bus of this size offering this level of automation 	5.2
	FU2	<ul style="list-style-type: none"> • Introduction of modern pedestrian technology to use the service • Modern and future proof propulsion technology to inspire other manufacturers 	5.2 4
User Requirements	US1	<ul style="list-style-type: none"> • Seating optimised for comfort and space including leg room, offering at least 20% more spacing for seated passengers and 30% more area for standing passengers above regulation value • Adaptive and comfortable suspension with road surface vibration isolation 	2 1.4.2 3.1
	US2	<ul style="list-style-type: none"> • A two-door system implemented to aid the flow of passengers 	5.5
	US3	<ul style="list-style-type: none"> • Automated wheelchair ramp and space for wheelchair provided 	5.4
	US4	<ul style="list-style-type: none"> • Modern Mobile Application based payment implemented 	5.2
	US5	<ul style="list-style-type: none"> • Electrical and Crash safety implemented into design 	6.1
Performance Requirements	PE1	<ul style="list-style-type: none"> • Proposed vehicle can perform in an example business scenario 	1.2.4 4.2.2
	PE2	<ul style="list-style-type: none"> • A simulated drive cycle of energy usage is simulated in Section 4, resulting in a range of 202.7 miles fully laden 	4.2.2
	PE3	<ul style="list-style-type: none"> • The use of hydrogen and battery electric power means the bus can adapt to either scenario where either power source is available or produce a larger range • The automated driving feature of the bus saves an average of 1 minute of bus cycle time per day 	4.2 5.2
Environmental Impact	EI1	<ul style="list-style-type: none"> • Various weight saving optimisation processes are completed in this design report 	
	EI2	<ul style="list-style-type: none"> • The fully electric powertrain has no pollutants at the vehicle 	4.5

	EI3	<ul style="list-style-type: none"> The electric motor cuts noise from a conventional internal combustion power bus by 5 dB(A) 	4.3.4
Cost	CO1	<ul style="list-style-type: none"> The proposed vehicle is profitable design due to the ability of a larger cost to the customer for the use of the advanced technology 	1.1.1
Manufacturing	MA1	<ul style="list-style-type: none"> Steps were taken where possible in the choice of design to reduce any unnecessary manufacturing cost however due to the purpose of the vehicle to be future inspirational, this is not always the case to provide a keen competitive advantage, like the chassis and body panel design 	2-6
	MA2	<ul style="list-style-type: none"> Various consideration of physical maintainability considered in design of particular aspects of this bus 	2-6

1.1.3 Hydrogen Review

This section outline the feasibility of Hydrogen as an energy source and the uses in this design case. While at the current stage of Hydrogen use it is expensive, with investment into this sector it is expected Hydrogen and other fuels will become more readily available and cheaper to the user.

Hydrogen Requirements

The concept report concluded that 95.85kWh would be provided by battery power, meaning for 70:30 battery to hydrogen power split, hydrogen energy capacity would be 41.08kWh. This provides a full total capacity of 136.93kWh, which is enough for one and half days of bus service. As shown in Section 4. The summary of use of Hydrogen is formalised in Table 1D. It shows that enough Hydrogen for the minimal case is provided by one hydrogen tank. Where there is market requirement, a further 8 hydrogen tanks could be added to increase the Energy capacity to 382.5kWh or a range of Approximately 550 miles.

Table 1D: Hydrogen System Specification [3] [4] [5] [6]

Dimension	Constant	Required	Actual	Unit
Energy Capacity		41.08	42.5-382.5	kWh
H2 Energy Density (55% Efficiency)	18.48			kWh/kg
H2 Density (at 350bar)	0.023			Kg/L
Tank Capacity		96.6	100-900	L
H2 Mass Capacity		2.22	2.3-20.7	kg

Hydrogen Cost and Weight Comparison

Table 1E considers the system weight and refuelling cost of a full hydrogen, full electric, full diesel and hydrogen electric hybrid system, using an energy capacity requirement of 137kWh. The analysis here is simplified as it assumes all energy within each fuel type is converted to kinetic energy in the drivetrain, to have a more accurate measure of the effectiveness of each fuel, efficiency should also be considered.

Effective mass for range is approximately how much weight of fuel or equivalent power of system is required to provide the required energy capacity, Diesel excludes the weight of the tank as this is marginal, Hydrogen includes the weight of the tanks as these are much more than the fuel itself. This proves that the hybrid mix provides an achievable alternative to electrical power only weight disadvantage while not relying too heavily on Hydrogen due to cost and availability issues. In the future, when Hydrogen cost to consumers reduces, we would like to offer multiple powertrain options on buses to offer a different split of hydrogen/battery capacity.

Table 1E: Powertrain System Comparison [7] [8] [9]

Type	Energy Density	Effective Mass for Refuel Cost Range	
	kWh/kg	kg	£
Diesel ICE	12.92	10.60	16.22
Battery Electric	0.27	516.98	13.70
Hydrogen Electric	33.60	154.07	61.16
Hydrogen/ Battery Hybrid (30:70)	10.27	413.11	27.94

It should be noted that if a transportation business employed its own Hydrogen generation facility for a long-term fuelling of a large fleet of vehicles, the cost for refuelling would considerably lower. For the purposes of this project, the aim is to promote hydrogen as a future fuel and customers of this vehicle would be looking to spend extra to promote their ethos of exploring new technology.

1.2 Vehicle Requirement Review and Performance

This section discussing how effective the bus design solution is at meeting each of the requirement criteria developed from the Concept Report.

1.2.1 Legislative Performance

Table 1F shows the progress of each of the specified legislative requirements determined in the Concept Report [10] [11] [12]. This shows the proposed Bus design is legislative conformant in this case and other legislative requirement performance for areas like passenger safety, autonomy and vehicle dynamics are tracked in further sections of this report.

Table 1F: Legislative Performance

Specification	Unit	Legislative Value	Actual Value
Length	m	<13.716	10.25
Gross Vehicle Weight	kg	<19500	16767
Width	m	<2.55	2.546
Engine Power/ Tonne G.V.W.	kW/1000kg	>5	10.3

1.2.2 Market Research Alliance

Based on the main objective of this vehicle type; to carry passengers, it is imperative to ensure that bus passengers are considered in the design process. In the Concept Report market research was conducted on an existing shuttle company's customers. Table 1G shows the design considerations committed based on data from this Concept Report market research. The full results are supplied for reference in Appendix B.

Table 1G: Market Research Design Alliance

Market Research Criteria	Design Decision Implemented
Customers dissatisfied with reliability of service loop frequency	Full Level 4 autonomy integrated into the bus design to automate loop driving, to communicate between buses to ensure reliable frequency of service. Mobile app also provides live tracking of buses
Customers dissatisfied with amount of area per passenger	20% more seated passenger space; including legroom and seating space. 30% more spatial area per person for standing passengers above legislation, shown in Section 1.4.2.
Customer dissatisfied with condensation or uncomfortable air conditions	A high performance air condition system with advanced ducting is implemented to aid the comfort of passengers, described in Section 2
Survey of passengers opinions suggested the seating to standing ratio should be 31:69	The proposed design incorporates 22 seating passengers and 38 standing, a ratio of 37:63 although this can be altered by request of the bus operator
Survey of passengers opinions suggested 90% of people wouldn't feel comfortable traveling any faster than 30mph on an automated Shuttle Service	The top speed of the proposed bus powertrain is 30mph
Customer suggested the most important design factors for a new bus should be; inclusion of modern technology, obtaining a smooth and quiet ride and having pleasing aesthetics and lighting	<ul style="list-style-type: none"> • Modern technology includes hydrogen hybrid powertrain and Level 4 autonomy • A smooth and quiet ride is obtained by using a modern electric motor and sound insulation combined with modern suspension design solutions • The design is inspired by the modern vehicle vision including modern LED lighting

1.2.3 Competitive Position

To directly see how the new bus design compares to similar existing products, dimensions and other quantitative factors can be directly compared. This is done in Table 1H comparing the new bus with two direct competitors, the overall average for alternative powertrain vehicles only and the overall average for all 12 benchmarked vehicles in the Concept Report. [13-16]

Table 1H: Market Research Design Alliance

	Main Competitors		Benchmarked Averages		
Dimension	Mercedes Citaro K [9]	Volvo 7900E [10]	Alternative Powertrain Average	Overall Average	H2-60 New Bus
Height (mm)	3300	3280	3320	3010	3400
Width (mm)	2550	2550	2520	2220	2546
Length (mm)	10630	12000	11553	10048	10250
Wheelbase (mm)	4398	-	5250	5621	5400
Turning Circle (wall to wall) (m)	17.28	-	19	19	20.3
Powertrain Type	Diesel/Electric Hybrid	Electric	-	-	Hydrogen Hybrid
Range (miles)	452	-	195	347	202
Drivetrain Power (kW)	220	160	187	145.8	155
Passenger Capacity	86	105	94	69	60
of which seated	26	35	27	30	22
G.V.W (kg)	18745	19000	18782	13714	16767
Weight Distribution (F:R)	39:61	-	36:64	35:65	36:64

Table 1H shows that the new proposed bus design competes effectively in terms of bus sizes and capacities, but since this bus is designed for shuttle services, it does not require the range of a diesel-electric hybrid high passenger long touring bus, like the Mercedes Citaro K. The new bus offers a reduced weight but strong range when compared with its the average for alternative powered average bus.

1.2.4 Example Business Deployment and Performance

From research of the example business deployment from the Concept Report, the proposed bus is required to travel a maximum of 200 miles in the 16 hour shift. If two buses were deployed this would allow a bus at every stop every 10 minutes (with the average loop duration of 20 minutes). This deployment of the automated service would create a fixed number of buses per hour of 6. Further to this the looping could be set up to adapt to the busiest customer times of the hour, to transport customers in time for their next lecture, for example.

This usage would deplete the charge and hydrogen almost completely. To make this effective, a hydrogen refilling station would be required nearby, most efficiently in the bus depot, along with a high power charger at the depot to be charged overnight. If the bus is operated with staff on board, the buses could replenish with hydrogen when returning to the station at the end of each 8-hour shift and provide around 60 extra miles. Battery power only would allow a range of 140 miles.

1.2.5 Vehicle Selling Points Performance

Table 1J shows the successful performance of the proposed vehicle on the listed selling points in the Concept Report, showing overall success of the design and offering these as an advantage over competition bus designs.

Table 1J: Vehicle Selling Points Performance

Selling Point	Advantage	Performance
Technology	Full Level 4 SAE autonomy	<ul style="list-style-type: none">- Level 4 autonomy system is implemented, including LiDAR, Radar and Camera operating driving system
Range	Combination of battery and hydrogen power travel a minimum of 200 miles	<ul style="list-style-type: none">- Combined battery and hydrogen power of 137kWh provides a maximum range of 202 miles at fully laden conditions
Ergonomic Design	The interior is optimised for passenger space and comfort, targeting 20% more space than existing busses.	<ul style="list-style-type: none">- Seating provides more space for legs and seating width- Approximately 30% more space per person for standing passengers
Air Conditioning	Provide comfortable air that prevents steam up and uncomfortable environments	<ul style="list-style-type: none">- Advanced air conditioning system outlined in Section 2.
Emissions	The powertrain will have 0 CO ₂ emissions or other harmful pollutants.	<ul style="list-style-type: none">- Electric powertrain produces no emissions at vehicle, including emissions from Hydrogen Fuel Cell
Modern Design	Modern seating, materials, styling and lighting combined to give an overall satisfying experience	<ul style="list-style-type: none">- Modern stylistic features are shown in CAD Illustrative Views in Section 1.3.1

1.2.6 Vehicle Specification Targets Review and Performance

Table 1K shows the current specification status of design parameters at the end of the Design Stage.

Table 1K: Final Status of Specification Targets and Justification

Specification	Target	Current Status	Justification
Top Speed (mph)	30	30	On Target
Range (miles)	>200	202 (141/61 Battery/ H2 Split) up to 550 miles with 9 H2 Tanks	On Target
Length (metres)	10.3	10.25	10.25 is adequate
Width (metres)	2.55	2.55	Increased over Concept estimation due to including of rear view cameras for the driver
Wheelbase (metres)	5.4	5.4	On Target
Height (metres)	3.3	3.4	Within legislation for this bus type
Floor Height (millimetres)	380 kneeling to 250	400 (-20 near doors floor level) – suspension kneeling by 150mm	On Target
Track (metres)	F: 2.175 R: 1.775	F: 2.175 R: 1.775	On Target
Turning Circle (metres)	< 21	20.3	Not identified as a crucial design factor, however still performs within tolerance of competition
Stopping Distance from 30mph (metres)	9	9.17	Within acceptable tolerance
Passenger Capacity	60, 22 seated	60, of which 22 are seated	On Target
Gross Vehicle Weight (kg)	<16800	16767	Difficult to get complete estimate without knowing every component weight
Number of doors	2	2	On Target
Wheel Layout (FxR)	2x4	2x4	On Target
Weight Distribution (F:R) Unladen	35:65	36:74	Within reasonable tolerance to accuracy of weight data obtained

1.3 Complete Vehicle Packaging and Illustrations

1.3.1 CAD Illustrative Views

Figures 1B:1G show various isometric views of the final assembly of the proposed design, features are annotated where appropriate.

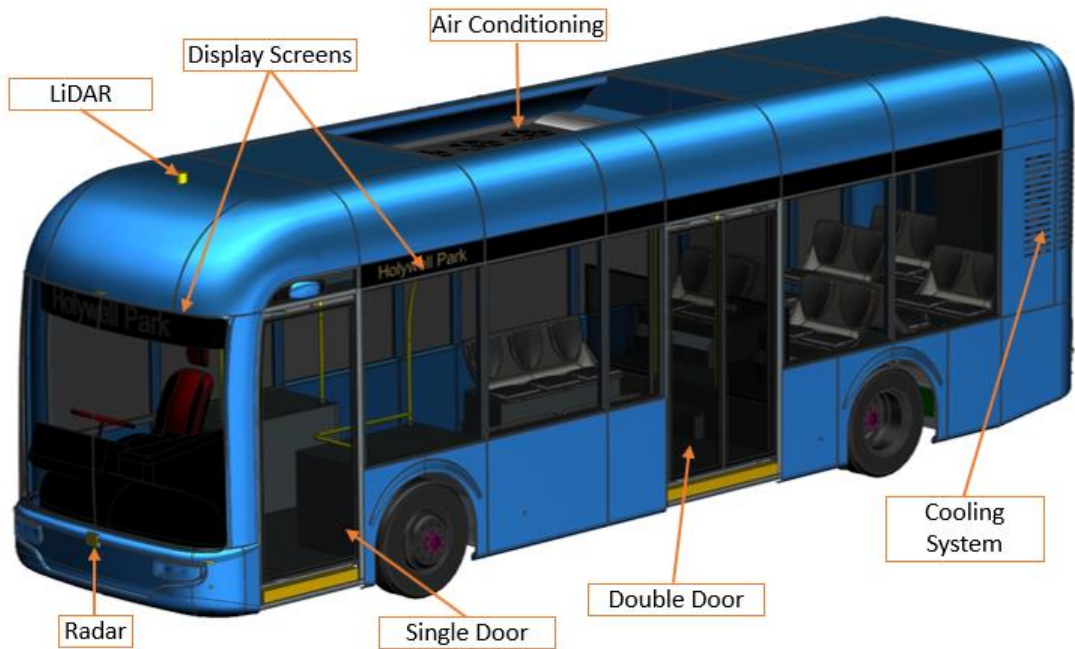


Figure 1B: Labelled Front Isometric View

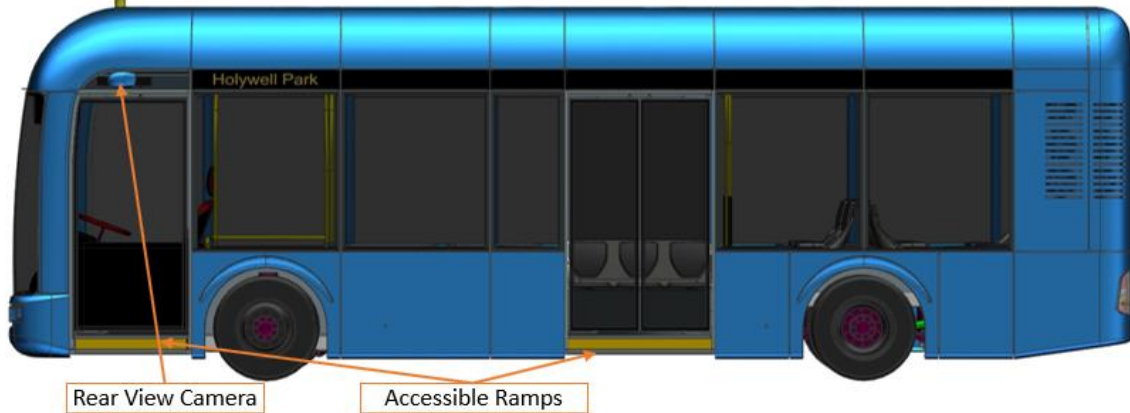


Figure 1C: Labelled Side View

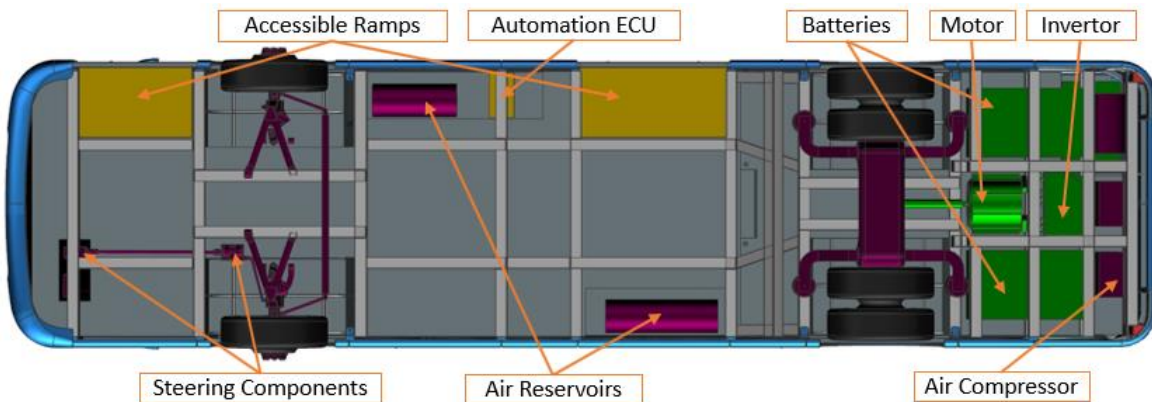


Figure 1D: Bottom View

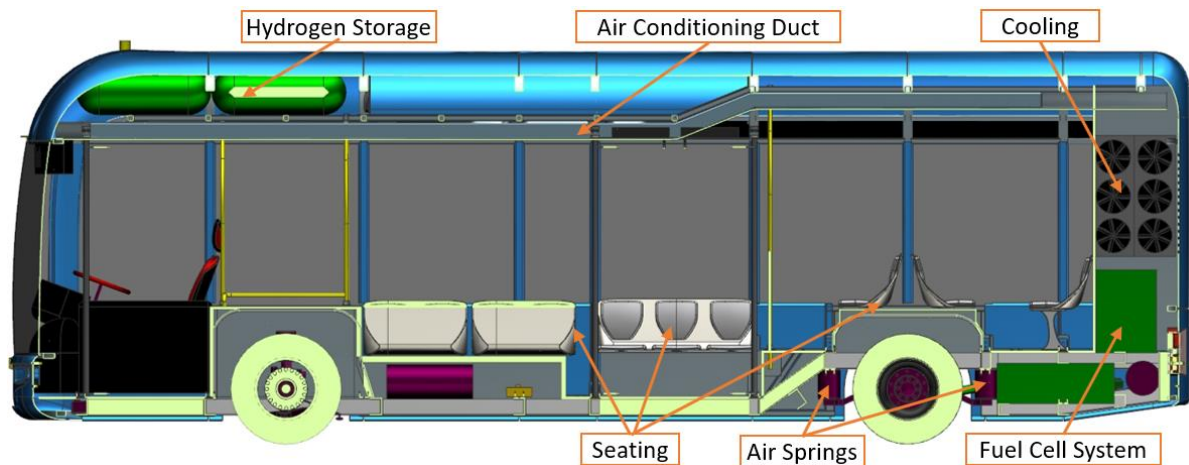


Figure 1E: Section Side View

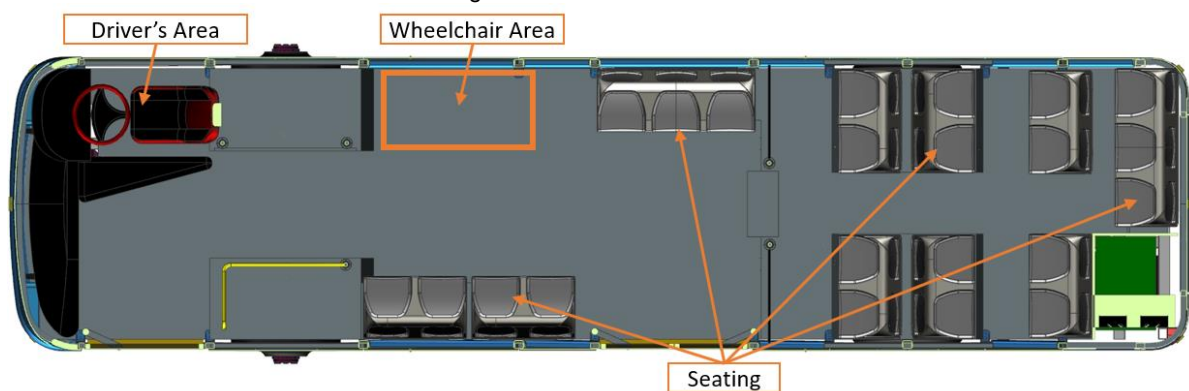


Figure 1F: Section Top View

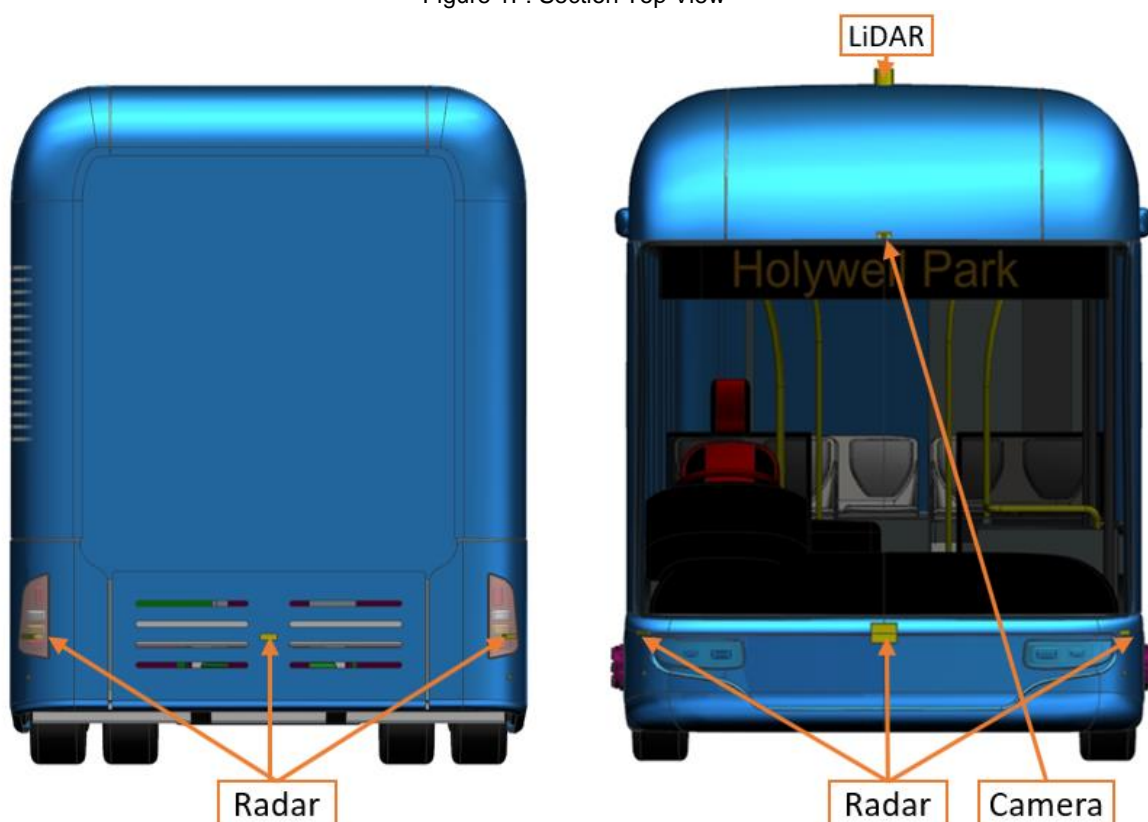
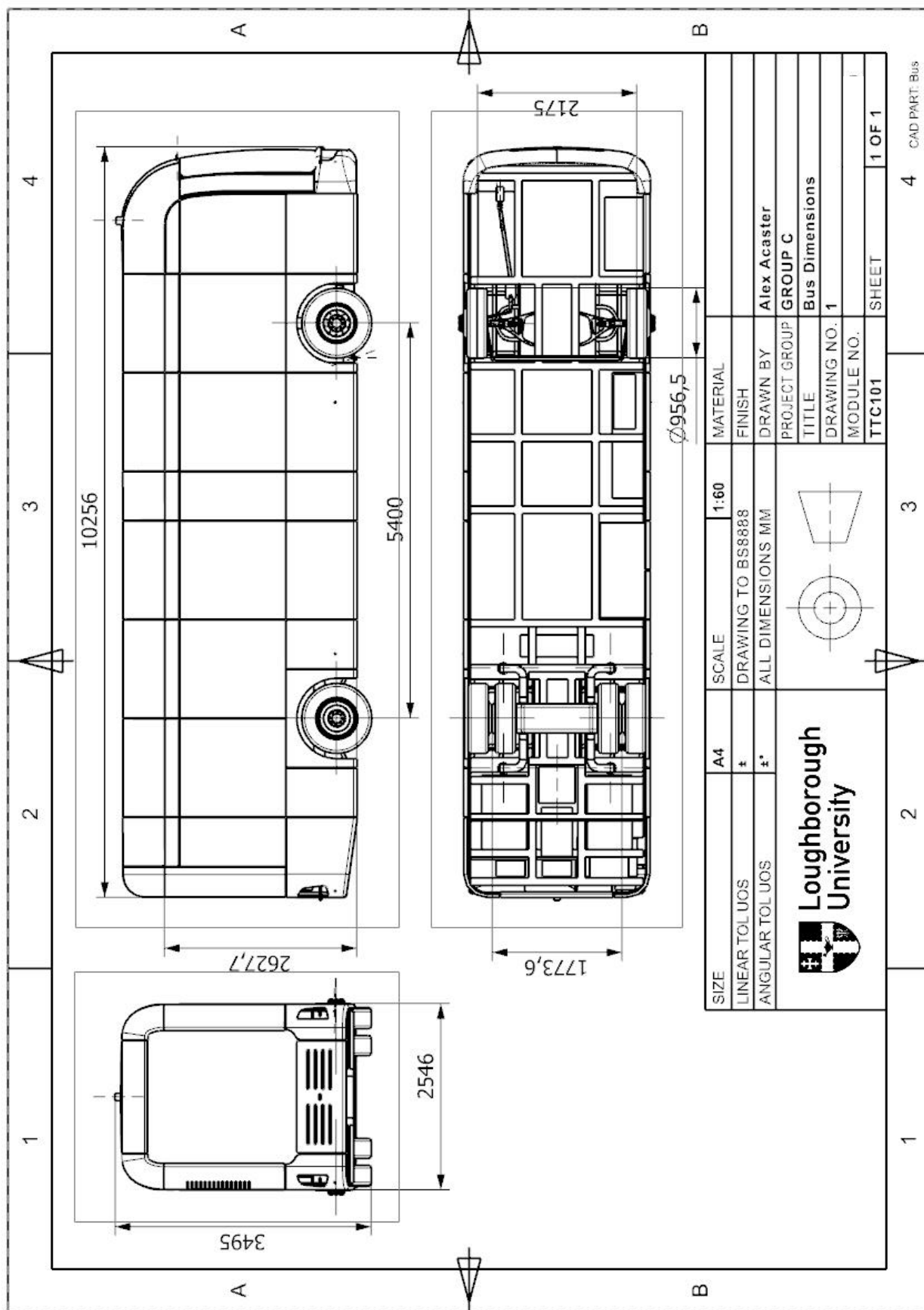


Figure 1G: Front and Rear View

1.3.2 Dimensioned Technical Drawings



1.4 Weight Distribution and Vehicle Load Cases

The overall final weight and distribution shown in Section 1.4.1 is accurate at the time of the end of the Design stage. Other subsections in this section (1.4.2 – 1.4.3) are relevant to the weight and distribution from the end of the Concept stage. The reason for this is that subsequent design work can be completed before the final weight data is obtained very late in the process. In order to complete the design stage another design iteration would have to be completed with the final weight data. While the design solutions in this report do not use the exact weight and distribution, they are still relevant as the weight data at the concept stage does not change significantly to the design stage.

1.4.1 Overall Distribution

Table 1L shows the mass and centre of gravity data for the bus at the end of the design stage.

Table 1L: Mass and COG Summary

Dimension	Value	Unit
Unladen Weight	9767	kg
Laden Weight	16767	kg
Unladen Weight Distribution	36:64	F:R
Laden Weight Distribution	38:62	F:R
Unladen Height of Centre of Gravity	1.18	m
Laden Height of Centre of Gravity	1.29	m

Figure 1H show the positions on the vehicle on the centre of gravity Un-laden (Green) and Laden (Red)

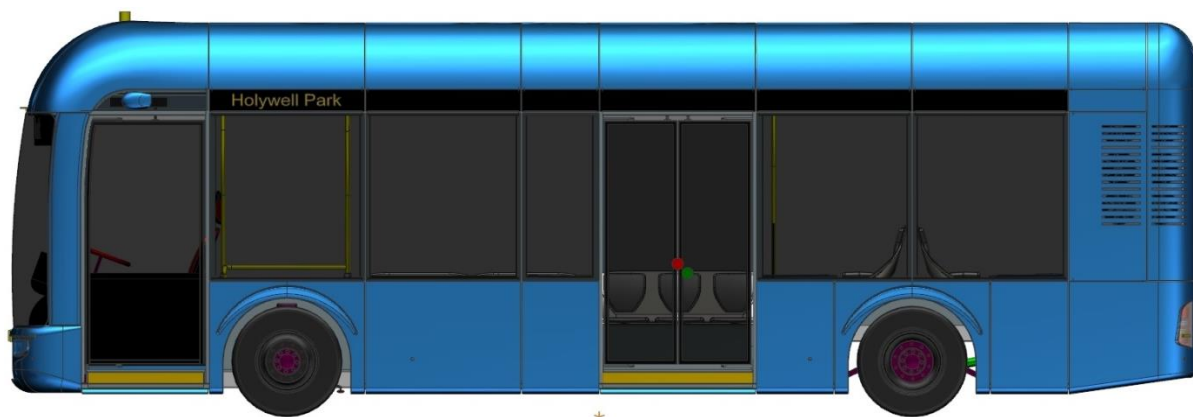


Figure 1H: Vehicle Mass and COG CAD Visualization

1.4.2 Passenger Distribution and Loading

With the main objective a vehicle of this type to carry passengers, it is highly important to consider the effect of passenger loading cases in order to provide a successful design that is safe to use, to achieve vehicle objective FO2. Calculations in this section are based on passenger weight estimation as found in Table 1M. Regulations state the safe maximum passengers per area is 6.25 people per square metre and there should be no passengers at the side of the driver or within 200mm on the seating edges, this is accounted for in the seating illustrated size. [17]

Table 1M: Summary of Passenger Mass

Type	No. [#]	No. Safety Factor ~ [*]	Average Mass [kg]	Luggage Mass [kg]	Mass Safety Factor [*]	Total Mass per Passenger [kg/pp]	Total Mass [kg]
Driver	1	1	68	4	1.25	90	90
Disabled	1	1	68 + (25 chair)	9	1.25	127.5	127.5
Seated	22	1	68	9	1.25	95	2090
Standing	38	1.3	68	9	1.25	95	4693

[~] is the realistic extra people that can fit into the standing space on the bus (beyond suggested level of 38 standees)

Approximation of Bus at Full Capacity

An approximate location or area for all passengers can be found, shown in Figure 1J. This figure shows the maximum space for passengers using regulations, and the allocated number based on extra space for passengers. This can be used to work out the approximate load and location of loads across the longitudinal direction of floor of the bus, as shown in Figure 1K.

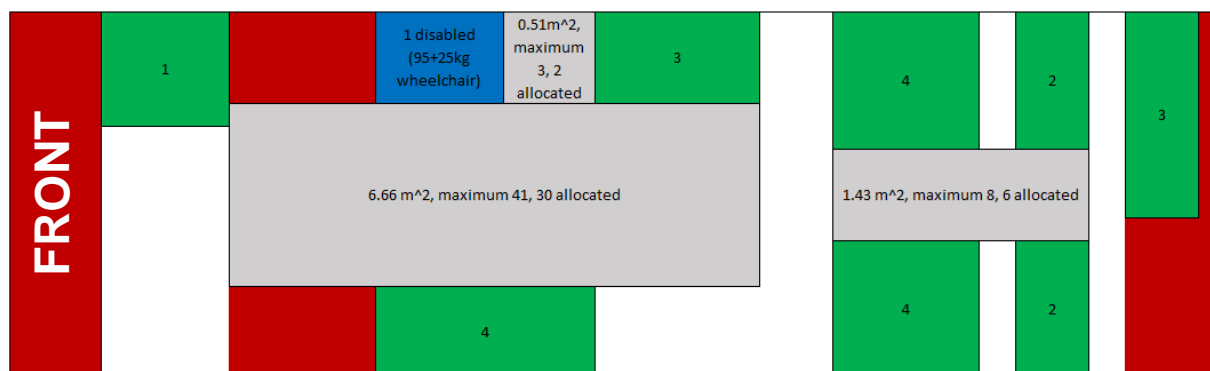


Figure 1J: Static Full Laden Passenger Positions (Green – Seated, Grey – Standing)

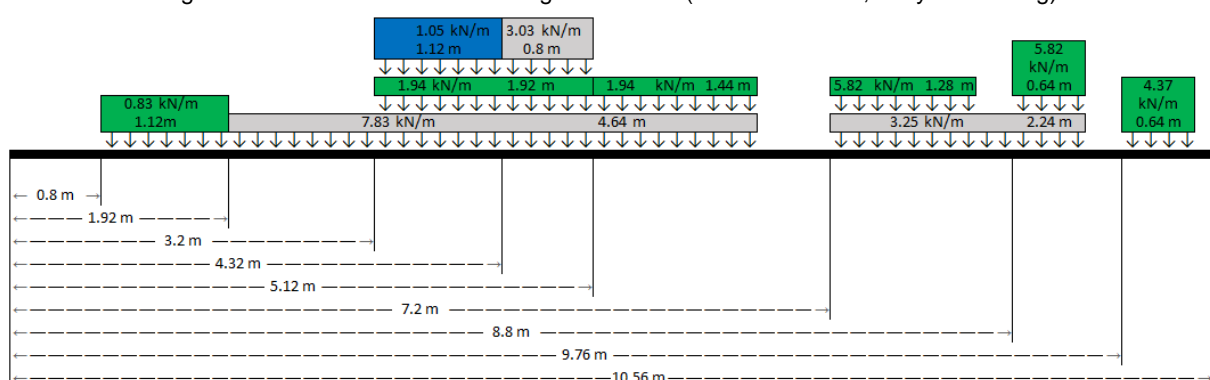


Figure 1K: Static Full Laden Longitudinal Loading Diagram (Green – Seated, Grey – Standing)

Approximation of All Passengers Entering/ Exiting:

This case can be simplified to the extreme example of all passengers (at full capacity) leaving equally at either door, which simulates the full bus capacity disembarking, half the bus disembarking and half embarking or the full capacity getting on an empty bus. This load case is shown in Figure 1L, Figure 1M shows the longitudinal weight distribution and Figure 1N shows the lateral weight distribution.

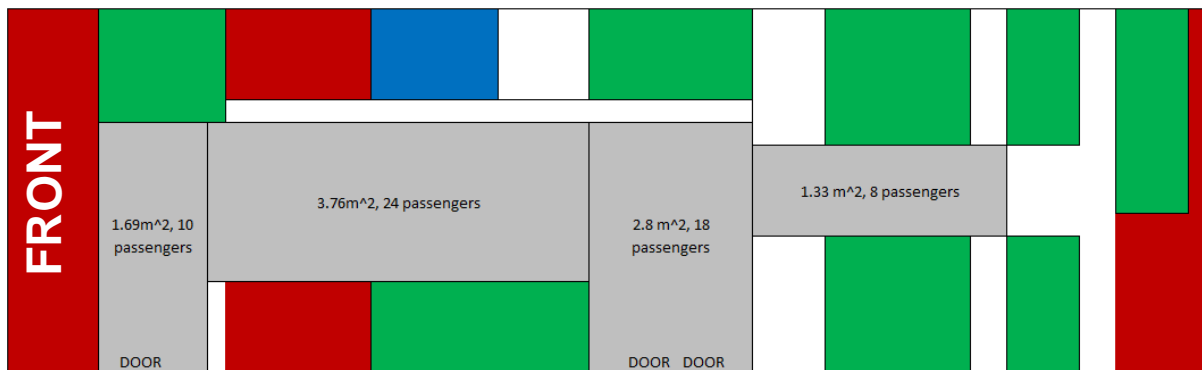


Figure 1L: Static Full Laden Passenger Entering/ Exiting Positions (All Standing)

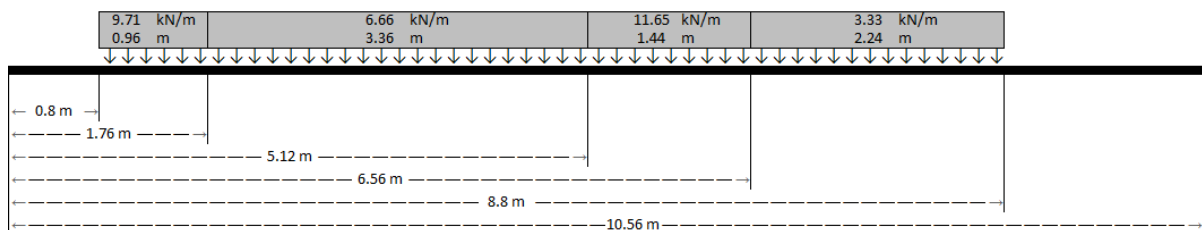


Figure 1M: Static Full Laden Passenger Entering/ Exiting Longitudinal Loading Diagram

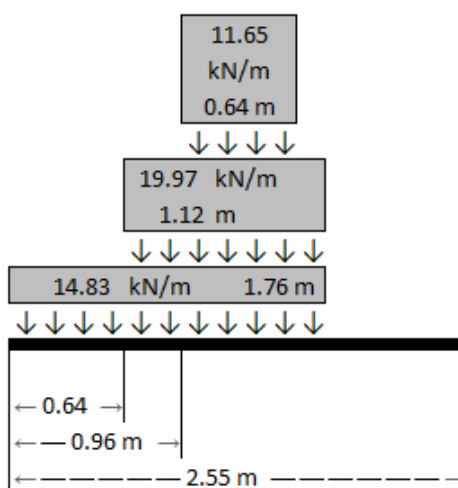


Figure 1N: Static Full Laden Passenger Entering/ Exiting Lateral Loading Diagram

1.4.3 Unified Loading Cases for Team Member Use

As well as considering the static loads and loads associated with passengers as above, it is also important to consider loads based on the dynamics of the vehicle, these are summarised and justified in Table 1N.

Table 1N: Unified Load Cases

Load Case	Value	Unit	Justification
Bending	3x static		
Crash	10	g	From Bus Crash SAE Paper [18]
Lateral	0.3 (@25mph)	g	Calculated in Section 3
Longitudinal Acceleration	0.11	g	Maximum acceleration rate, calculated in Section 4
Longitudinal Braking	1	g	Maximum achievable braking rate calculated in Section 3
Asymmetric (Kerb Strike)	120000	N	Based on research on kerb strikes [19]

1.5 Vehicle Design Conclusions and Team Performance

This section details the overall success of the project along with team success and lessons learnt.

1.5.1 Overall Vehicle Conclusions and Success Review

Strengths:

- The proposed vehicle offers a considerable marketing advantage over competitors of having fully autonomous driving and utilising power from a modern method- combination of Hydrogen and modern Battery power, offering an increased range of 202 miles, 7 above the alternative powered bus average and over 70 more than the range of the main competitor- the Optare Solo EV with a range of 130 miles. The bus also combines the modern envisage of passenger transport with meeting the needs of passengers through offering more space for passengers and providing comfortable ambient conditions with air conditioning and pleasing aesthetics.
- This design is focused on the functionality and feasibility of the bus in dealing with operation. This report clearly shows how the bus is designed to deal with loads based on high passenger numbers, particular load cases focused on bus manoeuvres and being functional in terms of seating and standing space while accommodating for disabled use. Since the targets for these sections are met, this offers a strong bus design that could be produced but also provides an acceptable starting point for any further refinement.
- With current government initiatives and investment into the public transport sector for clean and modern technology means that this design proposal lies deep in an area of demand of customers and promises to be a very financially promising venture for a manufacturing business.

Improvements:

- While a considerable amount of time was used to create the futuristic and interesting design of this bus, with more development time and researching, the final outcome could have been more ground breaking in terms of clever design functions and packaging of components. More time could also be spent light-weighting more components to improve the overall efficiency of the bus.

- To appeal to more of the market, further interior design iterations could be made to offer a different ratio of seated to standing passengers based on customer requirements. This is also important if the bus was to be operated with no staff, the driver's position could be removed for more passenger space, if the regulations where the customer is operating the bus allows. The ratio of Hydrogen and Battery power could also be adjusted dependant on consumer requirements. For example if the purchaser has access to Hydrogen at a lower cost, which may be true in the future, the bus could hold more hydrogen storage tanks in the roof as there is space.

1.5.2 Lessons Learned

Area	Explanation	Improvement Action Implemented/ Advice
CAD Organisation	In the Concept Stage iterations of CAD files became confusing for the assembly.	This problem was corrected for the Design Stage by adopting a numbering system that listed parts in the Parts List and added revision numbers.
Clinics	At the start, clinics seemed like critical scrutiny and members felt un-inspired.	This was improved by us becoming stronger as a team and beginning to present questions and area of weaknesses and mentors proved helpful. This therefore helped the development of our project.
Meeting Planning	Meetings could seem length and unproductive at some stages.	Meeting planning and approval of plans by team members was received to ensure everyone felt the meetings were useful and aired any concerns other members had. (example meeting minutes in Appendix C)
Vehicle Choice and Objectives	Some time was taken at the beginning by struggling to choose a vehicle and come up with suitable objectives	If we were to do this process again, the initial meetings would be much more focused into quickly deciding on an appropriate vehicle and coming up with strong objectives and targets as a team to then develop these fully throughout the following weeks.

1.5.3 Team Performance Review

Area	Rate (/10)	Explanation/ Improvements
Communication	9	All team members communicated effectively and any problems that arose were generally quickly resolved by a team member. Communication was achieved through weekly meeting plus the aid of messenger services along with OneDrive for sharing of documents and files.
Teamwork	9	Team members were all respectful of all members, everyone was encouraged to contribute to all outcomes and generally there were no issues between any individual members. Where any individual was struggling with time or their section any member of the team available would provide any assistance and this was well received by all members. Reviewing of each other's reports also was very useful and popular.
Motivation	8	Due to a convenient choice of design vehicle, along with enthusiasm from all team members, motivation was never a considerable issue as the team spirit was carried throughout. However timing with other modules and commitments was sometimes a small issue.
Time Management	8	All team members prepared a time plan for each stage of the process. From this an overall Gantt chart was created with deadlines agreed by all members. These were adhered to and allowed success in our final design proposal. Initial progress at the beginning of each stage seemed slow but as with any new team or task this was expected and didn't hinder progress too significantly. (Gantt Chart shown in Appendix C)
CAD	10	The use of an efficient CAD planning system and fantastic enthusiasm by team members meant that significant CAD results were achieved. The progress and attention to detail of some members in regard to CAD modelling inspired other members instead of detracting from their own work. CAD ability and knowledge was shared between members to help everyone produce an excellent final model.
Technical Ability	9	Generally everyone's ability was exceptional, where any issues arose, a solution was quickly found by another member. A good allocation of responsibility early on aided the strength of the team overall.
Creativity	8	Generally the team was inspired by the objectives of this vehicle to provide solutions that were 'modern' or 'creative'. However the extent of this was limited by the time available to members to explore other options. To improve this group sizes could be larger to allow small groups of people to team up on individual areas to consider all possibilities and share the time usage.

Appendix

Appendix A

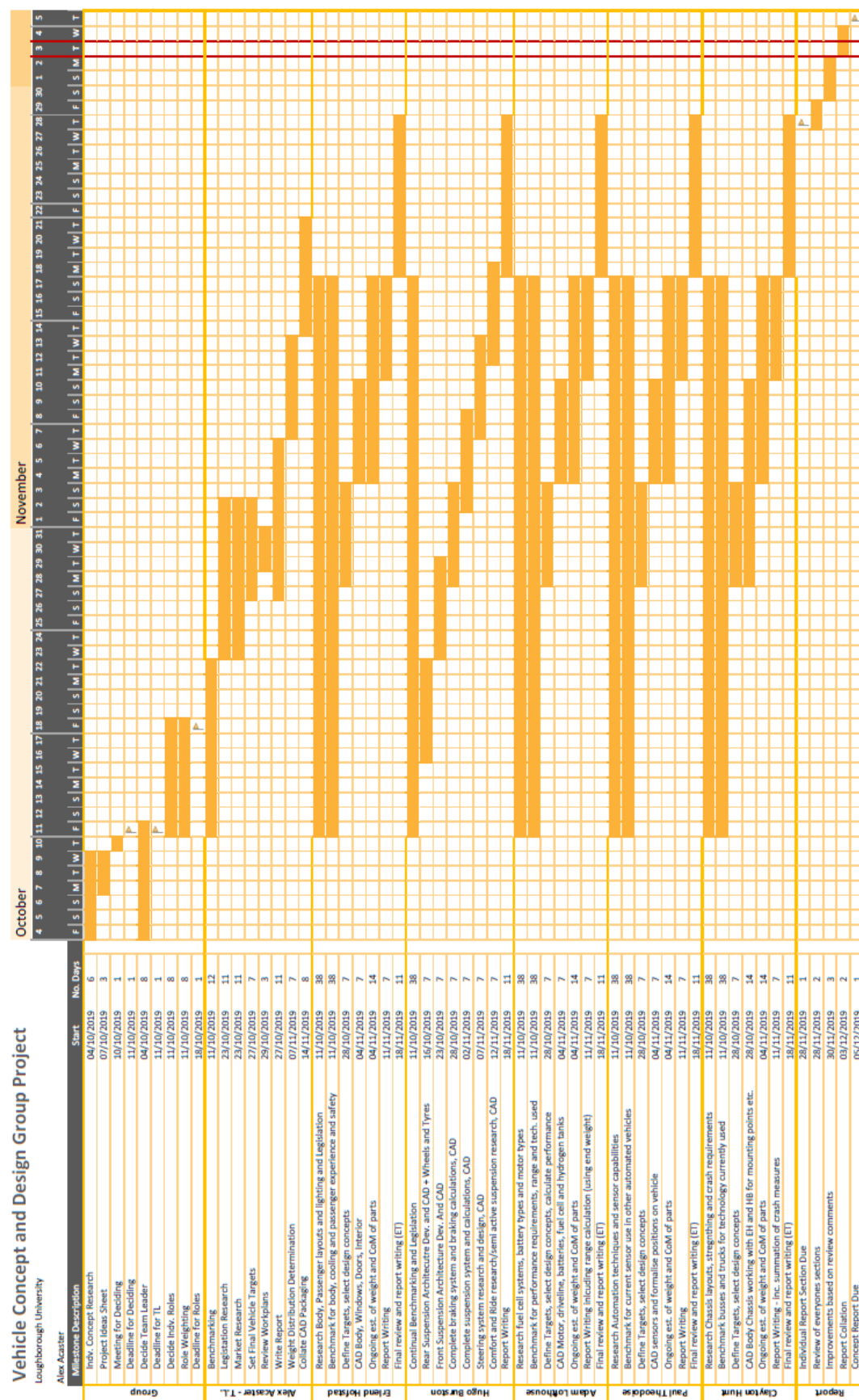
Name	Part Description	Part Dimensions			CoM on Vehicle			Raw Material per bus £	Production Cost per bus £
		Weight [kg]	x [mm]	y [mm]	z [mm]	x [mm]	y [mm]		
Alex	All passengers (standing x1.25x1.3, seated x1.25 (+driver and wheelchair))	7001				-550	0	1438	
Erlend	Air Conditioning (HVAC system)	258	2500	2000	300	660	0	3100	6000
	Superstructure	545				-465	-30	2090	980
	Lower Interior Panels	46	1390	50	800	560	0	843	900
	Panels, Windows, Doors	1873				-105	35	1995	3000
	Water Pump	3.9	154	203	154	-4425	660	1570	80
	Radiator	9.6	700	48	900	-4720	882	2126	240
	Coolant piping	2.3	6400	25	25	-4560	460	1295	124
	Spal Fan x 6	9	255	52	255	-4720	882	2126	331
	HVAC duct x 2	67				0	0	2655	500
	Interior Railing	220				1000	0	1910	400
	Seats (Double Bench)*12	240	620	900	1200	-2600	0	1010	3000
Hugo	Roof x 3	18				-500	0	3400	1000
	Ceiling	171				-130	0	2816	700
	Drivers Area	100	1300	900	2400	4100	-700	1500	600
Clayton	Air Compressor X1	30	400	220	600	-4750	-630	755	350
	Dryer etc	30	400	220	600	-4750	0	755	300
	Air Reservoir Brakes front (45 litres)	14.2	300	300	750	1627.6	920	540	500
	Air Reservoir Brakes rear (60 litres)	17.5	300	300	1000	-1708	0	492	500
	Air Reservoir Wet Tank	11.1	300	300	530	-4742	713	570	500
	Steering Column	6.1				2200	0	206	400
	Steering Shaft X2	1.5				2450	0	210	400
	Bevel Box	2.2				3150	-700	395	200
	ZF Rear Axle System AV 133 inc. whe	1088			2074	-2700	0	400	15000
	Front Axle RL 82 EC inc. wheels	597.2				2700	0	400	17300
	Electrohydraulic Steering Pump	11.5				440	-800	320	300
Adam	275/70/22.5 Tyres x6	330				0	0	138	600
	RB Servocom Steering System	43				3550	-600		500
Clayton	Chassis	1193	9730	2350	887	-1319	-0.8	467	2150
	Kilovac K1K High Voltage Contactor	0.1	114	96	80	0	0	0	100
	Resettable Inertia Switch Crash Sens	0.1	30	20	20	0	0	0	40
Paul	Flooring	413	###	2350	412	117	10	396	518
	Wheel Arches	57.1				416	0	1012	130
	Front Ramp	92.26	1000	600	130	3920	950	310	295
	Rear Ramp	92.26	1300	660	130	-675	920	320	295
	Continental MFC500 camera	0.2	88	70	38	4960	0	2650	300
	Velodyne VLP-32C Ultra Puck lidar	0.925	100	100	87	4100	0	3450	6500
	Continental ARS540 long range radar	0.4	130	101	32	5090	0	700	40
Paul	Bosch MRR rear medium range rada	0.19	70	82	30	-5150	0	700	35
	Continental SRR520 short range rada	0.68	83	69	22	200	0	700	140
	Bosch Ultrasonic sensor *8	1.12	26	26	44	200	0	500	960
	NXP Bluebox ECU	2.5	400	220	80	-1400	220	2800	4631
	Garmin GPS16-HVS	0.032	86	86	42	-1400	0	2800	66
	Door bracket *6	10	300	30	10	2500	950	1500	45
	Door turning column *3	128.2	55	55	2240	2500	950	1500	581
	Pneumatic system *3	6	75	75	105	2500	950	1500	225
	Sliding System	13.5							39
	Ramp motor *2	9							108
	Unmanned systems tech IMU-P sensc	0.07	39	45	22	-1400	-50	2800	300

Appendix B – Market Research Results

Appendix B: Market Research

Topic	Outcomes	Percentage
Dissatisfactions about the Sprint service (participants could list 3 problems)	Un-reliable loop frequency of shuttle service Low passenger space on board Compensated and uncomfortable air conditions Other outcomes included; small entrance/ exits; uncomfortable ride and noisy environment.	95% 85% 38%
Suggested improvements to the Sprint service (participants could only list 1 problem)	Fix route looping timing and quantity of buses Remove some seating for more standing space Improve overall comfort for passengers	49% 28% 23%
Preference over sitting or standing on the bus (two option question)	Seating Standing	31% 69%
A speed in miles per hour which participants would feel safe on an autonomous bus (four speed range options)	≤10mph >10, ≤20mph >20, ≤30mph >30mph	21% 44% 25% 10%
Voted important factors for the creation of a modern feel, comfortable bus (open question)	Inclusion of modern technology Obtaining a smoother and quieter experience Having pleasing aesthetics and lighting	39% 33% 28%

Appendix C – Project Planning – Gantt chart



Appendix D – Example Meeting Minutes

Meeting Number: 7

Meeting Date: 21/10/2019

Meeting Time: 11.00

Attendance: Alex, Erlend, Hugo, Paul, Adam, Clayton

Meeting Content:

Autonomy:

- Notion questioning the outcome of an occurrence that prevents the bus from travelling the planned route. If there's a blockage or road closed.
- Outcome after discussion is that there will be a **permanent driving position** on launch that will allow the bus to adhere to current automation laws while providing the view to extend the seating capacity when automation is allowed. The bus can still be in complete auto mode but for safety a drive is in position to stop any dangerous activity.
- Initial idea of power consumption is that on cars it can take up to 30% of the power of the vehicle to operate (in a city)

Vehicle Target Market Confirmation:

- The bus will use pre-planned roads and looped journeys as we are aiming this vehicle at the shuttle type of bus industry (repetitive short journeys).
- A 2021 expectation date of allowed autonomous vehicle on public roads with a driver for safety.
- Small capacity bus for shuttle services, providing a prestige environment to make a high profile reputation of the business/ location employing this vehicle. – based on the Loughborough Sprinter bus service.
- Vehicle package needs to allow the integration of the vehicle into existing architecture with the only major changes occurring at the bus depot – inclusion of hydrogen and electric filling services.

Powertrain:

- Having the Hydrogen Fuel cell system as the main power source for electric motors is possible but increases weight and has less range/ system weight than inclusion of batteries.
- Relying on power from batteries with a hydrogen range extender is the chosen choice because it is lighter and can provide a larger range.
- Motor location is on the sprung mass (attached to the vehicle structure) using a differential because of the ease of packaging and reducing unsprung mass therefore passenger comfort through suspension characteristics. **How Many Motors/ what size do we need?**

Suspension:

- Air springs seem more realistic for packaging over active system.

Chassis:

- Targeted to be low and provide strengthening through the body as well as ladder structure.
- Needs to fit suspension and powertrain.

Future Actions/ Meeting Topics:

- Review time plan, check feasibility and update regularly
- Everyone to complete an individual work/ section plan on what they're researching/ how they're going to plan time and idea of what data they needs from others and when.
- Creation of individual areas on OneDrive to collaborate ideas and work to be easily accessible to all, including a section on 'amendments' so everyone can see decision made by the individual easily.

References

Project Specification:

[1] - <https://www.hydrogeneurope.eu/hydrogen-buses> - 1000000 Euros

[2] - <https://www.investopedia.com/terms/b/breakevenanalysis.asp>

Hydrogen Review:

[3] - <http://www.hyer.eu/wp-content/uploads/2016/04/4.-Hydrogenics-Martin-Troeger.pdf>

[4] - <https://www.sciencedirect.com/topics/engineering/compressed-hydrogen>

[5] - <https://www.aqua-calc.com/page/density-table/substance/diesel>

[6] - <https://www.sciencedirect.com/topics/engineering/compressed-hydrogen>

[7] - <https://www.theaa.com/driving-advice/driving-costs/fuel-prices>

[8] - <https://evchargingsolutions.co.uk/ev-charging-costs/>

[9] - <https://www.rac.co.uk/drive/advice/buying-and-selling-guides/hydrogen-cars/>

Legislation:

[10] – “Directive (EU) 2007/46/EC” - <https://eur-lex.europa.eu/legalcontent/EN/ALL/?uri=CELEX:32007L0046> [retrieved 8th October 2019]

[11] – “Directive (EU) 2015/719” - <https://eur-lex.europa.eu/legalcontent/EN/TXT/?uri=CELEX:32015L0719> [retrieved 8th October 2019]

[12] – “Directive (EU) 97/27/EC” - <https://eur-lex.europa.eu/legalcontent/en/ALL/?uri=CELEX:31997L0027> [retrieved 8th October 2019]

Benchmarking:

[13] – TI_Citaro_RL_2019-EN download - https://www.mercedes-benz-bus.com/en_GB/buy/services-online/download-technical-brochures.html#container_copy/content_element_385184368

[14] – Brochure_7900E_EN download - <https://www.volvobuses.co.uk/en-gb/our-offering/buses/volvo-7900-electric/specifications.html>

[15] – Alexander Dennis enviro200EV Brochure - <https://www.alexander-dennis.com/media/69774/enviro200-brochure.pdf>

[16] – Optare Solo Specification Sheet - <https://www.alexander-dennis.com/media/69774/enviro200-brochure.pdf>

Weight Distribution and Load Cases:

[17] - https://transportsafety.vic.gov.au/__data/assets/pdf_file/0005/39479/How-to-calculate-the-maximum-number-of-passengers.pdf

[18] – “Simulations of Large School Bus Crashes”, Technical Paper SAE2000, March 6 2000.

[19] – “Prediction of impulsive vehicle tyre-suspension response to abusive drive-over-kerb manoeuvres” June 2013

Vehicle Concept Definition and Design: Design Report

Section 2

Body & Styling, Passenger Compartment, HVAC & Thermal Management



(s) Erlend Strutt-Hofstad – B614287

Number of Pages: 25
Number of Words: 1711

Contents

2.1 Introduction	29
2.2 Targets	29
2.3 Superstructure.....	29
2.3.1 Calculations and Assumptions	30
Energy absorption	30
Maximum allowable displacement at roof header	30
Work Calculations	31
Cross Members	34
Reaction forces	34
Reaction moments	35
Maximum Stress.....	36
2.3.3 Final Specifications	37
2.4 Body Panels	37
2.4.1 Design for Minimum Weight.....	39
Requirements	39
Fastening concept.....	39
Material Selection.....	39
Calculations.....	41
2.5 Exterior Lighting	43
2.6 Passenger Compartment	44
2.7 HVAC System	45
2.4 Thermal Management	46
Appendix	48
Appendix A	48
Appendix B	49
References	50

2.1 Introduction

This section covers the development and optimisation of the components that make up the bus body. The final specifications for all areas including HVAC and thermal management systems are outlined.

2.2 Targets

Refined targets for the vehicle body relating to the relevant design areas are listed in Table 2A below. The actions outlined will be examined closer in each subsection.

Table 2A - Refined Targets

Code	Description	Actions	Design Areas	Status
EH01	The body must protect occupants in the event of a roll-over accident (ECE R66)	Optimisation of bay cross section dimensions	Superstructure	Target has been met
EH02	The body must support the HVAC unit and hydrogen tanks during 1.9g vertical acceleration (kerb strike)	Analysis of load cases at roof header	Superstructure	Original concept design satisfactory
EH03	The superstructure must weigh less than 1500 kg	Use of aluminium and efficient design	Superstructure	Target has been met
EH04	Body must be aesthetically pleasing and well-integrated (structural where possible) to meet objectives FO1 and FO2	Refinement of A-surface and fastening methods, DFMW	Body panels, superstructure	Target has been met
EH05	Exterior panels must be easily manufactured and replaced to meet objectives MA1 and MA2	Materials and manufacturing methods specified	Body panels	Target has been met roof panels (DFMW)

2.3 Superstructure

The design of the superstructure is optimised following a thorough assessment of the loading conditions. Initially, analysis for roll-over protection is carried out to determine final dimensions of each bay. The superstructure consists of 10 bays distributed evenly along the length of the vehicle as shown in Figure 2A. These are the main structural elements and need to be designed to absorb the required energy in a roll-over accident. The method used for evaluating bus roll-over protection is derived from a referenced study [1].

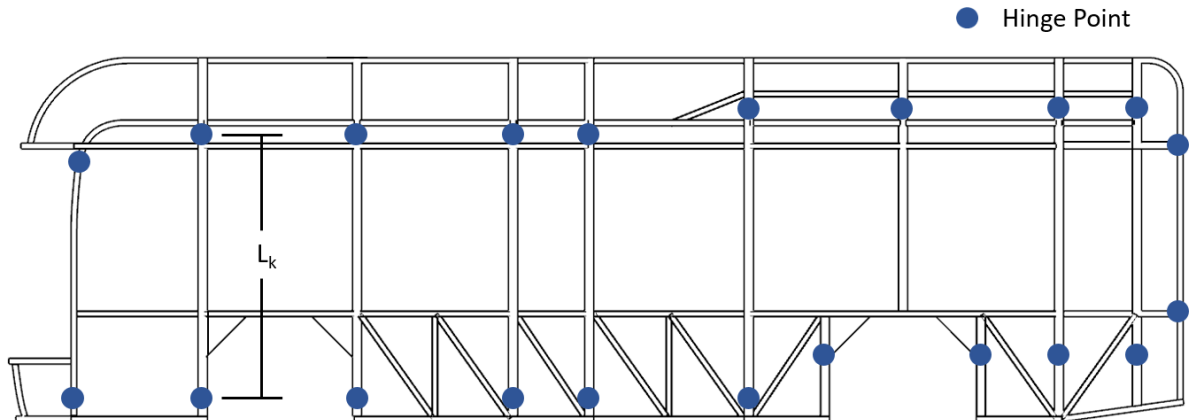


Figure 2A - Superstructure layout

Table 1B - Pillar heights [m]

L_1	L_2	L_3	L_4	L_5	L_6	L_7	L_8	L_9	L_{10}
2.21	2.41	2.41	2.41	2.41	2.66	2.26	2.26	2.26	1.80

2.3.1 Calculations and Assumptions

Table 2C - Assumptions for Calculating Rollover Energy Absorption

Assumptions	Explanation
All the energy absorption occurs through the deformation of each pillar element.	In reality, other components will absorb some energy. However, this simpler approach will yield a conservative result reducing the risk of failure.
The body is rigidly mounted to the chassis.	Chassis and mounting brackets are considered infinitely stiff as their deflection will be negligible in comparison to the deformation of each bay.
The body will rotate about the hinges determined in Figure 1.	From visual assessment, it is apparent that the maximum internal bending moments occur at the top and bottom of each pillar
No discrepancy between static and dynamic yielding.	Static material data has been used in previous studies with good agreement to experimental data [2]

Energy absorption

The total energy absorption requirement is calculated using the formula found in ECE R66 [3]:

$$\begin{aligned} \text{Energy} &= 0.75 \times M \times 9.8 \left[\sqrt{\left(\frac{W}{2}\right)^2 + H_s^2} - \frac{W}{2 \times H} \sqrt{H^2 - 0.8^2} + 0.8 \frac{H_s}{H} \right] \\ &= 58375 \text{ J} \end{aligned} \quad (1)$$

Where M is the vehicle mass excluding passengers as our city bus does not have individual seat belts [3]. W is the width and H and H_s are vehicle height and height of centre of gravity respectively.

Maximum allowable displacement at roof header

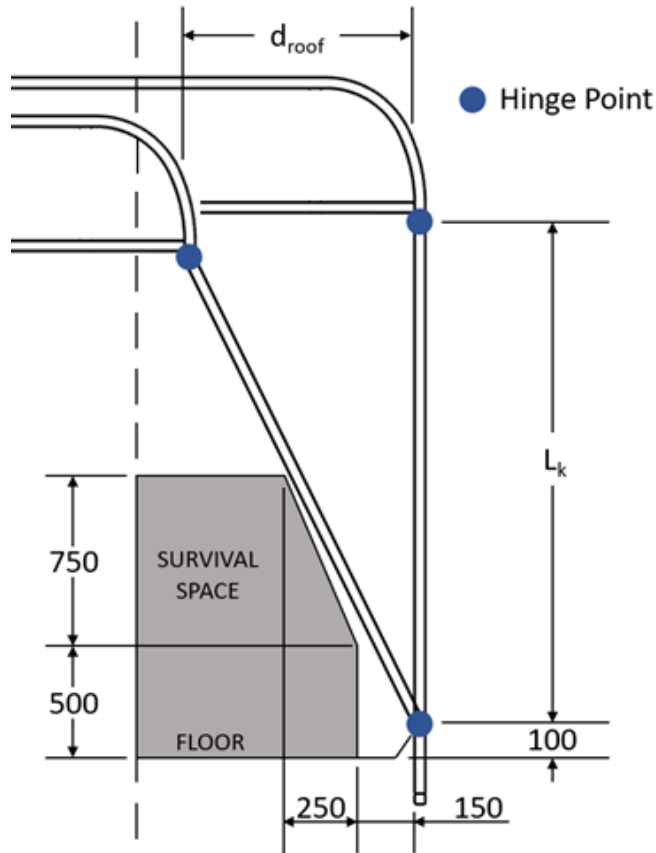


Figure 1B - Idealised model with survival space boundary [3]

Each bay is modelled as a plastic hinge mechanism with four hinges. The maximum allowable displacement at the roof header is determined using the following equation with dimensions derived from Figure 2B.

$$d_{roof} = L_{roof} \times \frac{400}{1150} = 838 \text{ mm} \quad (2)$$

Work Calculations

Initial section geometry and material from concept phase is used as baseline design (See Table 5). The energy absorbed at each bay is due to both elastic and plastic deformation of the pillars. Considered first is the work done due to elastic deformation

The plastic yield moment for the section is calculated using the Roark method.

Plastic modulus:

$$Z_{plastic_k} = \frac{W \times H^2 - W_i \times H_i^2}{4} \quad (3)$$

Maximum plastic yield moment:

$$M_{plastic_yld_k} = S_{yld} \times Z_{plastic_k} \quad (4)$$

Area moment of inertia:

$$I_k = \frac{W \times H^3 - W_i \times H_i^3}{12} \quad (5)$$

Yield moment for each hinge:

$$M_{yld_k} = \frac{S_{yld} \times I_k}{\frac{H}{2}} \quad (6)$$

Each bay has four hinges, except for bay number 7 which has an additional two lower hinges as illustrated in Figure 2A. Therefore, we can describe the lateral resisting force for each bay as follows.

For $k = 7$

$$F_{max_k} = 6 \times \frac{M_{plastic_yld_k}}{L_k} \quad (7)$$

Otherwise

$$F_{max_k} = 4 \times \frac{M_{plastic_yld_k}}{L_k}$$

Using the Slope-Deflection method to determine the energy absorbed through elastic deformation:

$$d_{elastic_k} = \frac{M_{yld_k} \times L_k^2}{6 \times E \times I_k} \quad (8)$$

$$W_{elastic_k} = \frac{F_{max_k} \times d_{elastic_k}}{2} \quad (9)$$

During plastic deformation, local buckling at the hinges cause the force vs lateral deflection curves to be non-linear. An approximate function for thin walled rectangular beams from the referenced study is used to account for this non-linearity. The lateral resisting force vs lateral deflection curve during plastic deformation for bay number 4 is shown in Figure 2C.

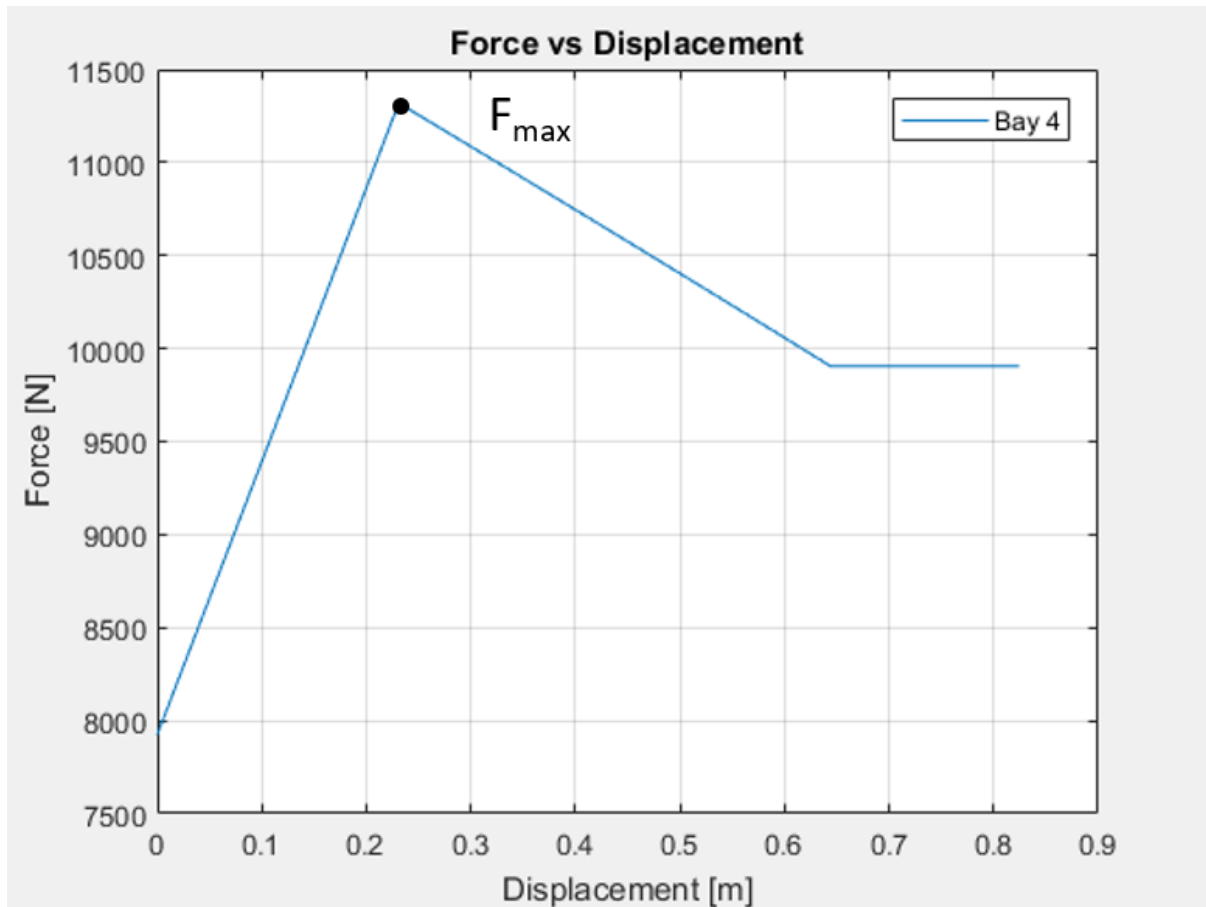


Figure 2C– Lateral Resisting Force vs Lateral Deflection at Roof Header – Bay 4

The work done due to plastic deformation can then be expressed as follows:

$$W_{plastic_k} = \int_{d_{elastic_k}}^{d_{roof}} Func(x) \times F_{max_k} dx \quad (10)$$

Where $Func(x)$ is the approximate function. The sum of the elastic and plastic work done for each bay yields the total absorbed energy:

$$W = \sum_{k=1}^{10} W_{elastic_k} + W_{plastic_k} \quad (11)$$

The superstructure will pass the roll-over test when $W > E$. The initial design from the concept phase can absorb 40279 J. Changes were made to the section geometry iteratively in Matlab in order to achieve $W > E$ and a safety factor of 1.2. The final design can absorb 70628 J before the pillars start to intrude into the survival space with section dimensions well within the recommended slenderness ratio limits [Appendix B]. Final specifications are outlined in Table 2E.

Cross Members

When considering the stresses in the lateral roof members, the maximum load caused by kerb strikes are used as a worst case scenario. From the quarter car suspension model, this was found to be 1.9g. The hydrogen fuel tanks will be fixed to both the upper and lower cross beams of the roof structure, distributing the load. Therefore, the load applied by the HVAC unit will be considered.

Table 2D: Assumptions - Roof Cross Members

Assumptions	Explanation
Lower cross beams are fixed at both ends.	These sections are to be welded to pillars at either end reducing their ability to rotate. In reality, flexure of the pillars will occur.
HVAC unit mass is uniformly distributed.	As the unit will be mounted flush with the cross members, it can be considered as a uniformly distributed load.
HVAC unit centre of gravity is located centrally	A reasonable assumption meaning that each cross member is required to support 1/5 of its weight.

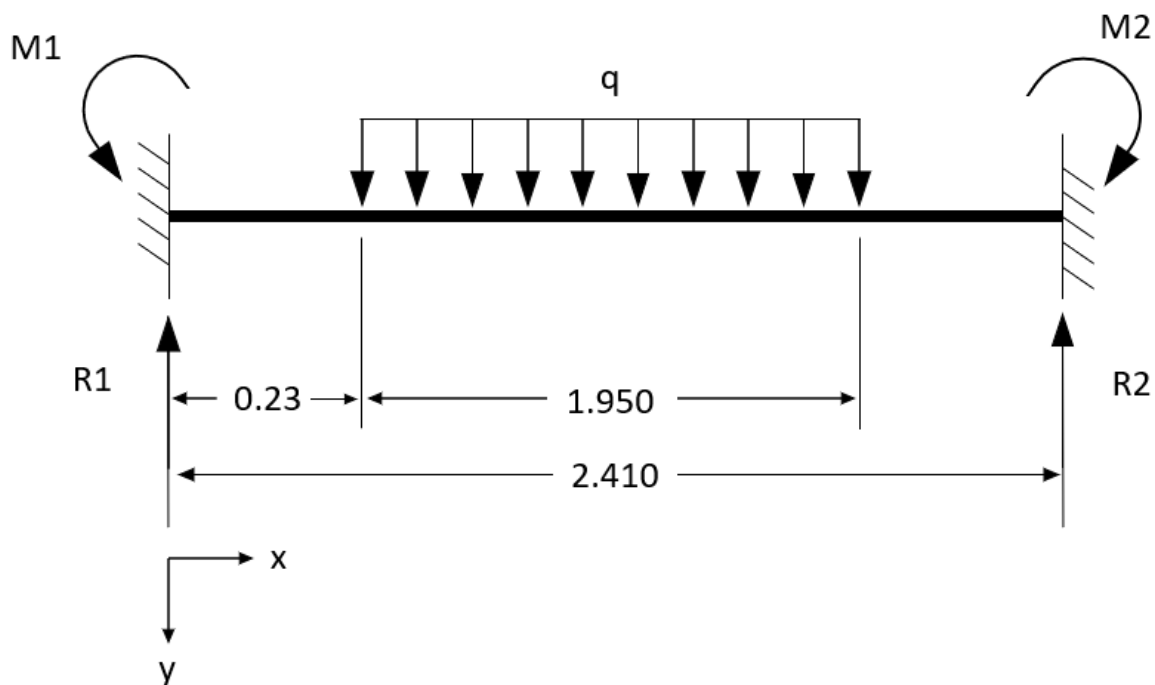


Figure 2D - Free Body Diagram - Roof Cross Beams

The mass of the specified HVAC from the concept phase is 258 kg, giving the following distributed load:

$$q = \frac{258 \times 1.9g}{5 \times 1.950} = 493 \text{ Nm}^{-1}$$

Reaction forces

$$R1 = R2 = \frac{q \times 1.95}{2} = 481 \text{ N}$$

Reaction moments

$$M1 = -\frac{q \times 1.95}{24L} \left(\frac{24 \times 1.205^3}{2.41} - \frac{6 \times 2.18 \times 1.95^2}{2.41} + \frac{3 \times 1.95^3}{2.41} + 4 \times 1.95^2 - 24 \times 1.205^2 \right) = \\ 1316 \text{ Nm}$$

$$M2 = -\frac{q \times 1.95}{24L} \left(\frac{24 \times 1.205^3}{2.41} - \frac{6 \times 2.18 \times 1.95^2}{2.41} + \frac{3 \times 1.95^3}{2.41} + 2 \times 1.95^2 - 48 \times 1.205^2 \right) = \\ 1316 \text{ Nm}$$

Cut 1 $0 < x < 0.23$

$$\sum P_y = -R1 + V = 0, \quad \therefore V = 481 \text{ N} \\ \sum M = M1 - R1x + M = 0, \quad \therefore M = 481x - 1316$$

Cut 2 $0.23 < x < 2.18$

$$\sum P_y = -R1 + 493 \times (x - 0.23) + V = 0, \quad \therefore V = 594 - 493x \\ \sum M = M1 - R1x + \frac{493(x - 0.23)^2}{2} + M = 0, \quad \therefore M = -1329 - 247x^2 + 594x$$

Cut 3 $2.18 < x < 2.41$

$$\sum P_y = -R1 + 493 \times 1.95 + V = 0, \quad \therefore V = -481 \text{ N} \\ \sum M = M1 - R1x + 493 \times 1.95 \times (x - 1.205) + M = 0, \quad \therefore M = -481x - 158$$

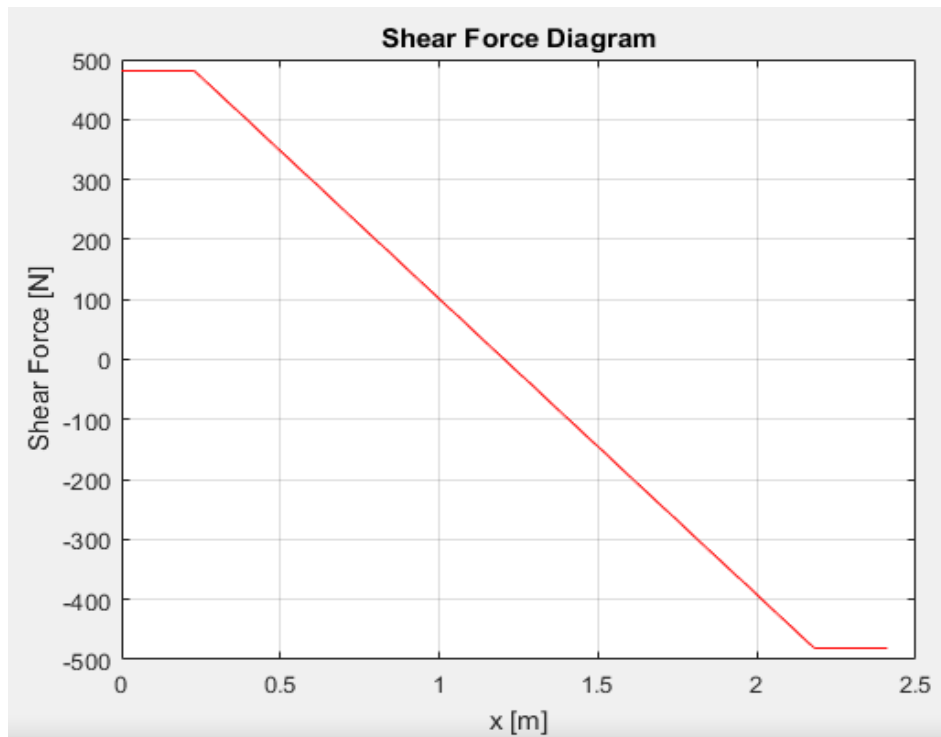


Figure 2E: Shear Force Diagram - Roof Cross Beams

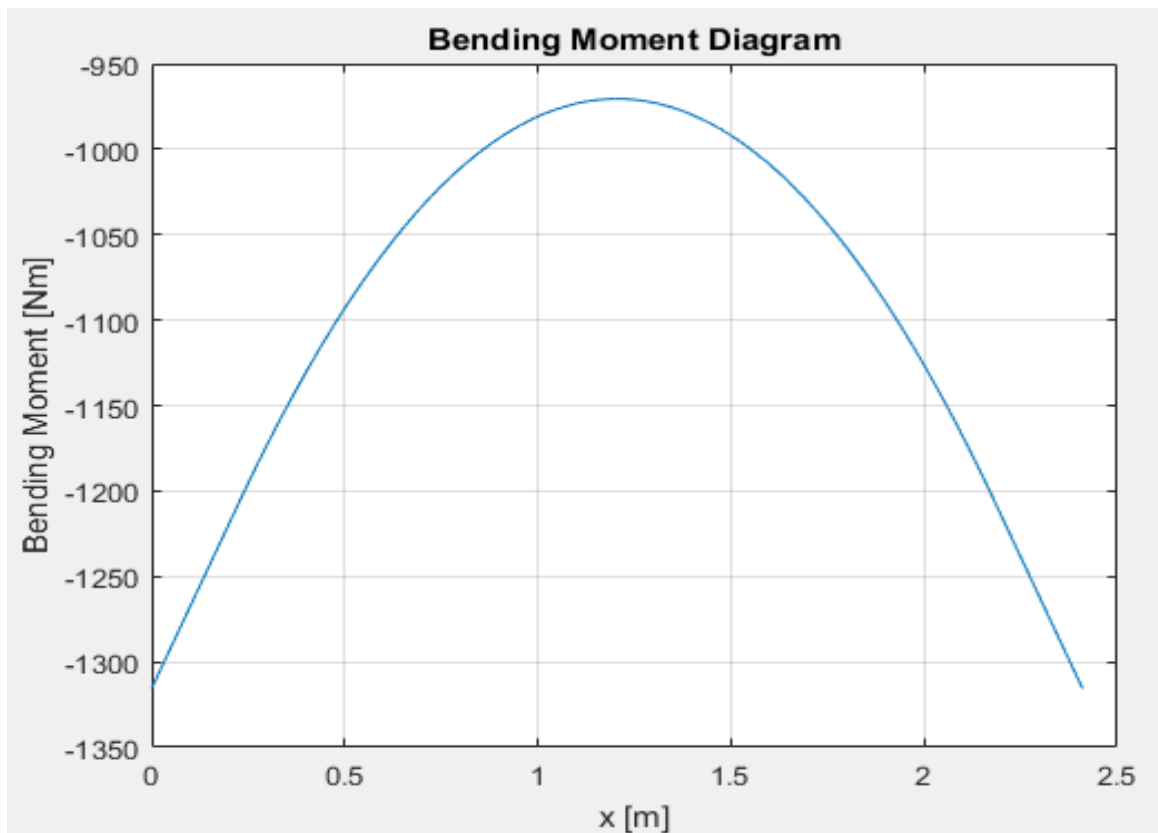


Figure 2F: Bending Moment Diagram - Roof Cross Beams

Maximum Stress

From Figure 2F, it is found that the peak bending moment occurs at the ends. This value is used to find the maximum stress in the beam. Cross section dimensions are listed in Table 2E.

Second moment of inertia of box section:

$$I = \frac{h^4 - (h - 2t)^4}{12} = \frac{0.05^4 - (0.05 - 2 \times 0.004)^4}{12} = 2.6 \times 10^{-7} m^4$$

Maximum stress:

$$\sigma_{max} = \frac{M_{max} \times y}{I} = \frac{1316 \times 0.025}{2.6 \times 10^{-7}} = 127 MPa$$

The chosen material yields at 260 MPa, meaning that the cross members can withstand the worst case loading scenario (kerb strike).

2.3.3 Final Specifications

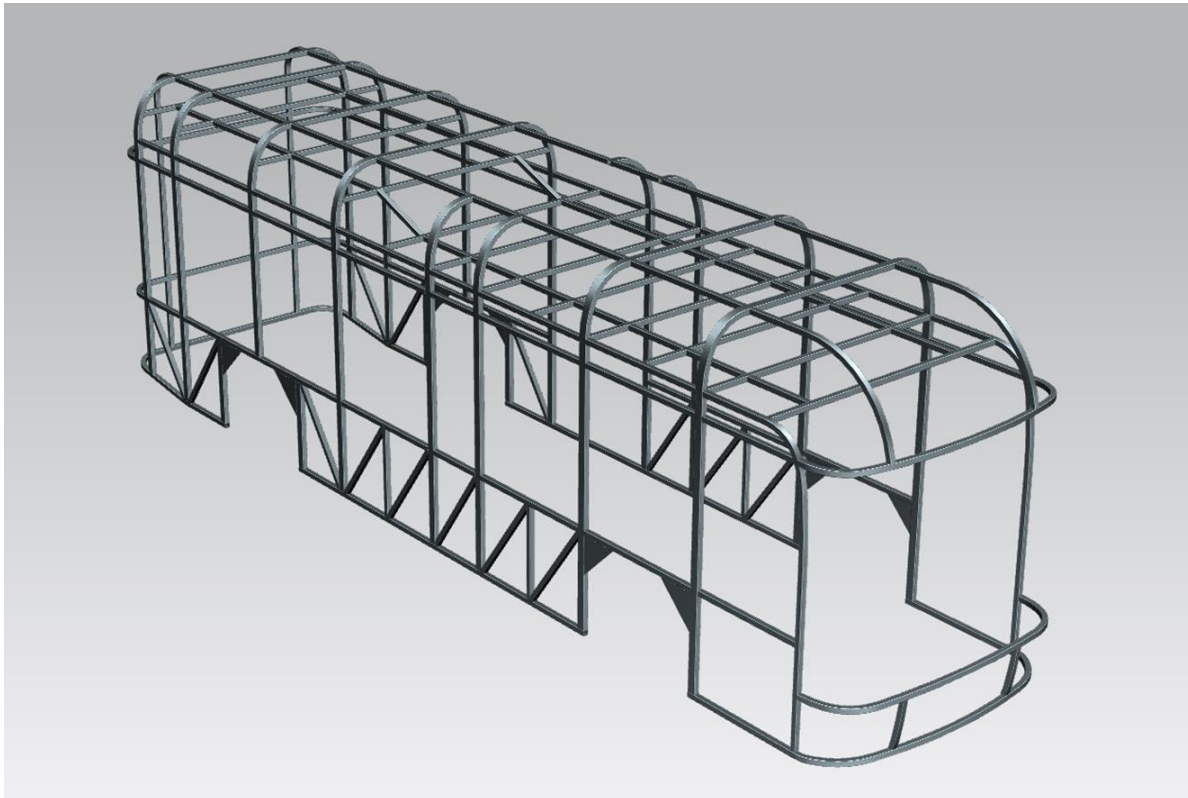


Figure 2G: Isometric View - Superstructure

Table 2E: Final Specification of Superstructure [12]

	Concept	Design
Material	Aluminium	Aluminium 6082-T6
Main beam cross section	50 x 50 x 4 mm	50 x 80 x 5 mm
Other beam cross section	50 x 50 x 4 mm	50 x 50 x 4 mm
Weight	466 kg	545 kg
Raw material Cost	£838	£980

Figure 2G shows the final design of the superstructure. Other alterations to the design include wheel arch plates for added stiffness and larger mounting surfaces, diagonal wall elements for improved side impact performance and mounting surfaces and longitudinal rails in the roof structure for handrail mounting points. The extruded elements that make up each wall will be welded together separately on jigs before being joined to each other along the centreline. The continuous pillar design, as opposed to the continuous waist rail design often used for buses, means that the welds will not significantly reduce the hardening effect in the main structural elements required for rollover protection [5].

2.4 Body Panels

The specification of the body panels remain mostly unchanged from the concept with the addition of insulation inserts as shown in Figure 2H.

Table 2F: Specification -Body Panels [6], [7]

Component	Concept	Design	Justification
Sills	GFRP, mechanically fastened	GFRP, mechanically fastened	Cost of replacement
Bumpers	ABS, mechanically fastened	GFRP, mechanically fastened (clips)	Manufacturing more cost effective for our production volume
Glazing	Bonded	Double glazing, bonded	Increased rigidity, clean aesthetic, reduced interior noise
Cant rail panels	GFRP, bonded	Aluminium, bonded	Reduces the risk of H2 tank penetration
Roof panels	GFRP, bonded	PLA sandwich construction	Allows maintenance access to H2 tanks
Insulation	Not Specified	Aluminium foil coated polyester	Thermal and noise insulation

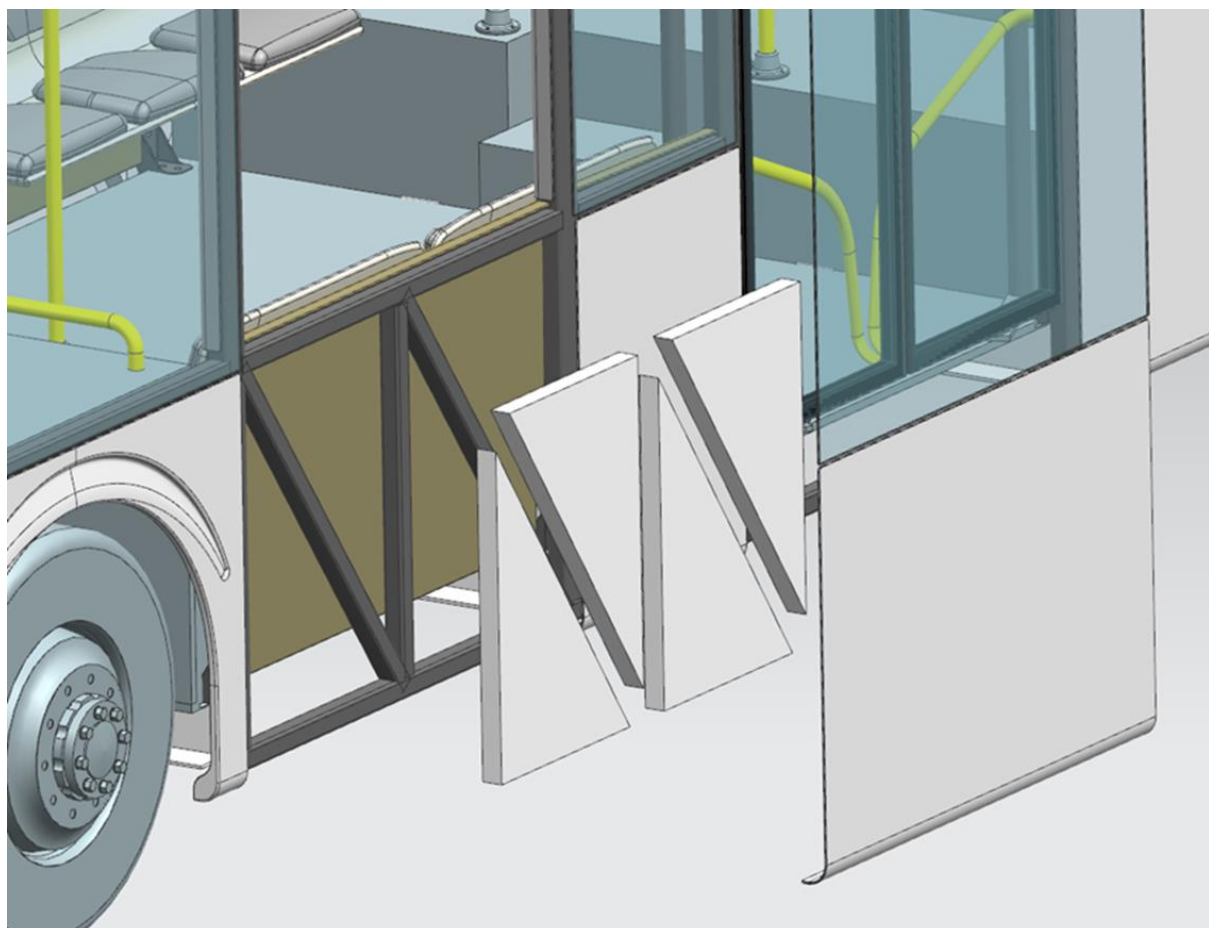


Figure 2H: Exploded View - Skirts and Wall Insulation

2.4.1 Design for Minimum Weight

A roof panel is chosen for weight optimisation. It is one of the largest exterior components and is required in three locations along the roof, providing room for considerable weight saving. A sandwich construction is selected as it is an emerging technology in modern bus manufacturing [12] [13].

Requirements

Table 2G - Roof Panel Requirements

Description	Explanation	Actions
Panel must be easily removable by one person	To allow maintenance access to H2 storage	Implementation of fastening method
A maximum deflection of 2mm	To maintain continuous A-surfaces and passenger compartment sealing.	The maximum distributed load case due to aerodynamic loading is considered
Panel must withstand moderate abuse	Panel must not yield during fitment and handling	Reasonable skin thickness and edging method

Fastening concept

To reduce the risk of water ingress and retain a clean outer surface, no fasteners will be visible on the top surface of the panel. Instead, the panel will be secured in place by M8 fasteners in one end and pins in the other [Appendix B]. This configuration allows the panel to be easily removed by lifting one edge and sliding the panel. Recessing of the inner surface allows easy alignment with the superstructure before fastening. The tolerances in the fit between pins and panel must be loose enough to allow one person to slide the panel off at an angle. The panel will also have an upper flange parallel to the top surface with a rubber seal so that it can rest on the superstructure and provide a continuous surface to the next panel.

Material Selection

When selecting appropriate materials for the core and skins, the following characteristics were considered

- Thermal conductivity
- Strength to weight
- Moisture permeability
- Fatigue due to UV radiation
- Sustainability

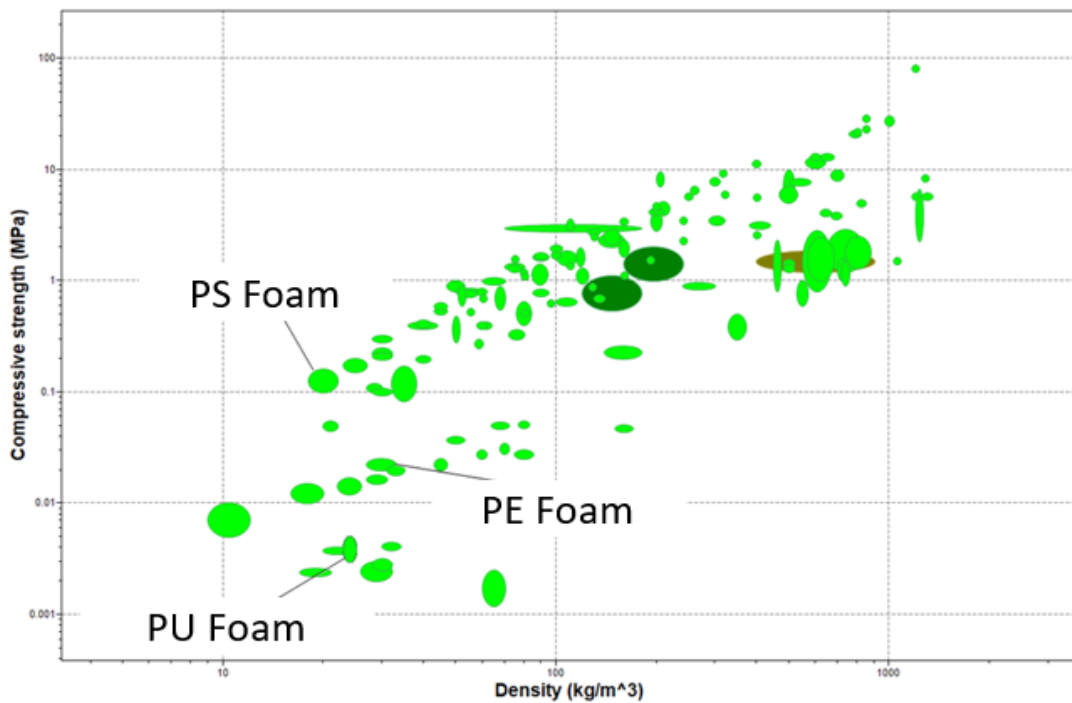


Figure 2J: Comparison of Various Core Materials [8]

Table 2H: Selected Materials [8] [13]

Material	Youngs modulus	Poisson's ratio	Density	Justification
Skins	PLA (30% natural fibre reinforced)	5.2 GPa	0.39	13000 kg/m ³ Biodegradable, high strength
Core	Polyurethane foam, closed cell	4.8×10^{-5} Pa	19 kg/m ³	Lightweight, good thermal insulation

Table 2J: Assumptions for Plate Bending

Assumptions	Explanation
Superstructure (to which panel is mounted) is infinitely stiff	Loads on panel are relatively low causing negligible deformation of the superstructure
Aerodynamic loads are evenly distributed over the panel	In reality, there are slight variations, however a uniformly distributed load is used for simplicity
Air-pressure inside the passenger compartment is ambient	Can vary depending on interior temperature and acceleration
Panel is simply supported along the edges	Given the fastening method, the panel is free to rotate, but not deflect along the edges.

Calculations

The panel will not be subject to any point loads during normal operation but requires a reasonable skin thickness for handling. This value is set to 0.8 mm. The coefficient of pressure close to the leading edge of a bus roof travelling at 80 km/hour is approximated from referenced studies to be -0.8 [15]. The pressure differential between interior and exterior of a bus is calculated below:

$$C_p = \frac{p - p_\infty}{\frac{1}{2} \rho_\infty V_\infty^2}$$

Rearrange for $p - p_\infty$

$$p - p_\infty = \frac{C_p \rho_\infty V_\infty^2}{2} = \frac{-0.8 \times 1.225 \times 22.2^2}{2} = -241.5 \text{ Pa} = q$$

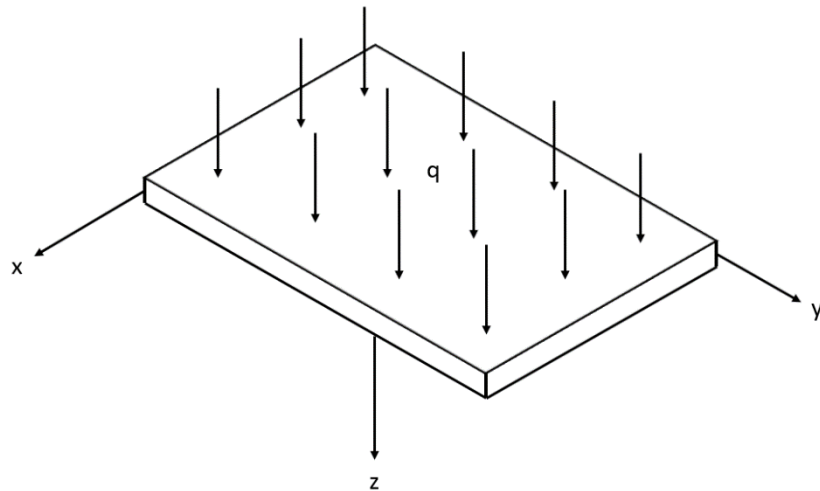


Figure 2K: Free Body Diagram of Roof Panel

The maximum vertical deflection at the centre of the plate can therefore be expressed as:

$$w_{max} = \frac{16(p - p_\infty)}{\pi^6 D_{eq}} \sum_{m=1,3,5}^{\infty} \sum_{n=1,3,5}^{\infty} \frac{\sin\left(\frac{m\pi}{2}\right) \sin\left(\frac{n\pi}{2}\right)}{mn \left[\left(\frac{m^2}{a^2} \right) + \left(\frac{n^2}{b^2} \right) \right]^2}$$

Where m and n are odd integers and a and b are the length and width of the panel respectively [Appendix B], [10]. For a symmetrical 3 layer sandwich structure, the following equation is used to determine the equivalent flexural rigidity [9]:

$$D_{eq} = \frac{2}{3} \left(E_p \frac{\left(\frac{t_c}{2} + t_p \right)^3 - \left(\frac{t_c}{2} \right)^3}{1 - v_p^2} + E_c \frac{\left(\frac{t_c}{2} \right)^3}{1 - v_c^2} \right)$$

The thickness of the core material t_c is altered iteratively in Matlab to achieve the required stiffness. With a core thickness of 28.4 mm deflection of the panel is 1.9 mm upwards.

Final specifications

Dimensions for the final design are shown in Appendix B. The layers will be bonded together using an epoxy adhesive and will feature an aluminium edging profile as shown in Figure 2L. A rubber seal is used around the flange of the panel to improve water tightness.

Table 2K - Final Weight and Cost

Category	Value
Weight	7.3 kg
Weight of equivalent aluminium panel	39 kg
Estimated cost	£245

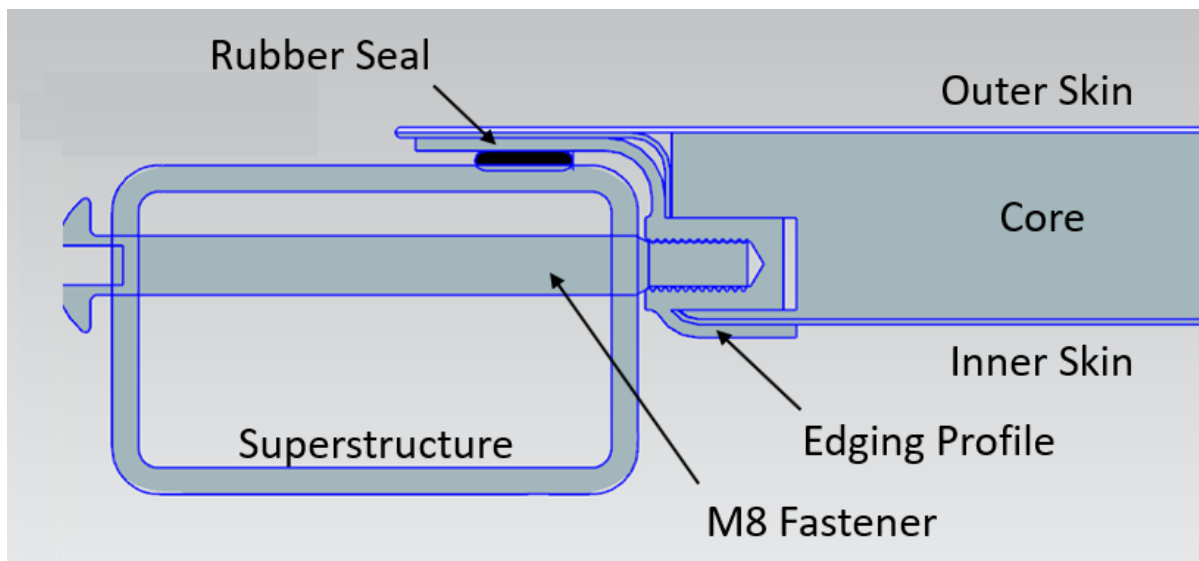


Figure 2L - Section View of Roof Panel Fixing Method

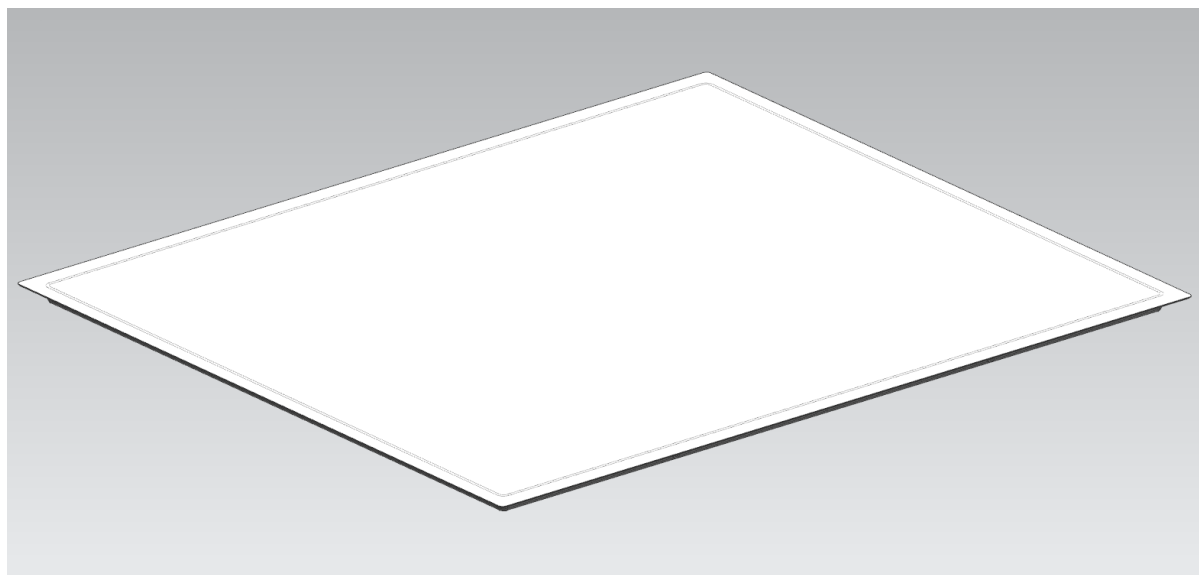


Figure 2M - Isometric View - DFMW Roof Panel

2.5 Exterior Lighting

The headlights and taillights have been designed to meet the legislative requirements [7]. The decision was made to use a bespoke lighting system rather than standard parts to stand out amongst the competition and meet vehicle objective FO1.

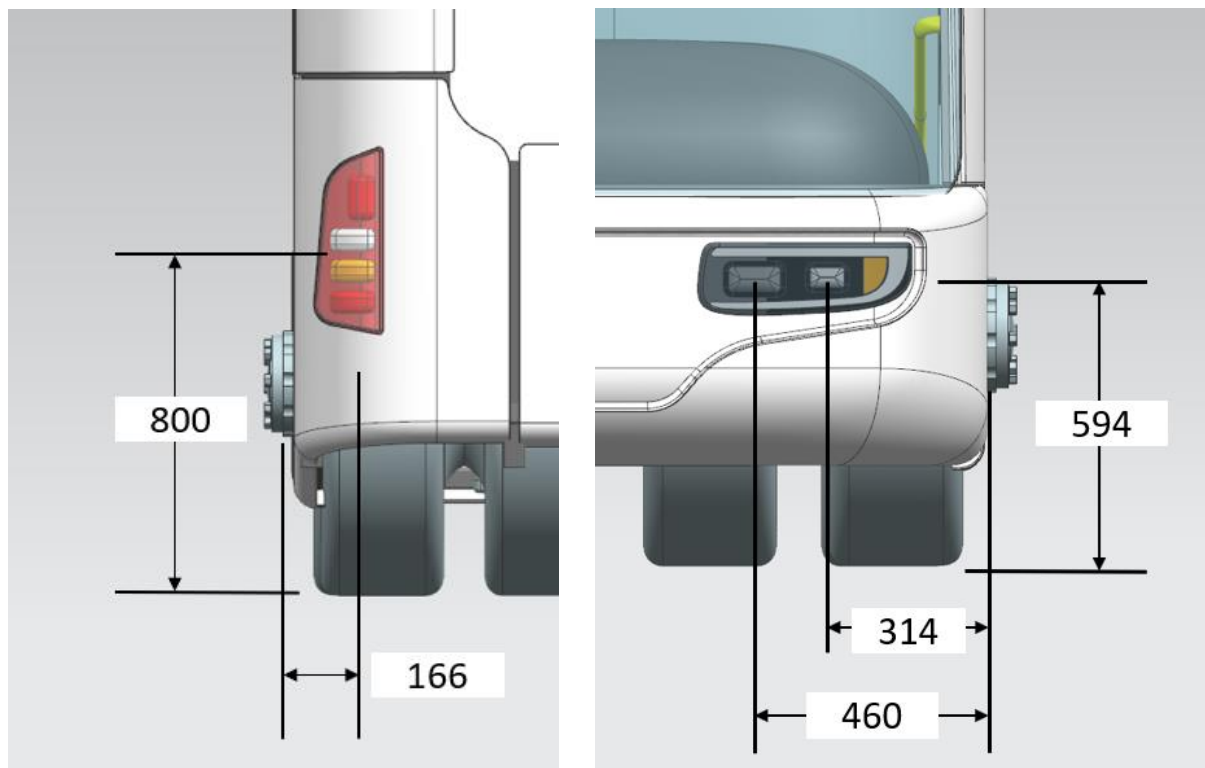


Figure 2N - Exterior Lighting Dimensions

2.6 Passenger Compartment

Handrails have been added to the interior in accordance with legislation and the optimal diameter for accessibility [14]. Central LED lighting is added to the ceiling to meet vehicle objective US1. Figure 2O shows the final interior layout when entering the bus.

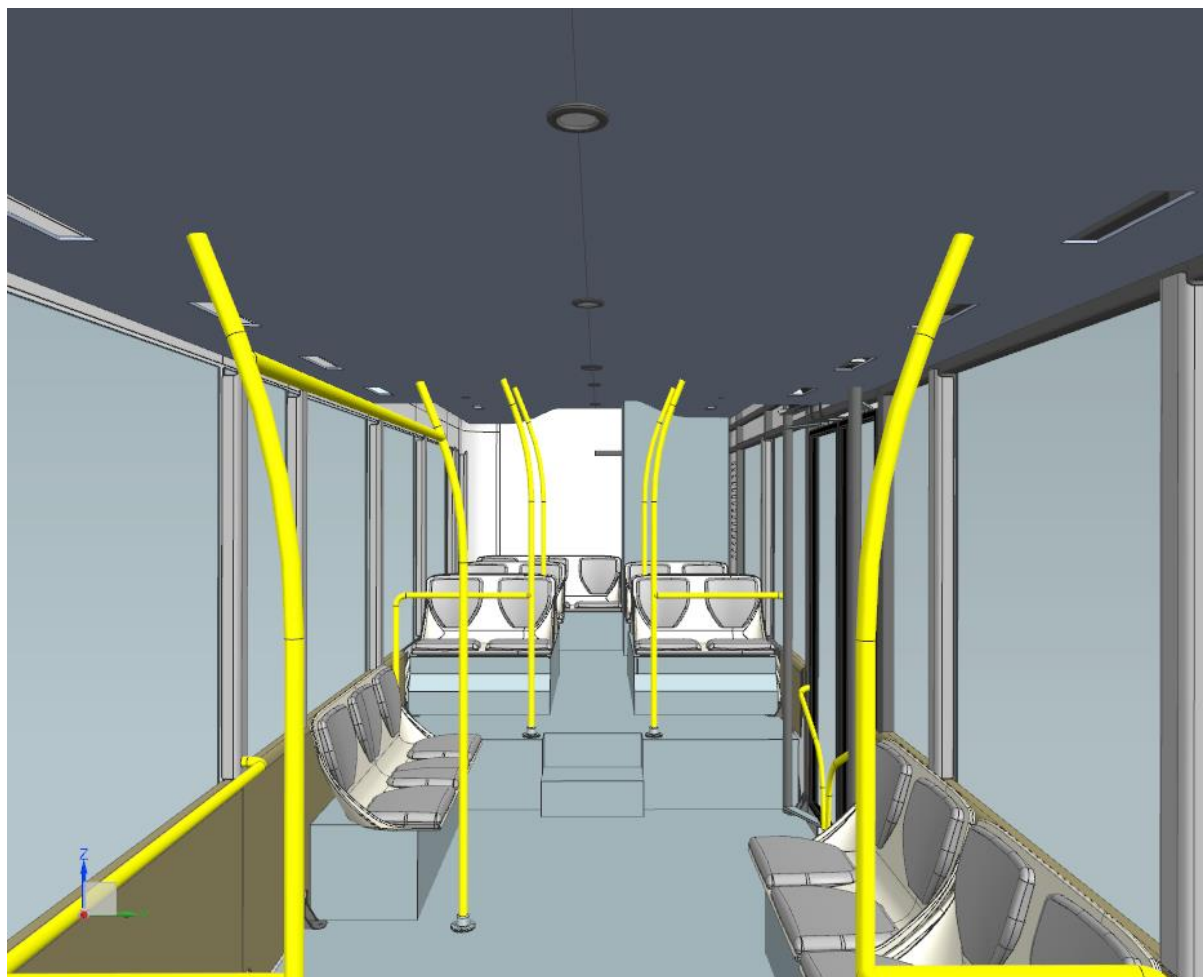


Figure 2O: Human View of Passenger Compartment

2.7 HVAC System

The chosen HVAC unit from the concept phase has been carried forward to the final design. The air flowing from the twin centrifugal impeller fans along the edges of the HVAC unit goes into two main ducts along the length of the bus before exiting through 18 diffusers. The air at the end of the duct will have greater pressure than at the centre. Therefore, the diffuser dimensions are reduced towards the end to achieve even flow rate distribution [29].

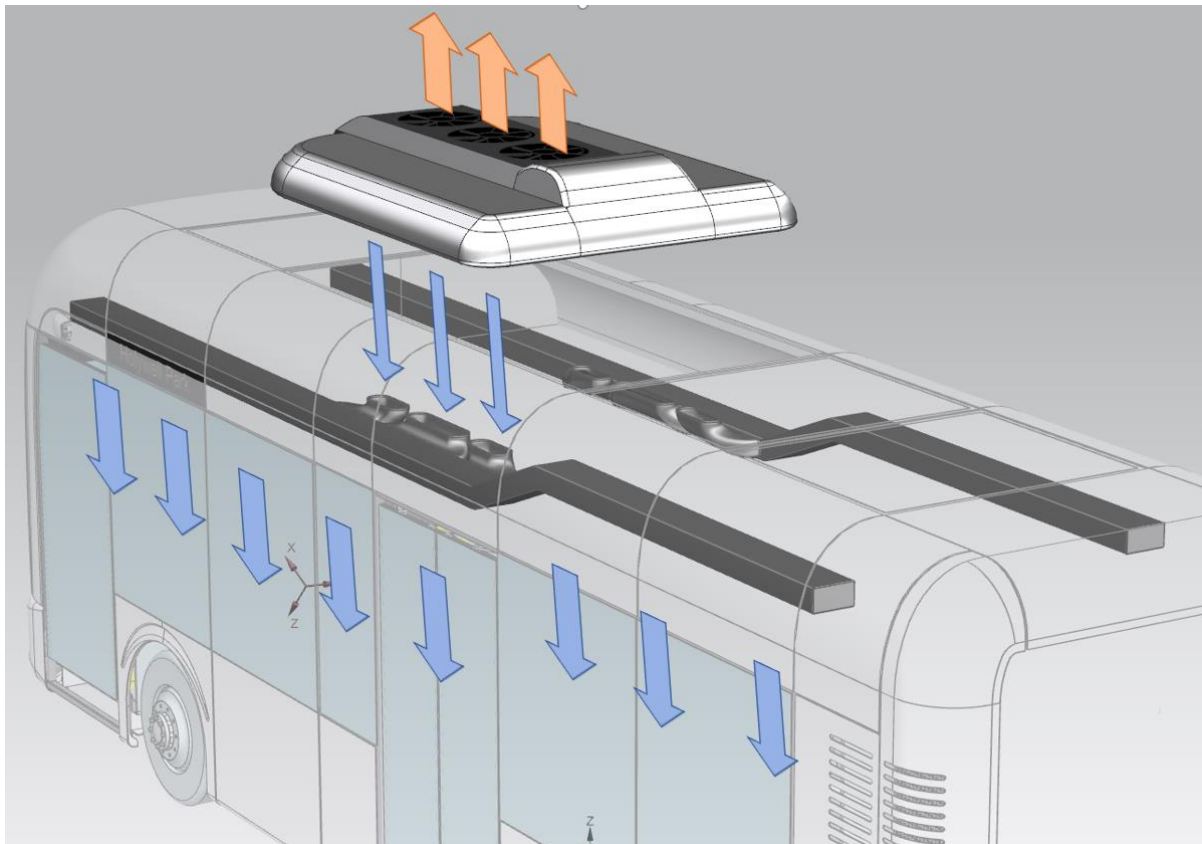


Figure 2P: HVAC System Overview

2.4 Thermal Management

Cooling system specifications have changed slightly from the concept report following the specification of an electric water pump and its optimal flow rate [17].

Table 2L: Changes to Cooling System

Value	Concept	Design
Volume flow rate, coolant	0.856 L/s	0.75 L/s
Volume flow rate, air	2.6 m ³ /s	2.27 m ³ /s

The components listed in Table 2M have been chosen to match the requirements. Fan speed will be controlled via a central control unit which monitors the temperatures in the motor and inverter.

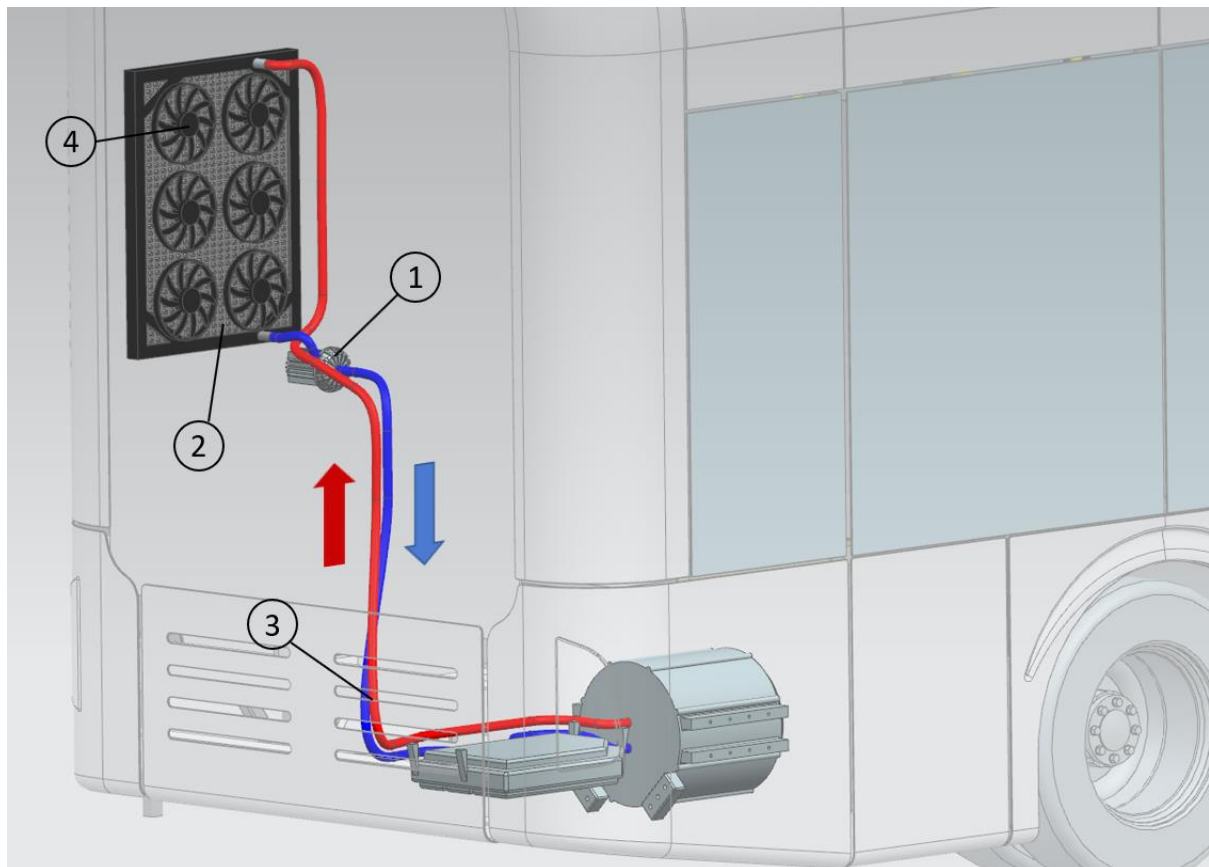
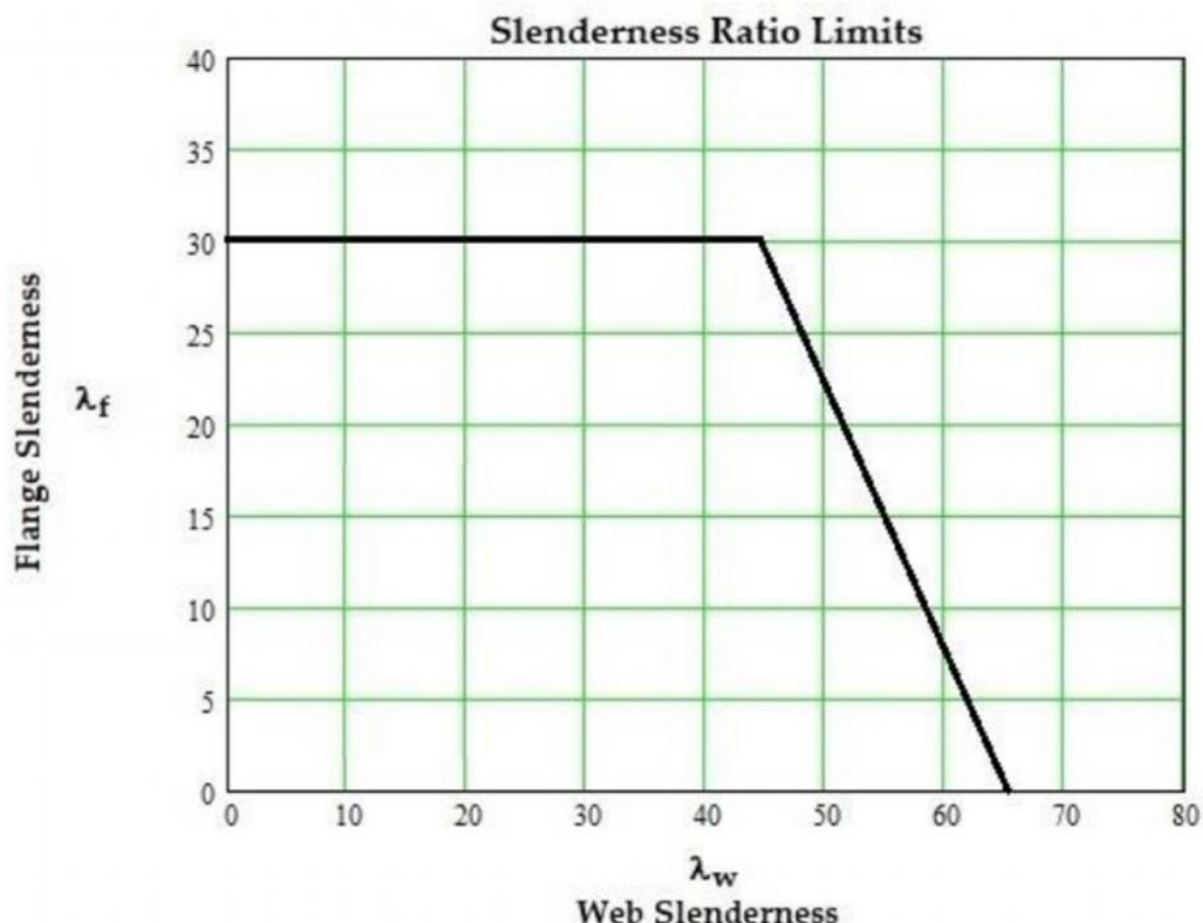


Figure 2Q: Cooling System Diagram

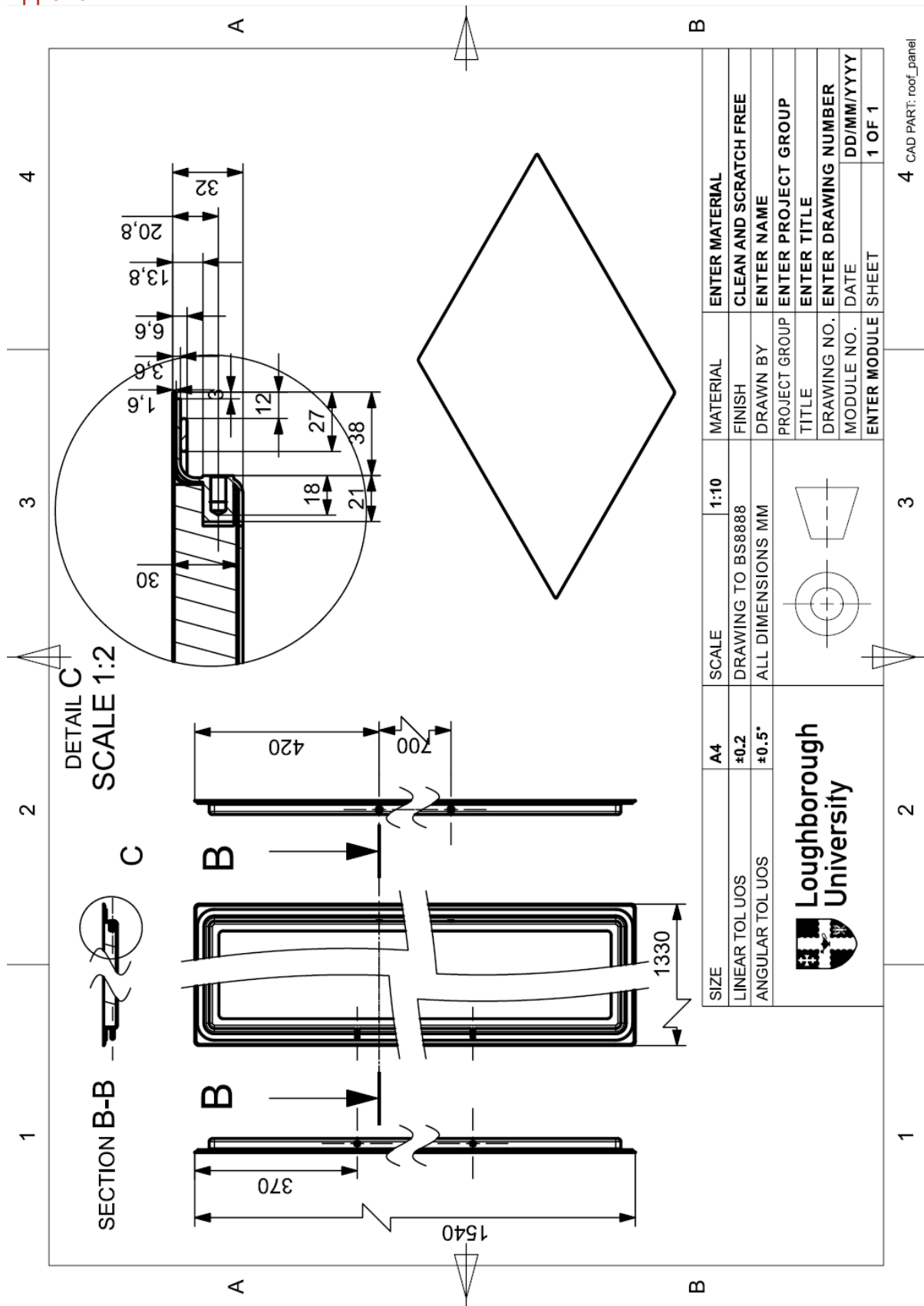
Table 2M: Final Specification for Cooling System [17],[21],[22], [23], [24]

Number	Component	Dimensions [mm]	Weight [kg]	Cost [£]	Justification
1	Grayson 24v Electric Water Pump	203 x 154	3.9	80	<ul style="list-style-type: none"> • quiet operation • includes CAN control configurations • low power consumption
2	Grayson Radiator	900 x 700 x 48	9.6	240	
3	Grayson Silicon Hoses 4 Ply	6400 x 25 x 25	2.3	124	<ul style="list-style-type: none"> • durability
4	Spal Cooling Fan x 6 (pulling)	255 x 255 x 52	9.0	331	<ul style="list-style-type: none"> • curved blades for quiet operation • meets airflow requirements
Total			24.8	775	

Appendix
Appendix A
[1]



Appendix B



References

Superstructure

- [1] – Pauls, L.S., "A Simplified Analytical/Experimental Method for Evaluating Large Buses and Motor Coaches for Rollover Protection," SAE Technical Paper 2018-01-5033, 2018, doi:10.4271/2018-01-5033.
- [2] – Kecman, D. (1983). Bending collapse of rectangular and square section tubes. International Journal of Mechanical Sciences, 25(9-10), pp.623-636.
- [3] – Unece.org. (2020). [online] Available at: <https://www.unece.org/fileadmin/DAM/trans/doc/2002/wp29grsg/TRANS-WP29-GRSG-83-inf08e.pdf> [Accessed 3 Mar. 2020].
- [4] – Engineersedge.com. (2020). Beam Deflection, Stress, Bending Equations and calculator for a Beam Fixed at Both Ends with Partial Uniform Loading. | Engineers Edge | www.engineersedge.com. [online] Available at: https://www.engineersedge.com/beam_bending/beam_bending52.htm [Accessed 26 Feb. 2020].
- [5] – European-aluminium.eu. (2020). [online] Available at: https://www.european-aluminium.eu/media/1295/aluminium-in-commercial-vehicle_en.pdf [Accessed 26 Feb. 2020].

Body Panels

- [6] – Aydin, K. and Esenboga, F. (2016). Improvement of the Heat and Sound Insulation of a Bus for Compliance with American Regulations. Advances in Automobile Engineering, 05(01).
- [7] – Welling, M. S. (1982). *Plastic uses in cars and commercial vehicles*. Germany, PA: VDI-Verlag.

DFMW

- [8] – CES Edupack, 2019. CES Edupack Materials Selection Software, s.l.: CES.
- [9] – Szilard, R. (1974). *Theory and analysis of plates*. New Jersey, PA: Prentice-Hall International, Inc.
- [10] – Megson, T. (2007). Aircraft structures for engineering students. Amsterdam [etc.]: Elsevier/Burttnerworth-Heinemann.
- [11] – Johnson, A. and Sims, G. (1986). Mechanical properties and design of sandwich materials. Composites, 17(4), pp.321-328.
- [12] – Zehnder, J., "Development Trends in Bus Manufacturing," SAE Technical Paper 2001-01-3330, 2001, <https://doi.org/10.4271/2001-01-3330>.
- [13] – JEC Group. (2020). Thermoplastic composites for mass transit applications. [online] Available at: <http://www.jeccomposites.com/knowledge/international-composites-news/thermoplastic-composites-mass-transit-applications> [Accessed 27 Feb. 2020].
- [14] – Bus design. (1996). Warrendale, Pa.: Society of Automotive Engineers.
- [15] – Velshankar, M., Senthilkumar, S., and Kannan, B.T., "Aerodynamic Drag Reduction of an Intercity Bus through Surface Modifications - A Numerical Simulation," SAE Technical Paper 2019-28-0045, 2019, doi:10.4271/2019-28-0045.
- [16] – Kim, M. (2004). Numerical study on the wake flow characteristics and drag reduction of large-sized bus using rear-spoiler. International Journal of Vehicle Design, 34(3), p.203.

Thermal Management

[17] – Graysons. (2020). Grayson 24v Electric Water Pump - Graysons. [online] Available at: <https://www.graysonts.com/products/grayson-24v-electric-water-pump/> [Accessed 24 Feb. 2020].

[18] – Danatm4.com. (2020). [online] Available at: <https://www.danatm4.com/wp-content/uploads/2018/08/TM4-SUMO-Product-Brochure.pdf> [Accessed 26 Jan. 2020].

[19] – Green Car Congress. (2020). Optare Introduces Battery-Electric Bus. [online] Available at: <https://www.greencarcongress.com/2009/03/optare-introduces-batteryelectric-bus.html> [Accessed 1 Mar. 2020].

[20] – Green Car Congress. (2020). Mercedes-Benz provides additional details on upcoming 12m electric Citaro bus. [online] Available at: <https://www.greencarcongress.com/2018/03/20180305-citaro.html> [Accessed 24 Feb. 2020].

[21] – Malpasairflow.co.uk. (2020). 12 inch Radiator / Air Conditioning Condenser Fans (12v) from SPAL Automotive | malpasAirflow.co.uk. [online] Available at: <https://www.malpasairflow.co.uk/s/c/spal-blowers-fans/axial-cooling-fans/12v-spal-radiator-condenser-fans/10-255mm-fans> [Accessed 3 Mar. 2020].

[22] – eBay. (2020). "FITS MAN M2000 (1994 - 2005) GRAYSONS RADIATOR ASSEMBLY RR-5214-000 | eBay. [online] Available at: <https://www.ebay.co.uk/i/174190041374> [Accessed 25 Feb. 2020].

[23] – Graysonts.com. (2020). [online] Available at: <https://www.graysonts.com/wp-content/uploads/2016/12/CV-Radiators-Brochure-REF-GL1034PG6K-Issue-1.pdf> [Accessed 25 Feb. 2020].

[24] – Graysonts.com. (2020). [online] Available at: <https://www.graysonts.com/wp-content/uploads/2016/12/Silicone-Hose-Brochure-REF-GL1030PG7-Issue-4.pdf> [Accessed 3 Mar. 2020].

Exterior Lighting

[25] – Learn.lboro.ac.uk. (2020). 19TTC101. [online] Available at: https://learn.lboro.ac.uk/pluginfile.php/190975/mod_resource/content/2/packaging_and_min_weight.pdf [Accessed 20 Feb. 2020].

Interior

[26] – Legislation.gov.uk. (2020). Public Service Vehicles Accessibility Regulations (Northern Ireland) 2003. [online] Available at: <http://www.legislation.gov.uk/nisr/2003/37/made> [Accessed 3 Mar. 2020].

[27] – Commercialhandrails.co.uk. (2020). Tube Bending, Tube Manipulation, Steel Fabrication Birmingham | Commercial Handrails. [online] Available at: <http://www.commercialhandrails.co.uk/our-services.html> [Accessed 3 Mar. 2020].

HVAC

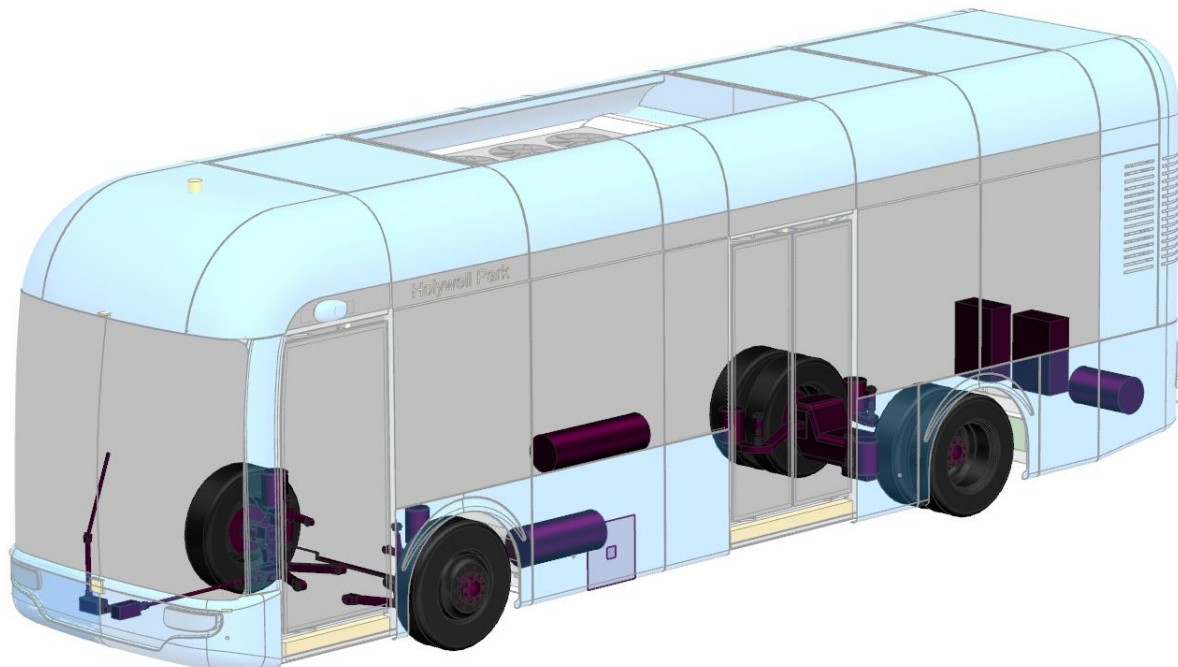
[28] – Bus and coach '96. (1996). London: Mechanical Engineering Publications for the Institution of Mechanical Engineers.

[29] – Kim, M., "A Numerical Analysis on the Optimum Distribution of an Air-Conditioning Duct with Multiple Outlets in a Medium Bus," SAE Technical Paper 2001-01-3330, 2001, <https://doi.org/10.4271/2001-01-3330>.

Vehicle Concept Definition and Design: Design Report

Section 3

Suspension, Braking, Wheel and Tyres



(s) Hugo Burston – B719796

Number of Pages: 25
Number of Words: 1996

Contents

3.1	System Specifications and Targets.....	54
3.2	Front Suspension Design.....	55
3.2.1	Kinematic Analysis	55
3.3	Rear Suspension Design	57
3.4	Force Analysis Front Suspension	58
3.4.1	Specification and Targets.....	58
3.4.2	Load Cases	58
3.4.3	Reaction Forces	59
3.5	Lower Wishbone Lightweighting	60
3.5.1	Targets and Specification.....	60
3.5.2	Load Definition	60
3.5.3	Material Selection.....	61
3.5.4	Shear Force and Bending Moments	62
3.5.5	Combined Stress Case	63
3.5.6	Deflection	63
3.5.7	Fatigue and Stress Concentration	63
3.6	Air Springs.....	64
3.6.1	Targets and Specification.....	64
3.6.2	Front Air Springs	65
3.6.3	Rear Air Springs	66
3.7	Dynamic Ride Analysis	67
3.7.1	Specification and Targets.....	67
3.7.2	Chassis Roll and Stiffness	67
3.7.3	Rollover Acceleration	67
3.7.4	Quarter Car Model - Damping.....	68
3.7.5	Half Car Model	69
3.8	Steering System.....	70
3.9	Braking and Pneumatic System.....	71
3.10	Cost.....	72
3.11	Appendix	73
3.11.1	Appendix 1 Lateral Weight Transfer.....	73
3.11.2	Appendix 2 Multibody Force Magnitudes	73
3.11.3	Appendix 3 Minimum Weight Design Calculations	73
3.11.4	Appendix 4 Chassis Roll and Stiffness [1]	74
3.11.5	Appendix 5 Pneumatic Calculations.....	75
3.12	References	76

3.1 Introduction

This report serves as a development to the subsystems discussed in the concept report, creating a more complete design that can be guided towards production.

3.2 System Specifications and Targets

Table 3A – Global system targets

Code	Global Design Target	Achieved	Justification
G1	Suspension components must withstand all load cases.	Yes	Detailed load cases have been calculated and a sufficient safety factor chosen. Section 3.6 shows an example of the approach to component design according to maximum load cases.
G2	Safe and efficient pneumatic control system.	Yes	Reservoir size accounts for pneumatic demands minimising the frequency of re-pressurising. The established control system ensures efficient operation with failsafe systems.
G3	Maximise passenger comfort	Yes	Implementation of semi-active suspension enables ride characteristics to be optimised through model tuning (3.7.4-5). Kinematic design further complements this with low roll centre moment arms and high levels of anti-dive.
G4	Ensure the floor height during operation does not exceed 400mm	Yes	The spring height at static laden results in a ride height of 200mm and a floor height of 350mm. Springs are selected with no facility for excess travel to improve packaging.
G5	Capabilities to enhance the un/loading of passengers	Yes	Kneeling is facilitated by the air suspension, increasing the efficiency of passenger loading.
G6	Vehicle braking performance should be adequate and suspension must cope with induced loading and pitching.	Yes	Calculated values in concept report show braking distances are sufficient for service and parking. Spring selection is designed for pressures experienced under maximum front end loading with pressure relief valves as a failsafe.

Table 3B – Global system parameters

Parameter	Value
Total Mass (Inc 1.625 Passenger SF)	16021 kg
Sprung Mass (Inc. 1.625 Passenger SF)	14226 kg
Sprung Mass (Exc. 1.625 Passenger SF)	12112 kg
Tyre Size	275/70 R22.5
Loaded Weight Distribution (F:R)	(38:62)
Loaded C.o.M. Height	1.31 m

3.3 Front Suspension Design

3.3.1 Kinematic Analysis

A developed suspension design proposal from the concept stage defines the kinematics, hardpoints and force analysis for the front suspension system.

Table 3C – Kinematic suspension targets

Code	Design Target	Action
K1	All control arms should have full range of movement whilst not compromising passenger space.	Refer to packaging model for hardpoint and design volumes, making design adjustment to balance geometric performance and packaging requirements.
K2	Required suspension travel of 150mm in bump to allow for kneeling during passenger loading.	Ensure acceptable suspension characteristics at full bump, and full articulation is allowed.
K3	Suspension should have good returnability and steer characteristics. Steering articulation should be maintained.	Consideration of mechanical trail, KPI and caster angle to influence steering returnability. Ensuring outer hardpoints are not intrusive on steering articulation. Alter upright to utilise the KPI/caster characteristics.
K4	Anti-dive should be considered to reduce the pitching moment.	Analysis of the inner wishbone pivot axes and pitch to ensure vertical loading is transmitted to the chassis.

Given the low-speed, predictable nature of the application, priorities lie with packaging and functionality rather optimising for performance. Packaging parameters such as the volumes in which hardpoints can exist are defined from the packaging CAD model to ensure no geometric interference (K1). Tuning of the suspension kinematics to obtain favourable characteristics was carried out resulting in the geometry shown in Figure 3A.

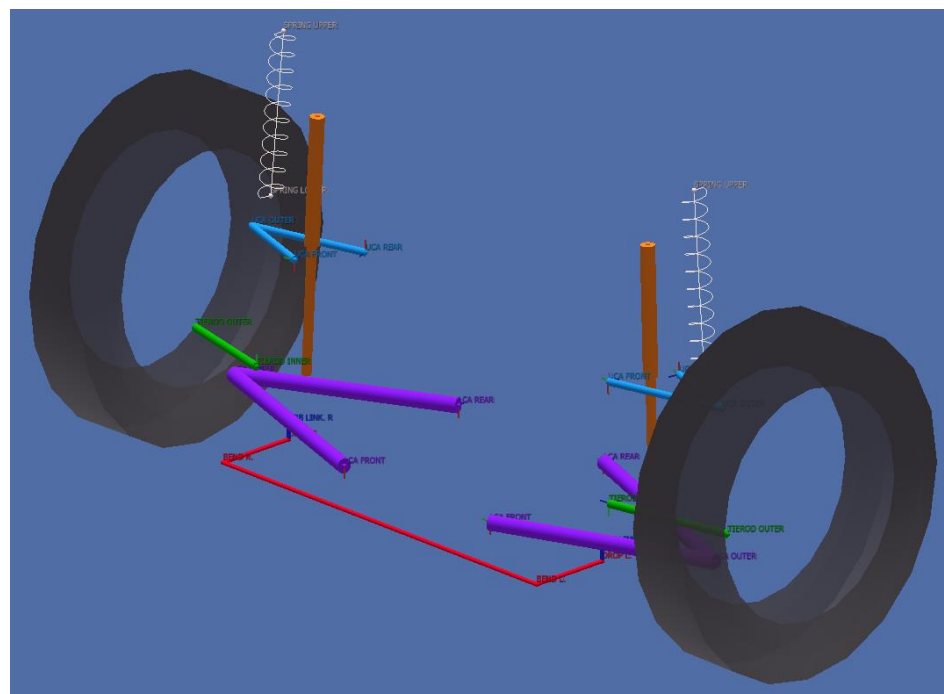


Figure 3A – Front Suspension Geometry

Table 3D – Front suspension kinematic characteristics

Characteristic	Achieved Value	Explanation
Anti-Dive	39% at static see fig 3C1	<ul style="list-style-type: none"> Pitch of revolute wishbone joints creates an angle between IC and ground plane, determining the proportion of normal force transferred through the control arms directly to the chassis. Ultimate reduction of pitching motion due to reduced spring compression. (K4)
Camber	0 degrees at static see fig 3C2	<ul style="list-style-type: none"> Compromise made between camber change and other characteristics due to tight packaging constraints of the upper wishbone. Despite this, as minimal wheel travel is expected during operation with low lateral accelerations, camber is not of great importance.
Roll Centre Height	2mm at static see fig 3C3	<ul style="list-style-type: none"> To minimise roll torque, reduction of distance between roll and mass centres is preferable. Due to the low floor and packaging restraints, the location of the roll centre is far from ideal. It is found in section 3.8 that the spring stiffness is sufficient to negate the effect of the low roll centre.
Bump Steer	1.5 degrees at static	<ul style="list-style-type: none"> 1.5 degrees of static toe in ensures the toe angle remains above zero for all wheel displacements, which is preferable for the front axle on a rear wheel drive vehicle. To minimise bump steer, the inner tie rod ball joint lies on the line connecting the instantaneous centre and the lower outer ball joint. (K3)
Motion Ratio	1.29 at static see fig 3C5	<ul style="list-style-type: none"> The motion ratio defines the relationship between contact patch load and spring load. The magnification has been reduced through the inclination of the spring to reduce loading as described in section 3.7. (K2)
KPI/Scrub Radius	3 degrees/ 212mm	<ul style="list-style-type: none"> Slight positive KPI promotes steering returnability. Large scrub radius resulting from large KPI offset, must be accounted for with EHPS. Minimal variation with bump, reducing lateral loading during kneeling. (K3)
Caster/ Mechanical Trail	6 degrees/ 53mm	<ul style="list-style-type: none"> Positive caster angle results in mechanical trail, providing steering returnability and straight-line stability, preferable for this application. (K3)

The upright design was adjusted from the concept to incorporate ball joints and the pitched KPI. This allows an increase in length of the lower wishbone, further allowing a more preferable scrub radius and KPI, reducing steering effort and improving returnability. [1] An anti-roll bar was introduced between the lower front wishbones for added roll stiffness as demonstrated in section 3.8.1. (K2/3)

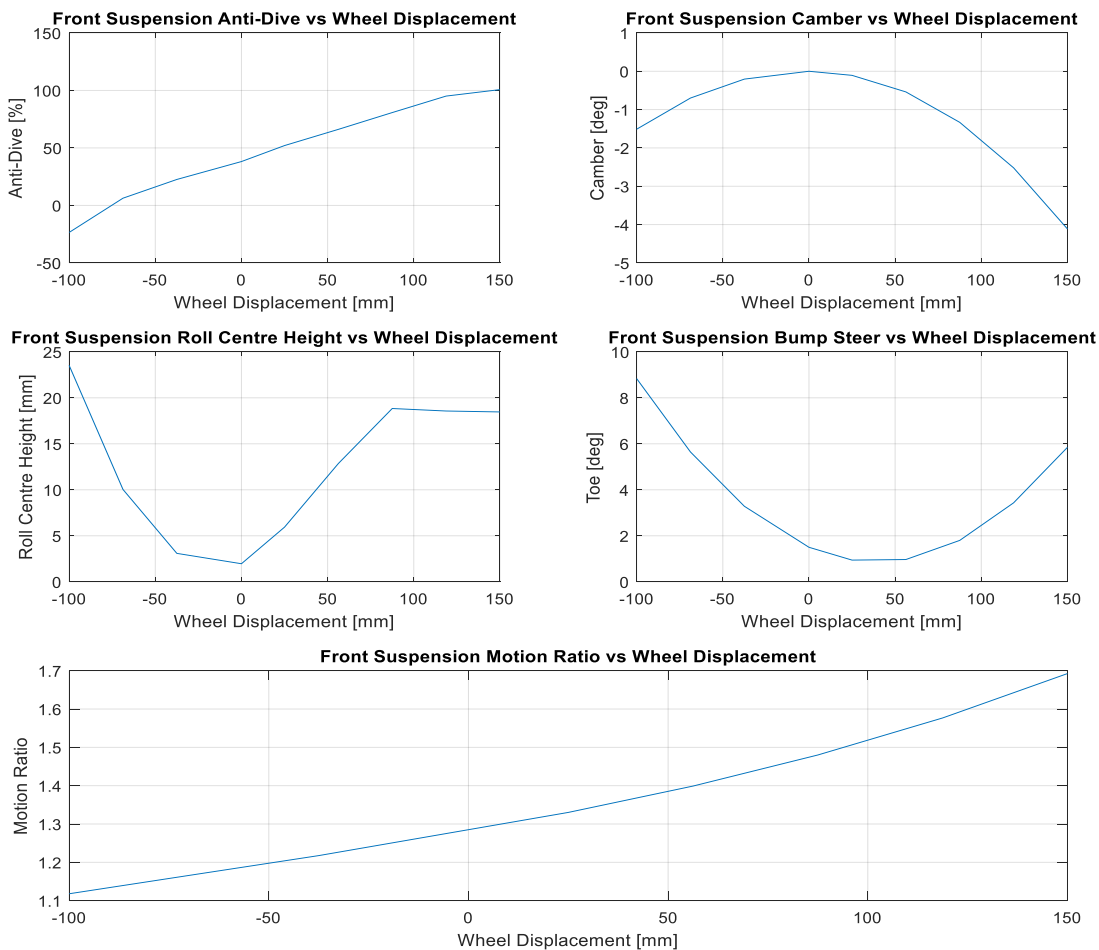


Figure 3B1-5 (Left to Right) - Front suspension geometry kinematic properties vs wheel displacement.

3.4 Rear Suspension Design

The rear suspension is a solid beam axle therefore has two degrees of freedom; in heave and roll. A four link design is commonly utilised for beam axles and provides four degrees of restraint. Figure 3C1 displays the final geometry of the four link rear axle in which similar kinematic analysis is carried out. [1] The roll centre height is 384mm.

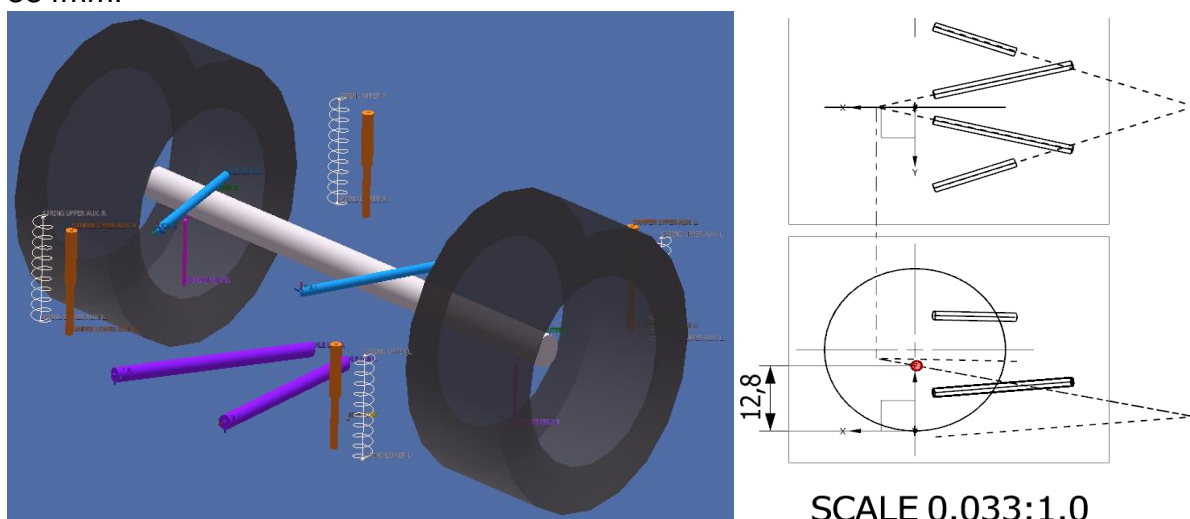


Figure 3C1 – Left - Rear Suspension Geometry – 3C2 Right – Roll Centre Height

3.5 Force Analysis Front Suspension

3.5.1 Specification and Targets

Analysis of the forces in the front suspension control arms for various load cases is carried out for stress analysis.

Table 3E – Suspension force analysis design targets

Code	Design Target	Action
F1	It must be ensured representative load cases are used to simulate real loading conditions.	Use quarter car models and kerb strike research to define an accurate extreme loading case.
F2	A range of load cases should be considered	This ensures all extreme eventualities are considered and no abnormal loading cases exist.
F3	A multibody analysis approach should be used	A multibody force moment balance allows all forces in all members to be determined for future analysis.

3.5.2 Load Cases

Forces induced at the contact patch in the single vertical degree of freedom are reacted by the spring, while longitudinal and transverse forces are reacted by the bushes and control arms. Although exists some minor axial torques on the control arms, these will be negligible in comparison to the tensile loads, hence are ignored and accounted for with a safety factor. Table 3F considers potential load cases.

Experimental data of top mount forces from a 135mm kerb strike at 40km/h using a Ford Galaxy peak at 43000N [2] (F1), corresponding to approximately 6g acceleration. Due to the increased compliance in the tyres of the bus, 4g peak acceleration is expected from a similar kerb strike event. Using the front quarter mass of the bus, this corresponds to an approximate vertical contact patch load of 120000N. Lateral weight transfer calculations are shown in appendix 3.12.1 [4].

Table 3F – Contact patch load vectors, with critical load cases highlighted (F2)

Load Case	Code	X [N]	Y [N]	Z [N]
Static Loading (Reference)	STA	0	0	29860
Maximum Acceleration (0.11g)	ACC	0	0	27780
Moderate Braking (0.4g)	MBR	14972	0	37430
Emergency Braking (1g)	EBR	48780	0	48780
Emergency Braking + Kerb	EBR + P	48780	0	168780
Maximum Lateral Acceleration (0.3g)	LACC	0	26140	7650

3.5.3 Reaction Forces

Reaction forces at all joints is calculated using a multi body force moment balance and solved via a matrix method [3], with results shown in appendix 3.12.2. (F3) This allows the x, y, z components of the reaction forces at the three lower wishbone links to be determined. Table 3G lists the forces calculated and notation used. Table 3G displays the global force vectors for the three reaction forces of the lower wishbone for use in lightweighting.

Table 3G – Resultant force vectors at lower wishbone hardpoints and upright joint

Force	STA (N)			MBR (N)			EBR+P (N)		
	X	Y	Z	X	Y	Z	X	Y	Z
FE21	-4070	10570	-330	36260	40810	5210	19900	83300	3880
FF21	-50	22920	370	140	-68360	-1120	-50	23750	390
FG24	4120	-33490	-40	-36400	27550	-4090	-19850	-107000	-4270

There is little reaction force in the z direction as the majority of this force is reacted by the vertical spring component, calculated from f2 and the spring direction vector. The sum of the above columns equals zero, confirming the validity of the approach

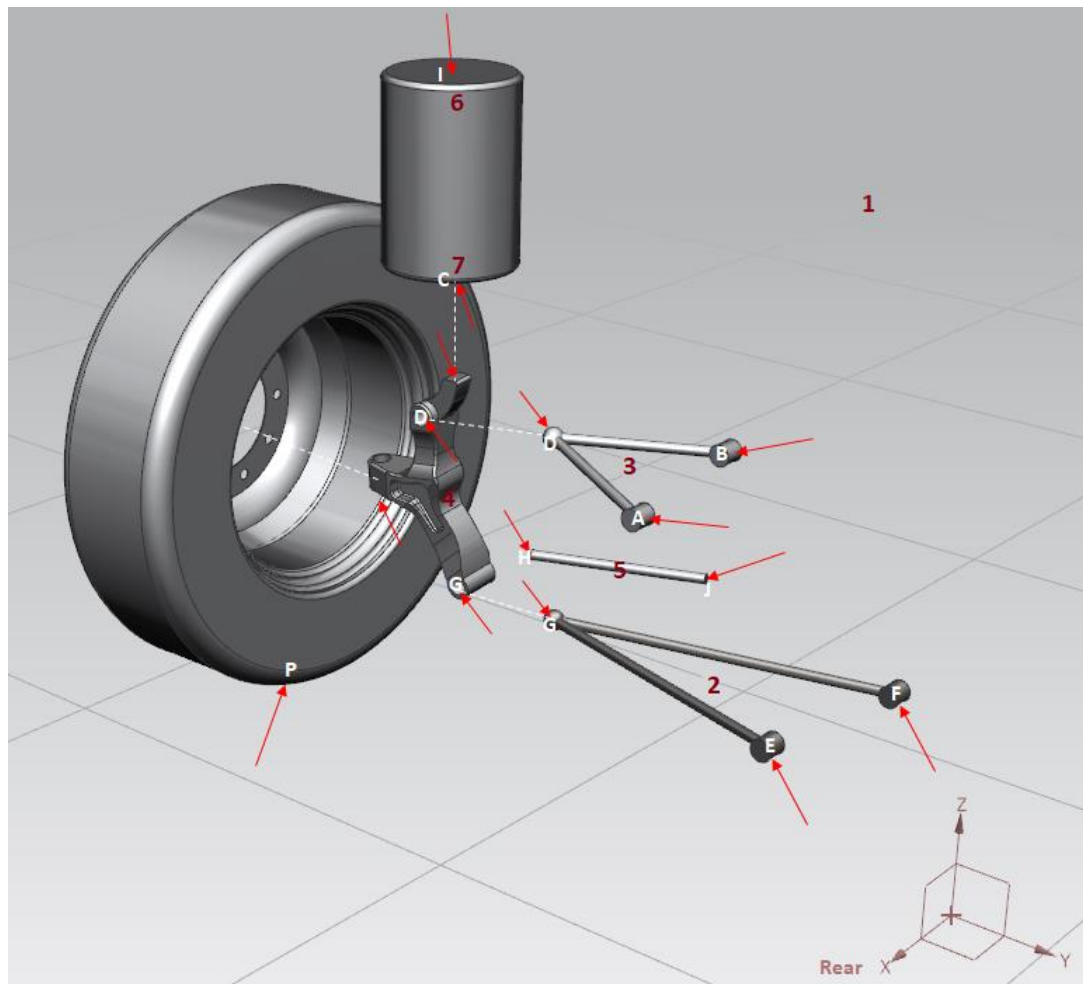


Figure 3D – Exploded drawing showing bodies and forces considered in multibody analysis.

3.6 Lower Wishbone Lightweighting

3.6.1 Targets and Specification

Table 3H – Lower wishbone design specification and targets.

Code	Design Target	Action
LW1	The wishbone must withstand all load cases within a reasonable margin.	Calculation of the magnitude of the forces experienced during a range of load cases in sections 3.4 ensures this target is met and use of a conservative safety factor.
LW2	An appropriate material and manufacturing method should be selected.	Selection should be made simultaneously alongside stress analysis as certain manufacturing methods may result in residual stresses.
LW3	A safety factor of 1.75 should be enforced with the design of all critical suspension components.	This ensures kerb strikes and abnormal loading conditions are accounted for, and that simplifications in the analysis shall not be critical.
LW4	Control arms should be sufficiently stiff as not to have an impact on suspension characteristics.	Analysis of the deflection according to Euler's beam theory should be carried out. Large deflections causing damage to the bushes are unacceptable

3.6.2 Load Definition

The critical load cases considered are ERB, ERB+P and LACC (table 3F). The focus of the lightweighting is in the main profile of the control arm, as the joints require further FEA. Table 3I shows the axial and transverse forces experienced in the control arms.

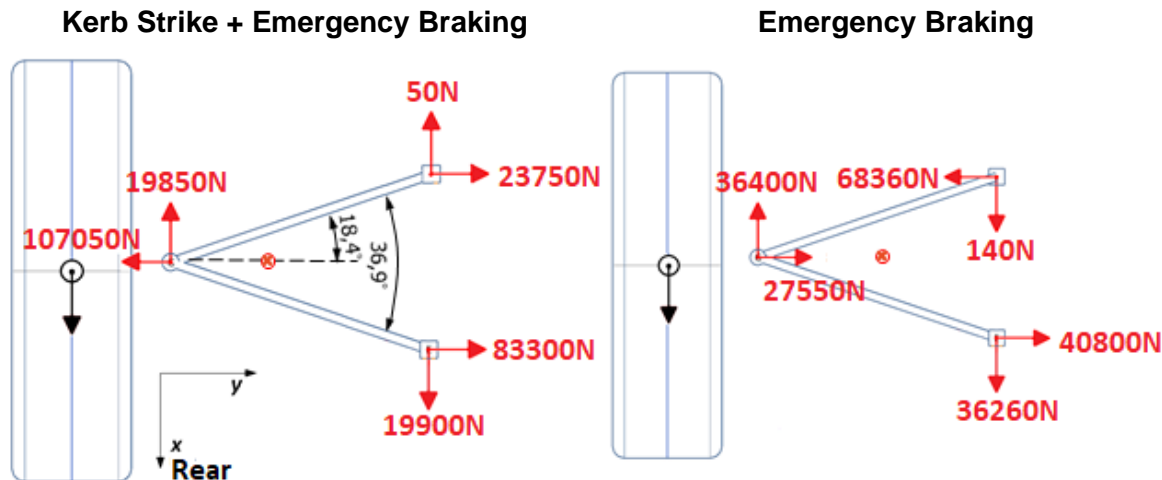


Figure 3E – Diagram of the magnitude of forces in the global coordinate system on the lower wishbone

The forces shown in table 3I are obtained through resolving the x y z forces along the length of the arms. The kerb strike loads are considered as steady state – in transient shock loading they may reach higher values; however this will be accounted for in the safety factor.

Table 3I – Lower wishbone forces with respect to the longitudinal/transverse coordinate system at the upright end

	Front Wishbone Axial (N)	Front Wishbone Transverse (N)	Rear Wishbone Axial (N)	Rear Wishbone Transverse (N)
KS + Braking	22550 (Tensile)	7450	85323 (Tensile)	7410
Braking (1g)	64810 (Compressive)	21445	50160 (Tensile)	21530
Cornering (0.3g)	3110 (Compressive)	1040	7847 (Compressive)	1020

Some force shall be transmitted via the damper mounting point, reacted by the hardpoints. A kerb strike of 50mm with a damping ratio of 0.4 (30000 Ns/m) is considered whilst experiencing -1G braking, such that the pitching moment and upwards movement of the wheel provide maximum front loading and relative damper speed. Utilising the half car model, the damper experiences a peak relative velocity of 2.6m/s (figure 3F), resulting in a vertical force at the damper link of 78000N. The minor pitch of the inner hardpoints in Z is neglected for simplicity.

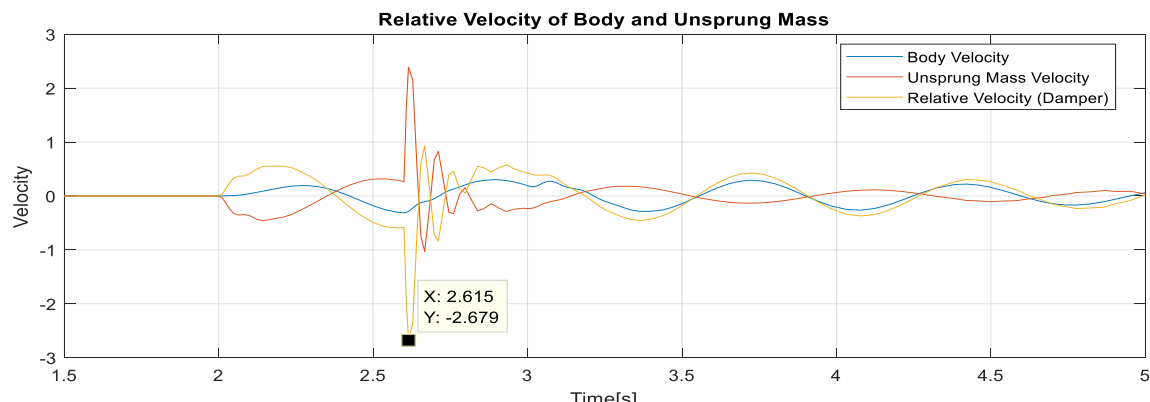


Figure 3F – Damper relative velocity during kerb strike and heavy braking

3.6.3 Material Selection

A selection of common materials used in wishbone and suspension components is shown in table 3J. [6],[7],[8]

Table 3J – Properties of viable material choices

Material	Yield [MPa]	E [GPa]	G [GPa]	Fatigue Strength at 10^7 cycles [MPa]	Density [kg/m^3]	Price [GBP/kg]	Part Weight [kg]
Low Carbon Steel AISI 1018	386	200	80	240MPa	7800	0.59	29.55
Low Alloy Steel AISI 4130	460+	210	80	280MPa	7850	0.65	29.74
Cast Iron (ductile)	440	175	67	255MPa	7100	0.27	26.90
Al Alloy (2000/7000)	380	72	30	160MPa	2700	1.97	10.23
Titanium Alloy	1100MPa	115	42	535MPa	4600	18	17.43

Titanium alloy has been selected for the wishbones. Design using steels and aluminium alloys under high loads results in the necessity for large section profiles – unsuitable for a tight packaging application. Therefore, titanium alloy is used (as in benchmarked systems) to obtain a smaller section. A safety factor of 1.75 is chosen, combined with the passenger loading safety factor, as larger kerb strikes at a varying oncoming angles and severities may result in larger load cases. Investment casting is the most suitable manufacturing method, without the requirement for expensive moulds or processes. Reasonably high tolerances can be achieved as well as a good surface finish, eliminating the need for post processing and reducing the likelihood of crack formation from fatigue.[8] (LW2)

3.6.4 Shear Force and Bending Moments

The two transverse bending load cases are analysed as shown in figures 3G(1-2), with supporting calculations in appendix 3.12.3. The shear force/bending moment diagrams are shown in figure 3I(1-2). The resultant bending moment is more significant by a factor of 2.4 in the X'Y' plane compared to the Y'Z plane, therefore a profile with a higher second moment of area in that plane should be chosen. An I beam is the most suitable for this application, as there is also no torsional loading considered. Typical control arms in this application have surface machined/forged channels derived from topological optimisation, therefore an I section replicates this in anticipation for further FEA. The profile section chosen and geometric properties are shown in figure 3H, with supporting calculations in appendix 3.12.3.

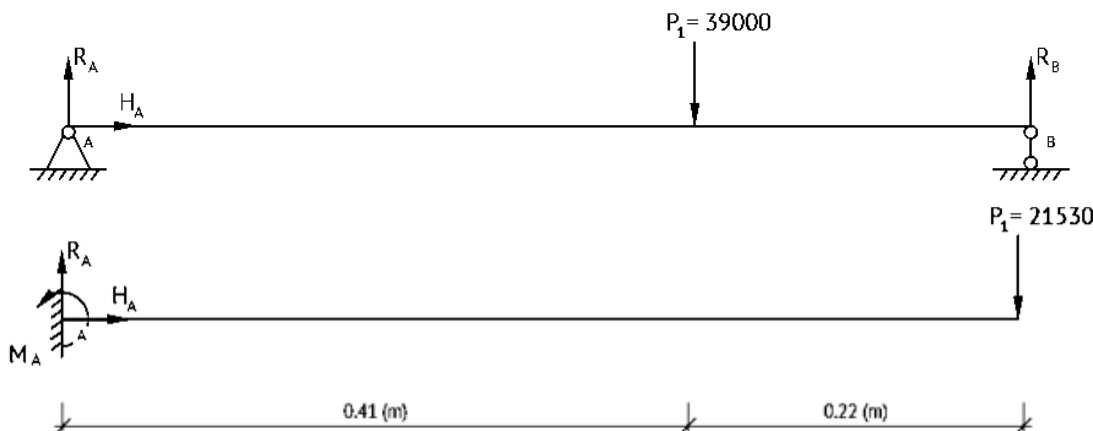


Figure 3G(1-2) – Euler beam bending diagrams showing the point loading conditions in Y'Z (top) and X'Y (bottom) planes for the rear control arm. Front arm load case in X'Y is near identical so only one analysis is carried out in bending.

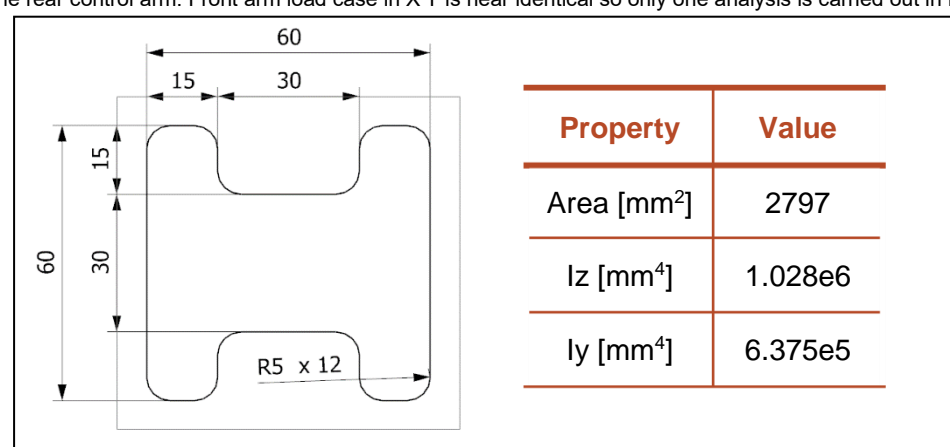


Figure 3H – Section profile of control arm and section properties.

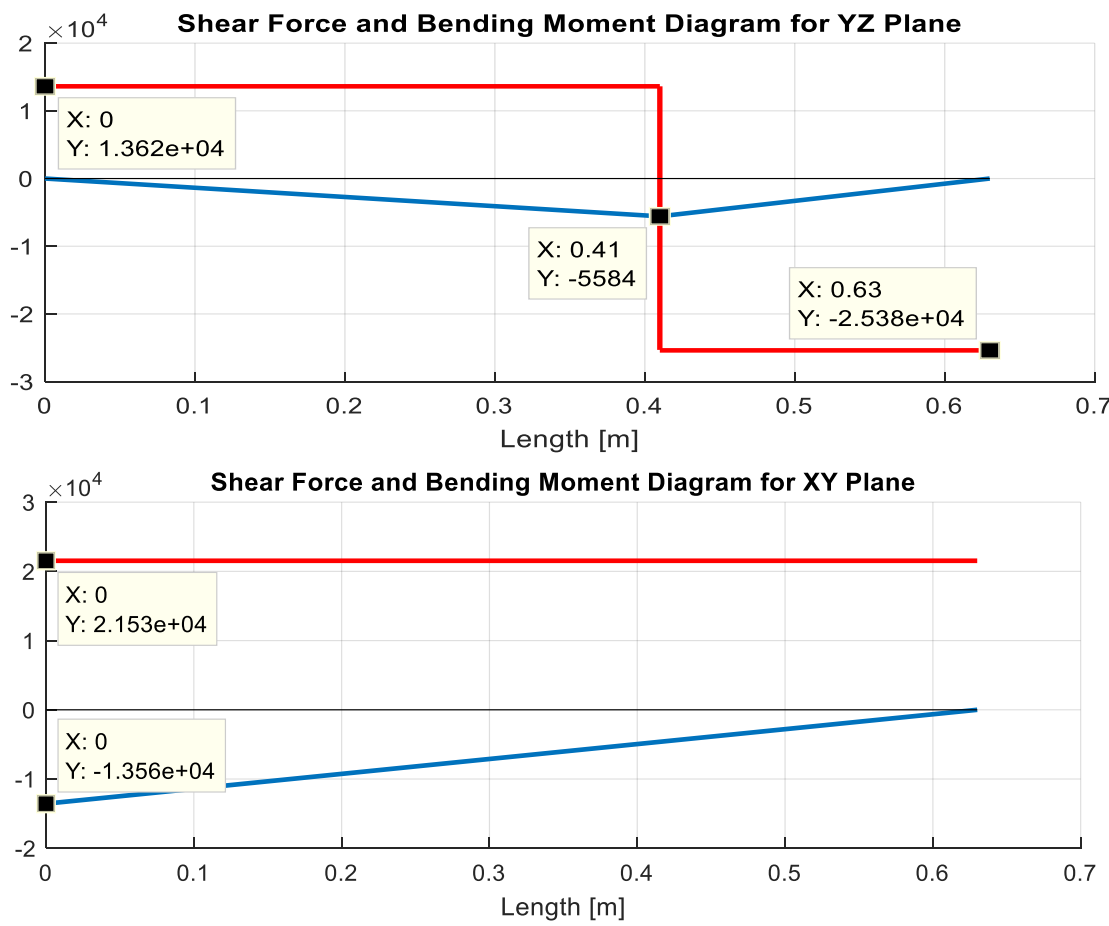


Figure 3I(1-2) – SF/BM diagrams for loading conditions in Y'Z (top) and X'Y (bottom) planes. Shear force is shown in red in N and bending moment in blue in Nm.

3.6.5 Combined Stress Case

Calculations in appendix 3.12.3 determine the maximum individual stresses experienced along the beam. The combined maximum axial stresses are summarised in Table 3K. (LW1/3)

Table 3K – Combined axial stresses in both load cases.

Braking + Kerb Strike Combined Axial Stresses		
Member	Axial Stress [MPa]	Safety Factor - (inc. Passenger Load Safety Factor)
Front Control Arm	635.5	1.57 (1.96)
Rear Control Arm	689.2	1.45 (1.81)

3.6.6 Deflection

Using Euler's beam theory, the tip deflection of the beam in the XY plane can be estimated with $\delta = \frac{PL^3}{3EI} = \frac{21530 \cdot 0.63^3}{3 \cdot 1115 \times 10^9 \cdot 10285 \times 10^{-6}} = 0.0152m$. This is deemed sufficiently small to be mostly accounted for by the compliance in the rubber bushes. (LW4)

3.6.7 Fatigue and Stress Concentration

Fatigue loading is defined by white noise road input and the resultant assumed cyclic stress case in the wishbone. The resultant stresses from small road displacements are assumed the peak cyclic load, providing a resultant combined maximum stress depending on the road surface. In most cases, this is far below the endurance

strength for titanium - 529MPa, hence fatigue is not a major consideration. Stress concentration factors such as those associated with sharp edges have been negated with fileted edges.

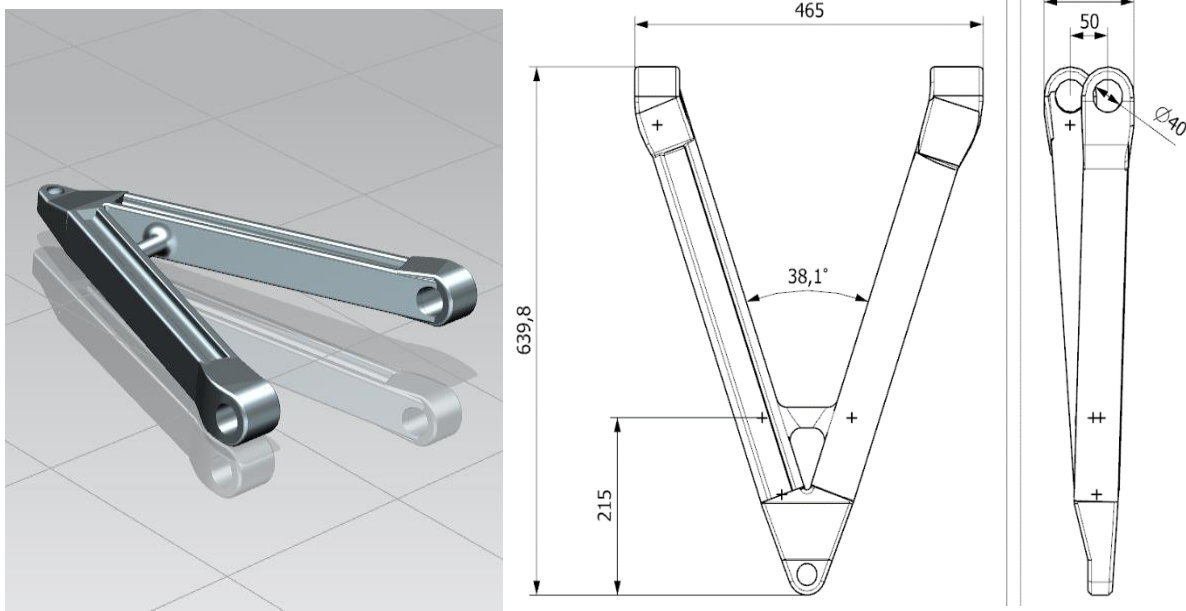


Figure 3J – Final lower wishbone design after designing for minimum weight.

3.7 Air Springs

3.7.1 Targets and Specification

Table 3L – Air spring design targets and specification.

Code	Design Target	Action
AS1	The springs must be able to withstand the maximum loads experienced during static and dynamic braking.	Selection of the springs is to be made with reference to tables 3L/M to ensure failure is avoided. The use of blow off valves increases loading capacity during extreme cases.
AS2	The springs must provide sufficient stiffness	The resultant spring stiffness should align with benchmarked values of current buses and should be sufficiently stiff to avoid large deflections.
AS3	The springs must allow for ride height adjustment and kneeling	An inherent property of air springs is the ability to vary ride height and stiffness dependent on sprung load and should be utilised accordingly.

The initial selection of air springs is dependent on the static load case of the bus, packaging requirements and kneeling stroke. The Firestone Airstroke 352 [5] is found to be the most suitable spring when considering the maximum front and rear static laden weights. (AS1) The equation for spring stiffness [5] is as follows:

$$K_s = \left[(P_g + 14.7) \left((A_c) \left(\frac{V_1}{V_c} \right)^{1.38} - (A_e) \left(\frac{V_1}{V_e} \right)^{1.38} \right) - 14.7(A_c - A_e) \right]$$

P_g = Pressure at DH, A_c = Eff. Area at $\frac{1}{2}$ inch below DH, V_1 = Internal volume at DH, V_C = Internal Volume $\frac{1}{2}$ inch below DH A_e = Eff. Area $\frac{1}{2}$ inch above DH, V_e = Internal volume $\frac{1}{2}$ inch above DH. Where DH = design height.

An active air system will vary internal pressure and therefore K_s as deemed appropriate to attempt to maintain constant ride height. The approach of spring limits triggers a release in pressure through blow off valves. Following this, tables 3L/M show estimated front and rear spring forces.

3.7.2 Front Air Springs

Spring 352 provides the following stiffness at an 11inch design height at 80 PSI [5], able to sustain front static loading of 26516N (5960lbs).

$$K_S = \left[(80 + 14.7) \left(\left(\frac{6250}{80} \right) \left(\frac{975}{940} \right)^{1.38} - \left(\frac{5750}{80} \right) \left(\frac{975}{1150} \right)^{1.38} \right) - 14.7 \left(\frac{6250 - 5750}{80} \right) \right]$$

$$K_S = 397000N/m - \text{Assumed constant. (AS2)}$$

The longitudinal weight transfer is used in a rearranged spring stiffness equation to obtain the wheel deflection for the respective load case. This then allows the current motion ratio to be obtained from figure X, hence the spring force can then be calculated. Only the increase in normal contact patch force due to weight transfer that is to be experienced by the spring i.e. $N1^*(1-ADR)$ shall be considered. The static laden sprung mass of 14226kg is used. (AS1)

Using the equation for spring rate:

$$K_S = K_W R^2 + S \frac{dR}{dx} \rightarrow \text{Substituting } K_W = \frac{W}{X} \text{ and } S = RW: \rightarrow K_S = \frac{W}{X} R(X)^2 + R(X)W \frac{dR}{dx}$$

From figure 3B1 we obtain the equation for R in terms of X: $R = 4.1957x^2 + 1.7801x + 1.3023$

Hence, $\frac{dR}{dx} = 8.3914X + 1.7801$, and substituting this into the above equation:

$$K_S = W \left(\frac{(4.20X^2 + 1.78X + 1.30)^2}{X} + (4.20X^2 + 1.78X + 1.30)(8.39X + 1.78) \right)$$

The variation of anti-dive with respect to wheel travel in the region of interest can be expressed by the linear equation $AD = 4.729x + 0.3934$. Subsequently, this can be substituted into an equation for the wheel force, $W = \frac{PZh}{2E}(1 - AD\%)$.

Table 3L – Front spring loading forces for varying load cases

Load Case Transfer	Wheel Force [N]	Approximate Wheel Displacement [mm]	% Anti Dive	Wheel Force (PZh/2E inc. Anti dive) [N]	Motion Ratio	Spring Force [N]	Cumulative Spring Force [N]
Base (Sprung Mass)	26516	0	39	26516	1.3	34470	34470
Normal Braking (0.19g)	+ 3463	8.6	43	1960	1.32	1826	37000
Moderate Braking (0.45g)	+ 8204	19.5	49	4220	1.34	4424	40100
Emergency Braking (1g)	+ 18230	38.9	58	7710	1.38	10570	45040
Kerb Strike	+ 120000	110	91	10800	1.45	15660	50130
Braking Kerb Strike	+ 138230	112	92	11060	1.53	16920	60360

Anti-dive values are purely theoretical. Transient forces will be transmitted before the spring can deflect fully and the analytical amount of anti-dive achieved, hence in reality bump stops may be reached during braking kerb strike.

Further analysis with the quarter car model provides top mount force. A kerb strike of 7cm yields a 600m/s^2 acceleration for the 200kg unsprung mass, corresponding to a 120000N contact patch load. Using the quarter front sprung mass of 3040kg and acceleration peak of 27m/s^2 , an additional top mount force of 82000N is experienced. This is greater than the calculated spring force because this entirely disregards anti effects, which is likely more accurate and conservative considering the transient nature of the kerb strike. (AS1)

3.7.3 Rear Air Springs

The static sprung weight to be sustained by one rear corner of the bus is 43600N, therefore 21800N per spring (4900lbs). 80 PSI and 12 inches design height provides sufficient force at static laden [5]. The stiffness of one spring at static laden is 372000 N/ms however as the two springs are orientated in parallel, the resultant corner spring rate is 744000 N/m. (AS2)

Table 3M – Rear spring loading forces for varying load cases

Load Case Transfer	Added Wheel Force per Spring (PZh/4E) [N]	Motion Ratio	Spring Force [N]	Cumulative Spring Force [N]
Base (Sprung Mass)	21800	1.14	21800	21800
Acceleration (0.11g)	$315 \times 0.95 = 300$	1.14	342	22142
Kerb Strike	$20000 \times 0.95 = 19000$	1.14	21660	43460

In bump scenarios, the suspension ratio is 1:1, however in roll situations, the suspension ratio 1:1.14 due to the 2DOF, calculated from the ratio between rear track and lateral distance between the springs resulting in a higher spring force, hence this shall be used for spring force calculation. A relatively constant 5% anti-dive is achieved with this geometry. (AS1)

3.8 Dynamic Ride Analysis

3.8.1 Specification and Targets

Table 3N – Dynamic ride and handling specification and targets

Code	Design Target	Action
DR1	Sufficient roll stiffness should be achieved to reduce body roll.	Calculation of front and rear roll stiffnesses shall ultimately allow the tuning for reduction nauseating roll motions.
DR2	Provisional optimal damping ratios for certain events should be determined	This is achieved through quarter car model analysis providing boundary values for a semi-active damper controller.
DR3	Natural frequencies should be identified for further tuning capabilities	Obtained through half car model analysis. Further identification of the implications of heavy braking and road displacements on the sprung body motion.

3.8.2 Chassis Roll and Stiffness

Chassis stiffness and roll calculations shown in appendix 3.12.4 are summarised in table 3O. This allows rollover acceleration and lateral acceleration values to be determined. A 60mm tubular anti-roll bar is introduced for the front suspension to improve roll stiffness. (DR1)

Table 3O – Rear spring loading forces for varying load cases

	Roll Stiffness (Nm/deg)	Roll Torque (0.3G LatAcc) (Nm)	Roll Angle (Degrees)
Front	12850	22300	1.87
Rear	15700	26800	1.71

This results in a total body roll stiffness of 28550Nm/degree.

3.8.3 Rollover Acceleration

A relatively accurate estimation of critical steady state cornering can be achieved by a quasi-static model by Guillespe [10]. This requires the conversion of roll stiffness from 28550 Nm/degree to 0.194 radian/g of lateral acceleration. h_r is height of roll axis at centre of gravity.

$$\frac{a_y}{g} = \frac{t}{2h} \frac{1}{\left[1 + R_\phi \left(1 - \frac{h_r}{h}\right)\right]} = \frac{2.175}{(2)(1.31)} \frac{1}{\left[1 + 0.194 \left(\frac{0.217}{1.31}\right)\right]} = 0.80g$$

3.8.4 Quarter Car Model - Damping

A quarter car model was constructed with the spring rates defined in table 3P [15]. Using state space representation, the frequency responses of the sprung and unsprung masses could be obtained. This is shown in the bode plot figure 3K(1-2), which displays the attenuation of different frequencies at different damping ratios. (DR2)

Table 3P – Rear spring loading forces for varying load cases

Front Spring Rate	397000 N/m	Rear Spring Rate	328000 N/m
Front Wheel Rate	1700000 N/m	Rear Wheel Rate	3400000 N/m
Front Body Bounce Rate	321840 N/m	Rear Body Bounce Rate	299140 N/m

The bode plot indicates the natural frequencies of the front suspension. It is important the gain is reduced in these areas by tuning the damping ratio whilst also functioning as intended – to minimise the transient oscillation and dissipate energy from the road springs, as shown in figure 3K(3) from a simulated kerb strike step input of 50mm. This information can be used to design a semi-active damping controller, with an identical analysis carried out for the rear axle. (DR3)

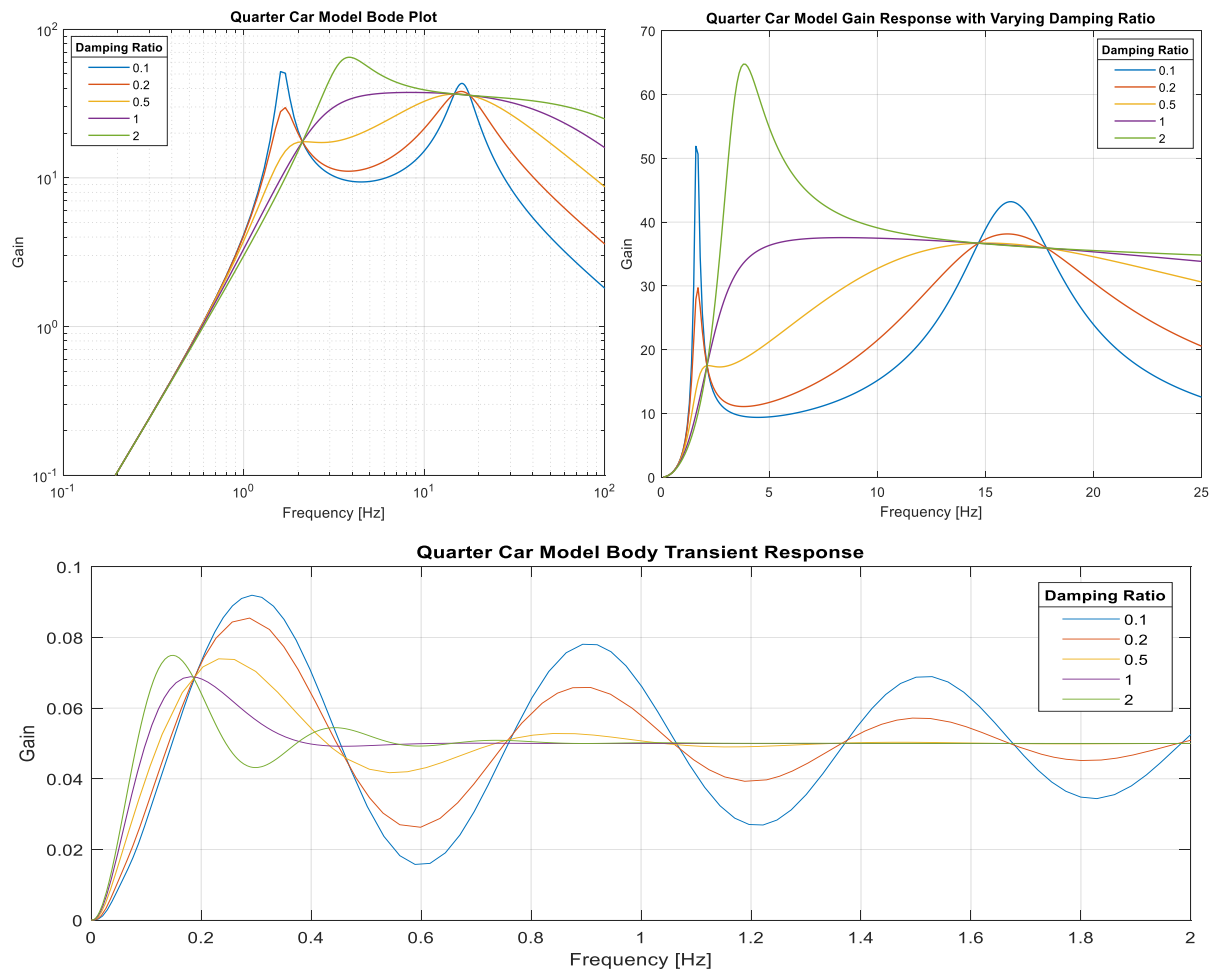


Figure 3K(1-3) – Bode plots of quarter car model response and transient oscillatory response for front suspension

Table 3Q – Range of optimal damping ratios for varying input frequencies (DR2)

Road Frequency	Amplitude	Optimal Damping Rate	Notes
Low (0.5-1.5Hz)	Large	0.4 - 0.5	Ensures the oscillatory decay is transient and would hence be used for large kerb strikes, also providing minimal gain for body bounce.
Medium (3-7Hz)	Medium	0.1	Reduces passenger discomfort. The visceral acceleration should be minimised, achieved by reducing the gain in this range. Visceral natural frequencies are found to be in the range of 4-6Hz.
Large (13-19Hz)	Low	0.7 - 0.8	White noise inputs are in line with the wheel hop natural frequency. This is harder to dampen; however a higher damping rate is more successful, despite the potential of stiff ride dynamics.

Semi adjustable dampers are to be employed on the vehicle to optimise ride response and contribute to anti-effects. Suppliers such as ZF [11] are readily producing effective semi-active dampers utilising this theory, which shall be employed in this application. An onboard IMU will detect pitching moments, whilst front and rear axle mounted IMU's and linear potentiometers will identify the oscillatory motion and adjust damping rates accordingly. (DR3) [12]

3.8.5 Half Car Model

Using the estimated optimal damping rate for body bounce (0.4) defined in the above section, analysis can be carried out for its effectiveness at reducing pitching oscillations with a half car model. A load case of the induced pitching of 1G deceleration shortly followed by a 50mm kerb strike is considered as the maximum load case. At 30mph the time between the two axles striking the kerb is 0.405s. In this case an increase in damping rate is required.

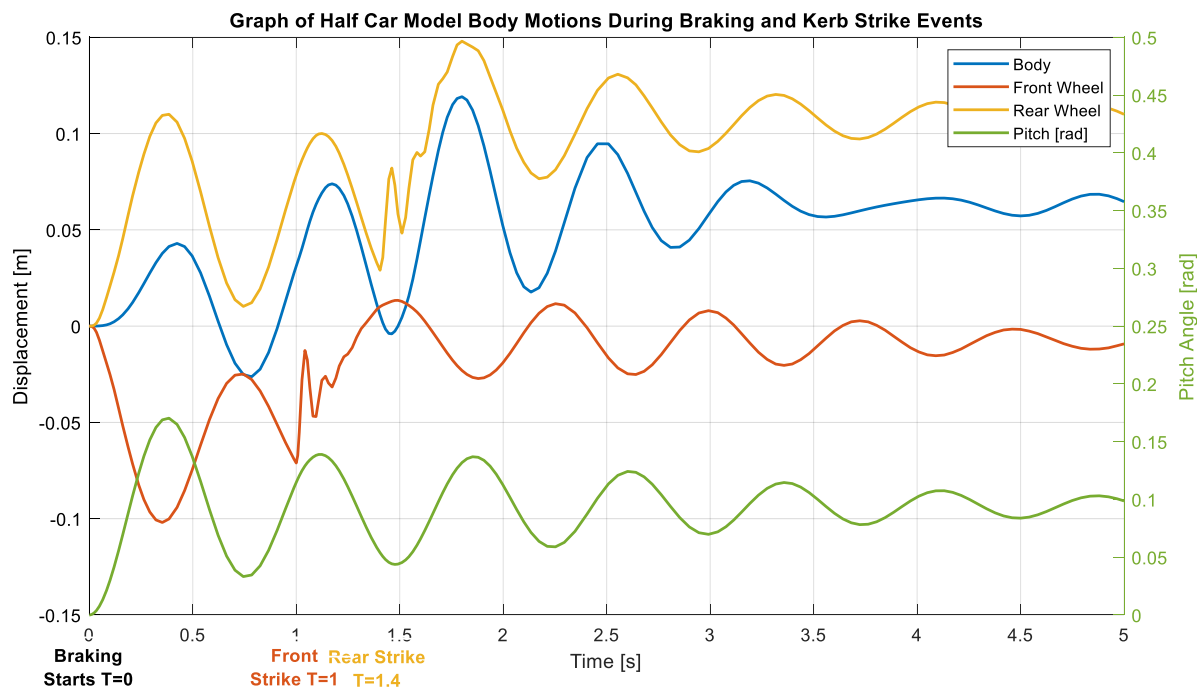


Figure 3K4 – Half Car model response for braking moment and kerb strike at 30mph with a 0.4 damping ratio

Calculating the eigenfrequencies from the state space transition matrix yields the following natural frequencies of the system: (DR3)

Figure 3R – Modes of the half car model system

Motion	Natural Frequency	Motion	Natural Frequency
Heave	1.58 Hz	Front Wheel Hop	11.31
Pitch	1.33 Hz	Rear Wheel Hop	9.18

3.9 Steering System

Table 3S – Steering system specification and targets

Code	Design Target	Action
S1	A suitable steering effort must be required by the driver.	Ensuring the EHPS is capable of reducing steering effort required to a level that shall not induce operator fatigue (when used).
S2	Minimal scrub should occur during steering.	This aids the reduction of steering effort and improves the longevity of tyres, increasing servicing/replacement intervals. 100% Ackermann.
S3	A steering radius of should be achieved with no geometric interference at maximum steer.	Rotating the knuckle and wheel assembly about the KPI to ensure no interference is necessary.

The components of the steering assembly are shown in table 3T with justifications found in the Concept Report.

Table 3T – Steering system assembly components

Component [13]	Weight (kg)	Characteristics
Bosch Steering Column	6.1	Provides a turning torque of <0.3Nm. Easily adjustable, with 82mm of height adjustment and 21 deg swivel angle.
Bosch Steering Shaft	Variable	Can retract and extend with 60N sliding friction dependent on steering wheel adjustability. 281mm – 3915mm installed length. 35 deg universal joint angle.
Bosch Bevel Box	2.2	1:1 transmission ratio able to turn drive through 90 degrees.
RB Servocom Steering Gear	41	Transmission ratio of 18, with maximum output torque of 8000Nm

Analysis of required steering effort is carried out to determine the steering gear model. These forces are about the equilibrium of zero steer.

$$\begin{aligned} \text{Torque}_{Wh} &= \text{Frictional Force} \cdot \text{Scrub Radius} = (16000)(9.81)(0.38)(0.5)(0.7)(0.212) \\ &= 4411\text{Nm} \end{aligned}$$

This torque must equal the torque applied by the tie rod.

$$4411\text{Nm} = (0.1298)(\text{Force}_{Tie}) \therefore \text{Force}_{Tie} = 33930\text{N}$$

The output torque of the steering gear is 8000Nm. Considering the Pitman arm:

$$Force_{Tie} \cdot L_{Pitman} = 8000 \therefore Force_{Tie} = \frac{8000}{0.222} = 36000N$$

Hence sufficient force is produced. A torque multiplication of 18 is installed in the steering gear, resulting in a shaft torque prior to the steering gear of:

$$Torque_{Shaft} = \frac{8000}{18} = 444Nm$$

An electronic steer assist module is installed in the steering column to assist torque production and control the autonomous steer driving and lane guidance. This has an effective low magnitude torque multiplication ratio of 20, resulting in a required driver input of 22Nm. With a steering wheel diameter of 540mm, this corresponds to a force input of 80N, or 40N per hand – within the typical 50N ergonomic limit. (S1)

Table 3U – Steering system assembly components

Final Parameter	Value
Ackermann	100% - The Ackermann geometry established in the Concept Report is retained as the steering linkages have not altered, based on the assumption of low operating speeds therefore minimal lateral scrub. (S2)
Turning Radius and Steer Angle	20316mm and 52 degrees – It was ensured these targets from the concept report were met through an efficient articulating upright and no geometric interference.
Steering Wheel Turning Force	80N – within a generally accepted 100N ergonomic limit (S1)
Steering Wheel Movement for Full Lock	For full steer the pitman arm must rotate through 20 degrees. Through a total gear multiplication of 38, this corresponds to 2.1 steering wheel rotations. (S2)

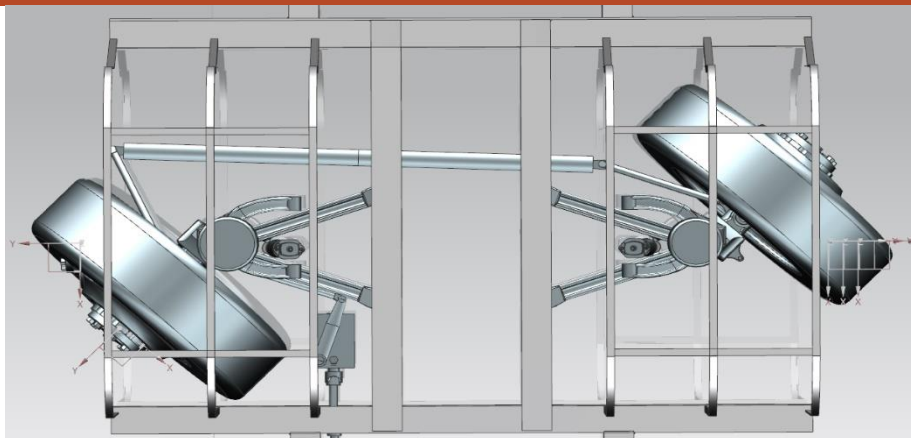


Figure 3L – CAD drawing of front suspension at max steer angle demonstrating no interaction (S3)

3.10 Braking and Pneumatic System

Table 3V – Braking and Pneumatic specifications and targets

Code	Design Target	Action
B1	Sufficient levels of deceleration available in an emergency event.	Ensure the brake assembly is capable of providing enough braking torque to generate sufficient deceleration.

B2	Braking system must meet legal requirements discussed in concept report.	The brakes must be applied in the event of a pressure loss, with sufficient chamber pressure to release if necessary.
B3	Pneumatic reservoirs must have sufficient volume and pressure for all systems and to avoid regular recompression	Analysis of required pressures of the brakes and springs will ensure reservoir size is sufficient

Based on the targets from the design and concept reports, and the calculations in appendix 3.12.5, the following components have been selected.

Table 3W – Braking and Pneumatic assembly components

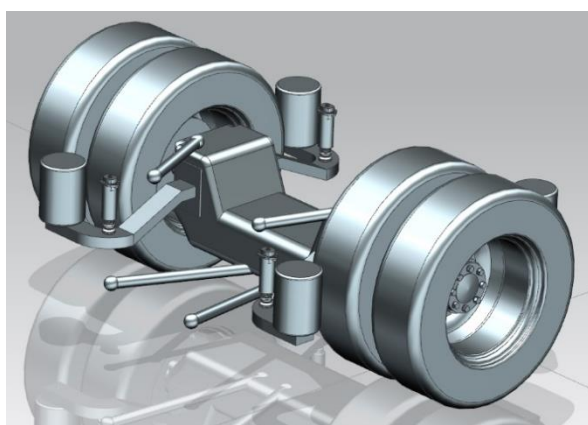
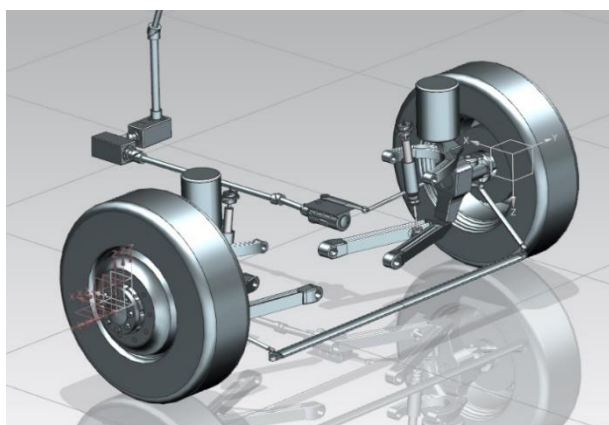
Component [14]	Characteristics
WABCO Ecomp	Maximum compression 181PSI at 220l/min. Designed for electric/hybrid bus usage. 4-14 kW power consumption.
WABCO Air Reservoirs (60 and 100 litres)	Capable of storage up to 275PSI. One reservoir per axle with dual circuit linkage; system can operate from one reservoir in the event of a pressure loss. (B2/3)
WABCO Type 24 brake chamber	Provides sufficient actuation force for the WABCO 24 callipers, with an internal diaphragm stroke of 1.3 litres. (B1)
WABCO Maxx 22 Air Brakes and Discs	Can provide a braking torque of 30,000Nm. With the type 24 brake chambers can provide the required braking torque of 23355Nm, shown in appendix 3.12.5.(B1)

3.11 Cost

Table 3X shows the costs associated with lower wishbone production/manufacturing for 20 units in year 1, whilst component costs are found in Section 1 of the report.

Table 3X – Estimated material and process costs

Material/Process	Cost per Unit [GBP]	Comments
Titanium Alloy Material Cost	313.74	Reasonable price considering the total cost of the bus and significance of the part
Investment Casting Process	350	Relatively low tooling costs over multiple runs, wax and ceramic being the only consumable to make expendable investment moulds.
Investment Casting Labour	500	The production time is approximately 7 days
Post Processing/Treatment	20	Application of anti-corrosive treatments to improve longevity of the component.
Rubber Bushes	8	Can be sourced externally from a wholesaler
Total	1191.74	



3.12 Appendix

3.12.1 Appendix 1 Lateral Weight Transfer

$$w_{tf} = \frac{C_F \theta}{t_f} + \frac{\text{Lateral}_F h_F}{t_f} + \frac{a_c m_f h_{uf}}{t_f}$$

$$M_s = 14325kg \quad M_F = 587kg \quad h_{uf} = 0.437m \quad h_f = 0.002m \quad h = 0.13m \quad C_F = 736kNm/rad$$

$$M_T = 16000g \quad M_R = 1088kg \quad h_{ur} = 0.55m \quad h_r = 0.384m \quad a_c = 0.3 \quad C_R = 900kNm/rad$$

Using system equivalence between total mass and un/sprung masses, taking moments about the ground plane with a lateral force applied:

$$h_s = \frac{M_T h - M_F h_{uf} - M_R h_{ur}}{M_s} = \frac{(16000)(1.3) - (587)(0.437) - (1088)(0.55)}{14325} = 1.39m$$

h' = distance of cog from roll axis

$$h' = h_s - \left(h_f + \frac{a_s}{E} (h_r - h_f) \right) = 1.41 - \left(0.002 + \frac{3.348}{5.4} (0.348 - 0.002) \right) = 1.17m$$

Under 0.3g lateral acceleration:

$$\theta = \frac{M_s a_c h'}{C_F + C_R - M_s g h'} = \frac{(14325)(0.3)(9.81)(1.17)}{736000 + 1720000 - (14325)(9.81)(1.17)} = 0.0215 rad = 1.23^\circ$$

$$\text{Lateral}_F = M_s a_c \frac{b_s}{a_s + b_s} = 26140N \quad \text{Lateral}_R = M_s a_c \frac{a_s}{a_s + b_s} = 16000N$$

Substituting into the above equation, the weight transfer for front and rear axles gives:

$$w_{tf} = \frac{(736000)(0.0215)}{2.175} + \frac{(26140)(0.002)}{2.175} + \frac{(0.3)(9.81)(587)(0.437)}{2.175} = 7650N$$

$$w_{tr} = \frac{(900000)(0.0215)}{1.774} + \frac{(16000)(0.384)}{1.774} + \frac{(0.3)(9.81)(1088)(0.55)}{1.774} = 15360N$$

3.12.2 Appendix 2 Multibody Force Magnitudes

Table of force magnitudes during braking + kerb strike load case corresponding to figure 3D.

FA31x	44107.51	FB31z	-86.6457	FE21y	-40805.5	FG24x	-36400.6
FA31y	-15189.3	FD34x	-44091.7	FE21z	5212.853	FG24y	-27554.3
FA31z	-8028.92	FD34y	-68281	FF21x	140.272	FG24z	-4090.68
FB31x	-15.8042	FD34z	8115.564	FF21y	68359.78	f1	-313.672
FB31y	83470.31	FE21x	36260.28	FF21z	-1122.18	f2	116.5415

3.12.3 Appendix 3 Minimum Weight Design Calculations

Tensile/Compressive Yielding

Front Wishbone:

$$\sigma_x = \frac{-64810}{A}$$

$$\sigma_x = \frac{-64810}{2797 \times 10^{-6}} = -23.2MPa$$

Rear Wishbone:

$$\sigma_x = \frac{85323}{A}$$

$$\sigma_x = \frac{85323}{2797 \times 10^{-6}} = 30.5MPa$$

Buckling

Buckling may occur during high compressive loads such as during heavy braking. The Euler buckling equation yields a reasonably accurate result for global buckling of constant cross sectional members. The smaller moment of inertia I_y is used:

$$\sigma_{crit} = \frac{\pi^2 E}{\left(\frac{l}{k}\right)^2} = \frac{\pi^2 EI}{l^2 A} = \frac{(\pi^2)(115 \times 10^9)(6.275 \times 10^{-6})}{(0.63^2)(2797 \times 10^{-6})} = 6.42 GPa$$

Due to the slenderness ratio ($\frac{l}{r}$) the beam shall yield far before the global critical loading stress is approached. Local buckling can also be considered, with the approximate critical stresses for the flange and web sections being defined by:

$$\frac{4\pi^2 E}{12(1-\nu)} \left(\frac{t}{h}\right)^2$$

Due to the thickness of the flanges and web, the local critical buckling stress is also extremely high, and the beam shall yield before this limit is reached. Resultantly, buckling is not a risk.

Shear and Bending Stresses

For maximum axial stresses produced by bending in the X'Y' plane at the hardpoint:

$$\sigma = \frac{My}{I_z} = \frac{(13584)(0.03)}{7.602 \times 10^{-6}} = 396 MPa$$

The maximum X'Y' shear stress produced at the hardpoint is:

$$\tau = \frac{F}{A} = \frac{21530}{2797 \times 10^{-6}} = 7.8 MPa$$

For maximum axial stresses produced by bending in the Y'Z plane at the hardpoint:

$$\sigma = \frac{Mz}{I_y} = \frac{(5583)(0.03)}{6.375 \times 10^{-7}} = 262.7 MPa$$

The maximum X'Z shear stress produced at the damper mount is:

$$\frac{-25381}{2797 \times 10^{-6}} = -9.07 MPa$$

Whilst the X'Z shear stress produced at the hardpoint is:

$$\frac{13619}{2797 \times 10^{-6}} = 2.14 MPa$$

These stresses can be combined in a stress tensor to determine the principal stresses in an element in the control arm. An element under maximum stress is considered – on the top surface of both bending situations, at the hardpoint ($x=0$). The beam theory coordinate system is used in which x is the length of the beam, y is vertically downwards. The load case on the front control arm under braking + kerb strike is considered:

$$\begin{bmatrix} \sigma_x & \tau_{xy} & \tau_{xz} \\ \tau_{yx} & \sigma_y & \tau_{yz} \\ \tau_{zx} & \tau_{zy} & \sigma_z \end{bmatrix} = \begin{bmatrix} 639.7 & 4.89 & 2.67 \\ 4.89 & 0 & 0 \\ 2.67 & 0 & 0 \end{bmatrix} MPa$$

Taking the eigenvalues:

$$\sigma_1 = -0.05 MPa, \quad \sigma_2 = 0 MPa, \quad \sigma_3 = 639.7 MPa$$

Due to the biased loading case in the axial direction and relatively small shear stresses, the usefulness in comparing this to the Von Mises or Tresca criterion is limited, and rather the combined axial loading presents an accurate yield criterion. This is used in section 3.6, table 3K.

3.12.4 Appendix 4 Chassis Roll and Stiffness [1]

Calculations are at zero wheel travel, with $K_s=397000 N/m$ and $R=1.3$, K_w therefore = $234911 N/m$.

Anti Roll Bar Calculations:

Considering 4150 Alloy Steel ARB: $E=210 MPa$, $\nu=0.3$. $G=E/2(1+\nu)$, $Od=80 mm$, $Id=60 mm$

$$K_T = \frac{GJ}{r^2 L} = \frac{(80.6 MPa) \left(\pi \left(\frac{0.08^4 - 0.06^4}{32} \right) \right)}{(0.04)^2 (1.24)} = 111670 N/deg$$

The anti roll bar motion ratio is estimated by the ratio between the distance between the lower control arm inner link and contact patch, and distance drop link and inner link.

$$R_{ARB} = \frac{848}{360} = 2.35 \quad K_{W\ ARB} = \frac{K_{ARB} \cdot T^2}{R_{ARB}^2 \cdot L^2} = \frac{(111670)(1.0875^2)}{(2.83^2)(0.56^2)} = 76260 \text{Nm/degree}$$

$$K_{Front_Roll} = \frac{t^2 \cdot K_{Ws} + K_{Warb}}{2\left(\frac{360}{2\pi}\right)} = \frac{2.175^2 \cdot (234900 + 76260)}{2\left(\frac{360}{2\pi}\right)} = 12850 \text{Nm/degree}$$

Torque = (Sprung Frontal Mass)(Lateral Acceleration[G])(9.81)(Sprung COG Height – Roll Centre Height)

$$\text{Torque} = (14336 \cdot 0.38)(0.3)(9.81)(1.39 - 0.02) = 22300 \text{Nm}$$

$$\text{Front Axle Roll Angle} = \frac{\text{Torque}}{\text{Roll Stiffness}} = \frac{22300}{11930} = 1.87 \text{ degrees}$$

Rear Chassis Roll Stiffness

At zero wheel travel, with $K=794000 \text{N/m}$ and $R=1.14$, K_w therefore $= 610957 \text{N/m}$. No ARB at rear therefore no additional wheel rate. Rear chassis roll stiffness is as follows:

$$K_{Rear_Roll} = \frac{t^2 \cdot K_{Ws}}{2\left(\frac{360}{2\pi}\right)} = \frac{1.773^2 \cdot (572480)}{2\left(\frac{360}{2\pi}\right)} = 15700 \text{Nm/degree}$$

From figure 3C2, it can be seen that the roll centre of the rear axle is 654mm, allowing the roll stiffness to be calculated. Considering the same 0.30g of lateral acceleration:

$$\text{Torque} = (14336 \cdot 0.62)(0.3)(9.81)(1.39 - 0.384) = 26800 \text{Nm}$$

$$\text{Rear Axle Roll Angle} = \frac{\text{Torque}}{\text{Chassis Stiffness}} = \frac{26800}{15700} = 1.71 \text{ degrees}$$

Roll stiffness of vehicle considering the roll axis: $12850 + 15700 = 28550 \text{ Nm/degree}$.

3.12.5 Appendix 5 Pneumatic Calculations

Air spring volume, 11inches at 80PSI = 9.83 litres

Air brake volume, type 24 actuator at 120PSI = 1.3 litres

WABCO E-comp compressor output pressure = 181PSI.

Air reservoirs for front and rear sub systems. Targets require ability to kneel 8 times and fully apply/release brakes 30 times before recompression. [9]

Front: $8 \times 9.83 \text{ litres} = 78.6 \text{ litres at 80PSI}$

$20 \times 1.3 \text{ litres} = 26 \text{ litres at 120PSI}$

$$(P1)(V1) + (P2)(V2) = (P3)(V3) \rightarrow (80)(78.6) + (120)(26) = (181)(V3)$$

$V3 = 52 \text{ litres} \therefore \text{WABCO 60 litre reservoir is selected.}$

Rear: $16 \times 9.83 \text{ litres} = 157.28 \text{ litres at 80PSI}$

$20 \times 1.3 \text{ litres} = 26 \text{ litres at 120PSI}$

$$(80)(157.3) + (120)(26) = (181)(V3)$$

$V3 = 86.7 \text{ litres} \therefore \text{WABCO 100 litre reservoir is selected.}$

Braking Calculations

The maximum developed braking force at 1G deceleration at front and rear axles including weight transfer is 97720N and 59240N respectively. Considering front force due to its higher magnitude, the braking torque required at one wheel is:

$$Torque_{Braking} = \text{Corner loading} \cdot \text{Wheel radius} = \frac{97720}{2} \cdot 0.4782 = 23355 \text{Nm}$$

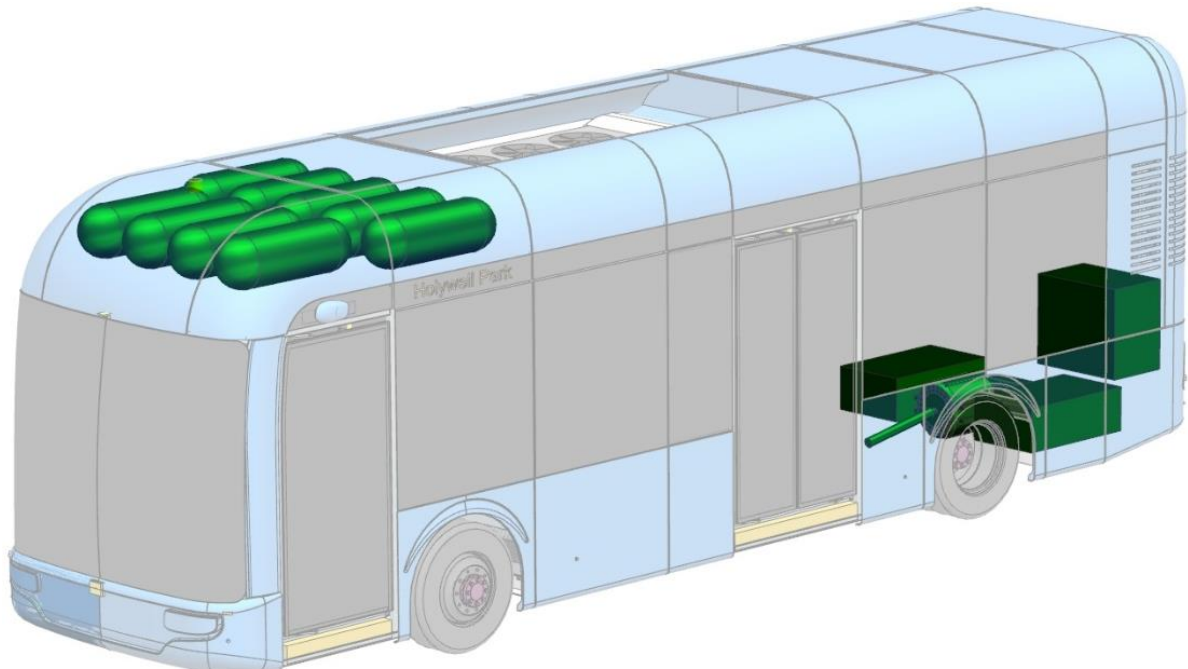
The WABCO MAXX 22 Air Disc Brake is selected due to its maximum braking torque of 30,000Nm.

3.13 References

- [1] – Metz, L., Milliken, W. and Milliken, D. (1998). *Race car vehicle dynamics workbook*. Warrendale
- [2] – Von Chappuis, H., Mavros, G. and King, P. (2013). Prediction of impulsive vehicle tyre-suspension response to abusive drive-over-kerb manoeuvres.
- [3] – Blundell, M. and Harty, D. (2014). *The Multibody Systems Approach to Vehicle Dynamics*. Oxford.
- [4] – Hugemann, W. and Nickel, M. (n.d.). [online] Unfallrekonstruktion.de. Available at: https://www.unfallrekonstruktion.de/pdf/itai_2003_english.pdf
- [5] – Firestone (n.d.). [online] Mrostop.com. Available at: https://www.mrostop.com/media/catalog/product/firestone_pdfs/w01-358-7096-firestone-air-spring-datasheet.pdf.
- [6] – CES Edupack, 2019. CES Edupack Materials Selection Software, s.l.: CES
- [7] – Matweb.com. (2020). *Online Materials Resource*. [online] Available at: <http://www.matweb.com/>
- [8] – Collins, J., Busby, H. and Staab, G. (2010). *Mechanical design of machine elements and machines*. Hoboken: John Wiley & Sons.
- [9] – Truck systems design handbook. (2002). Warrendale, Pa.: Society of Automotive Engineers
- [10] – Gillespie, T. (1992). *Fundamentals of Vehicle Dynamics*. Warrendale, Pa.: Society of Automotive Engineers.
- [11] – Zf.com. (2020). *Damping Modules*. [online] Available at: https://www.zf.com/products/en/cars/products_29132.html
- [12] – Guglielmino, E., Sireteanu, T., Stammers, C., Ghita, G. and Giuclea, M. (n.d.). *Semi-active suspension control*. London : Springer, c2010.
- [13] - Bosch-mobility-solutions.com. (2020). [online] Available at: https://www.bosch-mobility-solutions.com/media/global/products-and-services/commercial-vehicles/steering-systems/steering-systems/folder_for_steering_systems_for_commercial_vehicles.pdf
- [14] – Inform.wabco-auto.com. (2020). *WABCO INFORM Web*. [online] Available at: <http://inform.wabco-auto.com/intl/en/index.html>
- [15] – Learn.lboro.ac.uk. (2019). *19TTC066 – Vehicle Dynamics and Simulation*. [online] Available at: <https://learn.lboro.ac.uk/mod/resource/view.php?id=52957>

Section 4

Powertrain: Motors, Batteries, Fuel Cell System.



(s) Adam Lofthouse - B623365

Number of Pages: 24
Number of Words: 1943

Contents

4.1 Introduction	79
4.1.1 Targets & Requirements	79
4.2 Final Powertrain System	79
4.2.1 System Overview	79
4.2.2 Vehicle Drive Cycle	80
4.3 Motor Specification.....	83
4.3.1 System Overview	83
4.3.2 Regenerative Braking Overview	85
4.3.3 Final Drive Ratio.....	85
4.3.4 Noise Reduction.....	86
4.4 Battery Specification	86
4.4.1 System Overview	86
4.4.2 Charging System.....	87
4.5 Fuel Cell Specification.....	88
4.5.1 System Overview	88
4.5.2 Fuel Cell Chemistry	90
4.5.3 Hydrogen Refuelling System	90
4.6 Design for Minimum Weight.....	91
4.6.1 Part Selection.....	91
4.6.2 Assumptions & Load Cases.....	91
4.6.3 Material Selection.....	92
4.6.4 Numerical Analysis.....	93
4.6.4.1 Maximum Shear Criteria	93
4.6.5 Technical Drawing.....	95
Appendix	96
Appendix 4A	96
Appendix 4B	97
References	99

4.1 Introduction

In this section, an overview of the final powertrain of the bus is given. Changes made will be described/explained, and further justification will be given to areas not discussed in the concept report. A Design for minimum weight analysis will be completed on the driveshaft. This report will often refer to Section 4 of the concept report.

4.1.1 Targets & Requirements

Table 4A below shows the requirements and numerical targets set out for the vehicle and how the values have been proved.

Table 4A: A table showing the vehicle requirements and how they have been achieved

Code	Description	Numerical Target	Actual Value	Achievement Proved Via
PE2	To be able to last a full day's service including management of waste energy.	Range: 200 Miles	202.6 Miles	Drive Cycle created in Section 4.2.3
EI2	To not emit any damaging pollutants or material.	Emissions: 0 g/km	0 g/km	Fuel Cell Explanation in Section 4.5.2
EI3	To reduce noise of existing bus systems	Noise Decrease: Over 1 dB	Over 6 dB	Noise analysis completed in Section 4.3.4

4.2 Final Powertrain System

4.2.1 System Overview

Figure 4A below shows a system diagram for the powertrain of the vehicle. Boxes in red represent system components, purple boxes represent lost energy.

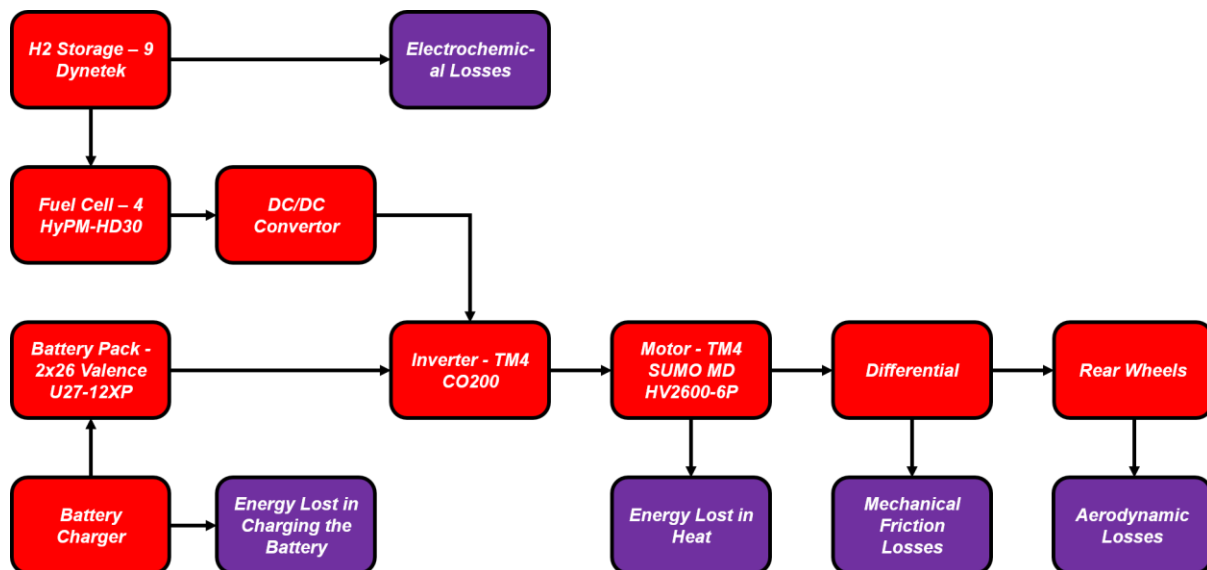


Figure 4A: A figure showing the overall System Diagram with flow of energy to components and losses

The percentage energy losses in the system stated in Figure 4A are shown in Table 4B below.

Table 4B: A table showing the sections of lost energy in the Powertrain System

Energy Loss Factor	Percentage Energy Lost
Electrochemical [4]	15%
Battery Charging [3]	10%
Heat [5]	8%
Mechanical Friction [2]	20%
Aerodynamic [3]	30%

Table 4C below shows the cost of each powertrain section and the final cost for the whole powertrain system.

Table 4C: A table showing the cost of Powertrain components

Powertrain Section	Estimated Cost (£)
Motor System	3300
Battery System	52250
Fuel Cell System	52000
Powertrain Total	107550

4.2.2 Vehicle Drive Cycle

To calculate vehicle range, a drive cycle has been created replicating how a bus would run on a daily basis. Figure 4B below shows the Loughborough University Campus Shuttle Bus route in which the drive cycle is based. Each number on the route represents a bus stop and areas circled in red represent a change in gradient.

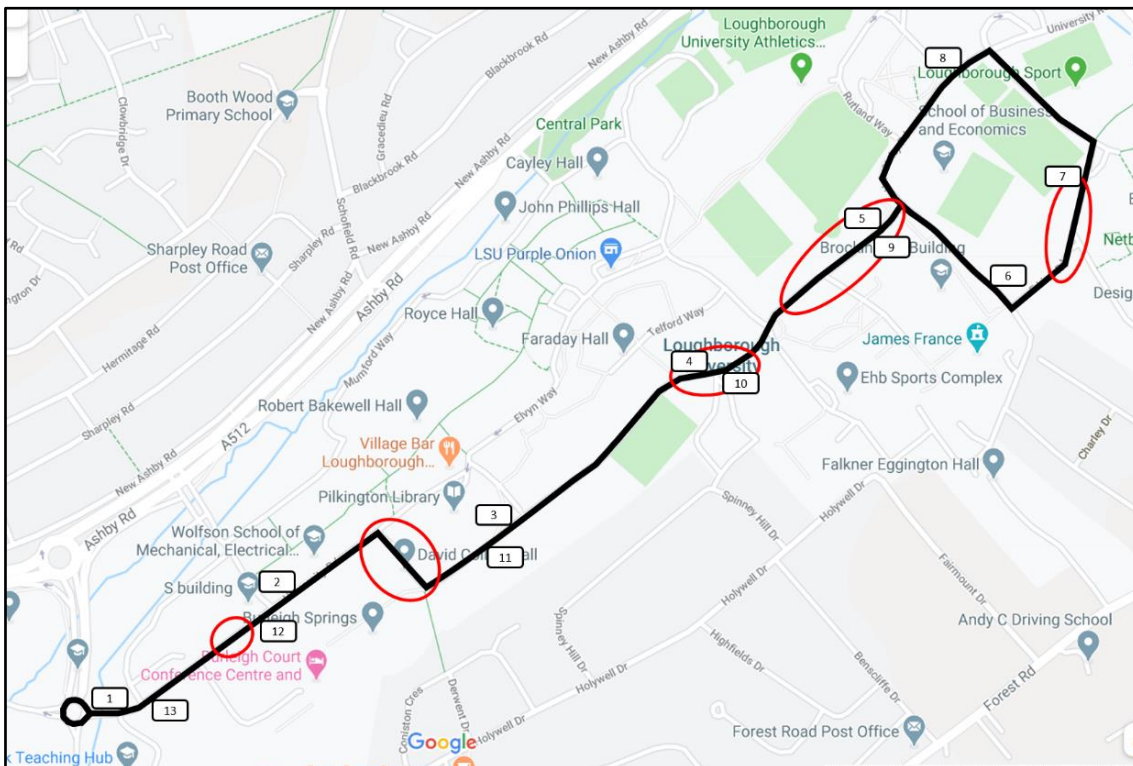


Figure 4B: A figure showing the Route used in the Drive Cycle calculations.

Table 4D below shows the lengths of each section of vehicle travel between the bus stops on Loughborough University campus and (where applicable) the size of the gradient and the state of it.

Table 4D: A table showing the relevant Drive Cycle Parameters.

Route Section	Section Length (Miles)	Gradient (Deg)
1 to 2	0.168	2 (downhill)
2 to 3	0.217	10 (Uphill)
3 to 4	0.217	2 (Downhill)
4 to 5	0.18	4 (Downhill)
5 to 6	0.118	2 (Downhill)
6 to 7	0.142	2 (Downhill)
7 to 8	0.174	N/A
8 to 9	0.174	N/A
9 to 10	0.162	4 (Uphill)
10 to 11	0.249	2 (Uphill)
11 to 12	0.217	10 (Downhill)
12 to 13	0.118	2 (Uphill)
13 to 1	0.137	N/A

Table 4E below shows the assumptions that have been made as well as how they could negatively impact the accuracy of the Drive Cycle Model.

Table 4E: A table showing the assumptions made in the creation of the Drive Cycle Model

Assumption	Impact on Accuracy
The Route has no Obstacles in Route doesn't always run perfectly, occasionally an obstacle the way (E.g. Slow Cyclist, Road Works, Flooding).	in the way which can slow the vehicle down. Difficult to model these scenarios as these events occur randomly.
Vehicle is always at full capacity during the drive cycle (Mass≈16252kg).	Buses are rarely at full capacity 24/7, difficult to model the random nature of passengers entering/exiting the vehicle. Shows the worst-case scenario for the drive cycle.

Figure 4C below shows the plot created for Vehicle Speed against Cycle Time, it is assumed in this case that the vehicle does not wait at the stop to pick up passengers, as this waiting does not affect the vehicle's range.

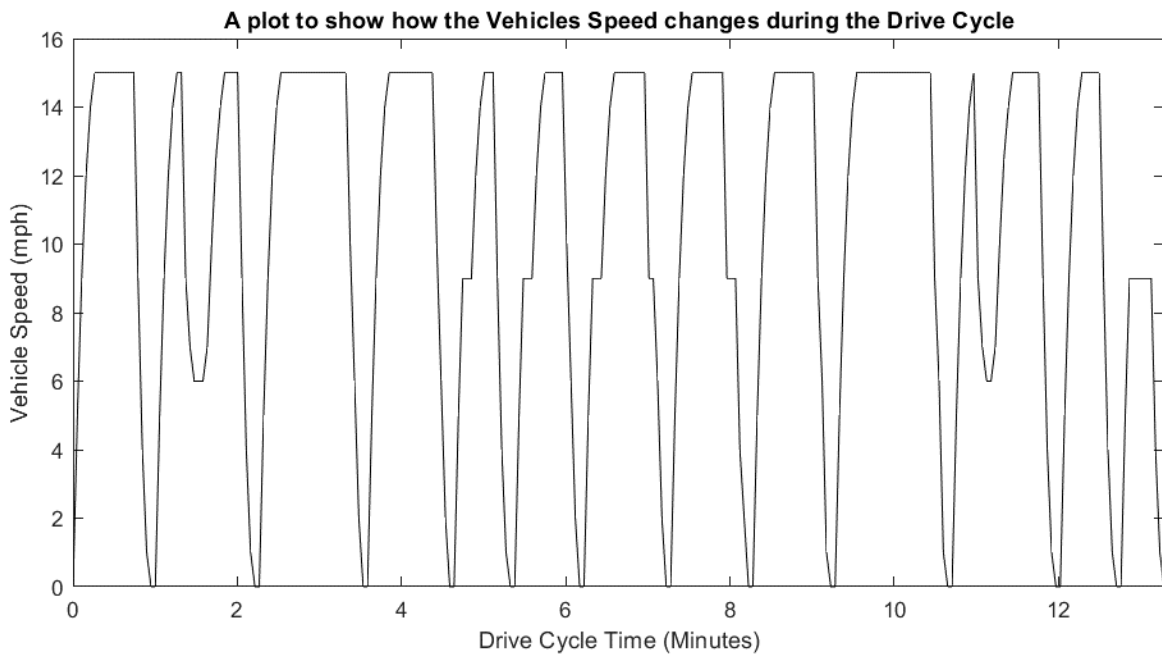


Figure 4C: A plot showing the Speed vs. Time Plot created by the Drive Cycle for 1 loop

The equation used to calculate the Energy (kWh) used between each data point (i and j) is shown below [1], the parameters represented by each symbol is explained in Appendix 4A.

$$E_{ij} = \frac{d_{ij}}{3600} \left[mg(A_d \cos\theta_{ij} + \sin\theta_{ij}) + 0.00386(\rho C_d A v_{ij}^2) + m \left(\frac{dv}{dt} \right)_{ij} \right]$$

Figure 4D below shows the Amount of Energy used during 1 route loop against cycle time.

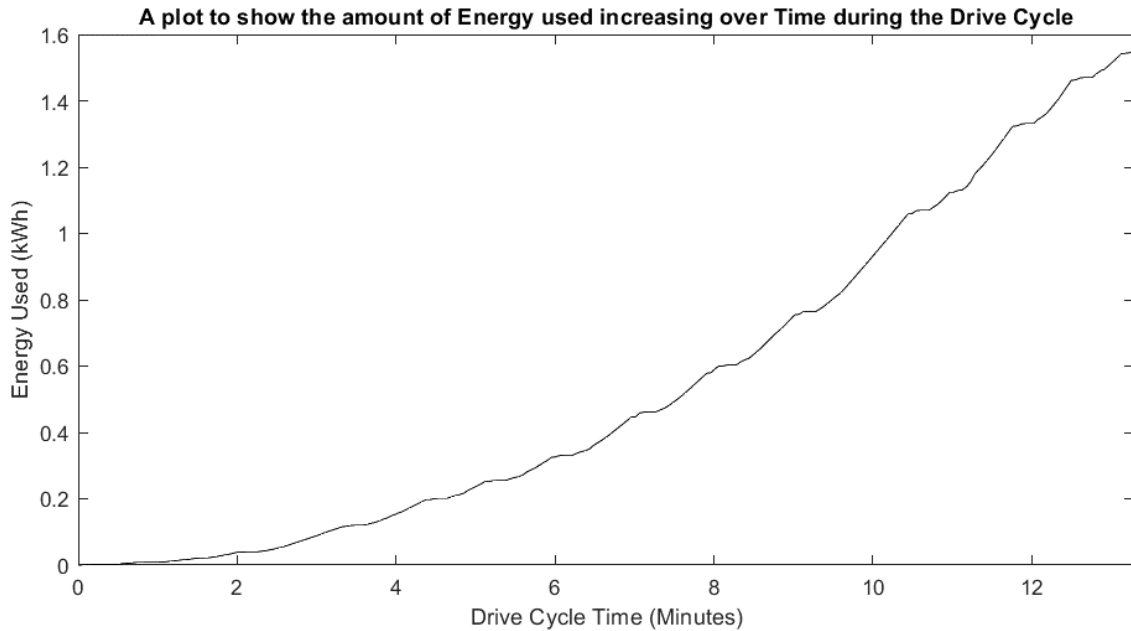


Figure 4D: A plot showing the Energy Used vs. Time Plot created by the Drive Cycle

From Figure 4D, it was calculated that during one complete loop of the Campus Bus Route, the Vehicle used 1.545kWh of Energy. Assuming a total Vehicle Energy of 136.93kWh , the total vehicle range can be calculated. The calculation and calculated value are shown below:

$$\text{Vehicle Range (Miles)} = \frac{\text{Total Vehicle Energy (kWh)} \times \text{Length of 1 Loop (Miles)}}{\text{Energy Used in 1 Loop (kWh)}}$$

$$\text{Vehicle Range} = \frac{136.93 \times 2.27}{1.545} = 201.5414 \approx 201.5 \text{ Miles}$$

As the vehicle range target set out in the concept report was 200 miles, the vehicle at maximum capacity exceeds this target. The number of loops which can be completed in a 16-hour workday is 71 (As 1 Loop takes 13 Minutes and 20 Seconds).

As shown in Section 1, to achieve a 70:30 Split between Battery and Hydrogen power, only 1 Hydrogen tank is required. The Drive Cycle was completed with the weight of these 9 Tanks being considered but the 70:30 split being in occurrence. If all 9 Hydrogen tanks are specified on the vehicle and supply hydrogen to the fuel cell, there would be an increase of range of 482.7 Miles.

4.3 Motor Specification

4.3.1 System Overview

Table 4F below shows the changes made to the motor system.

Table 4F: A table showing the changes made to the Motor System

Change	Reasoning
Addition of DC/DC Converter	Due to the nature of the DC voltage output provided by the Fuel Cell [8]. This outputted voltage is widely varying and has an overload capacity that is limited, to make the fuel cells act more like batteries a DC/DC Convertor is used.

The final choice of Convertor can be seen in Table 4G below, as well as the final choice of motor and inverter used.

Table 4G: A table showing the final component choices for the Motor, Inverter & Converter.

Component	Part Number	Component Choice
Motor	AL005	TM4 SUMO MD HV2600-6P
Inverter	AL006	TM4 CO200
Converter	AL007	Farnell HDD100-48S24-X

Table 4H below shows the final specifications for the Motor.

Table 4H: A table showing the specifications of the Motor [6]

Parameter	Concept Phase	Design Phase
Size – LxWxH (mm)	510x425x452	510x425x452
Mass (kg)	225	225
Max Speed (RPM)	3500	3500
Peak Torque (Nm)	2760	2760
Continuous Torque (Nm)	970	970
Peak Power (kW)	265	265
Continuous Power (kW)	155	155

Table 4I below shows the final specifications for the Inverter and Converter.

Table 4I: A table showing the specifications of the Inverter [6] and Converter [7]

Parameter	Concept Phase Inverter	Design Phase Inverter	Concept Phase Converter	Design Phase Converter
Size – LxWxH (mm)	424x670x143	424x670x143	-	88.9x149.7x42.4
Mass (kg)	26	26	-	0.71

Figure 4E below shows the final CAD produced for the Motor, Inverter and Converter.

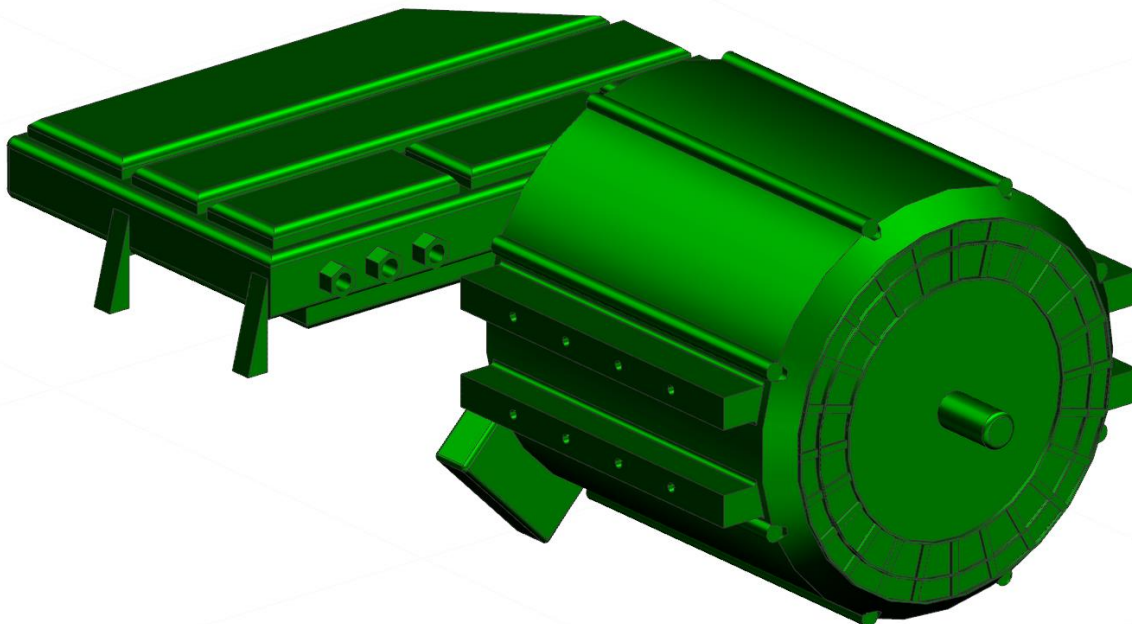


Figure 4E: A figure showing the CAD of the Motor, Inverter and Converter

Table 4J below shows the cost of each component of this powertrain section.

Table 4J: A table showing the cost of components

Component	Estimated Cost (£)
TM4 Sumo MD Motor HV2600-6P	3000
TM4 Sumo MD Invertor	250
Farnell HDD100-48S24-X Converter	50

4.3.2 Regenerative Braking Overview

The regenerative braking system recovers energy that was wasted when the vehicle brakes. When the brakes are applied, the electric motor becomes an electric generator due to the vehicle's inertia. This saved electricity then powers the vehicles motor reducing the energy wasted. On average, a regenerative braking system returns 34% of the energy lost in braking [3], this gives a 34% range increase giving a Total Range of 262 Miles.

4.3.3 Final Drive Ratio

When choosing a Final Drive Ratio for the vehicle, various values are considered, the equation used to calculate Torque at the wheels is shown below.

$$\text{Wheel Torque} = \text{Motor Torque} * \text{Final Drive Ratio} * \text{Driveline Efficiency}$$

Figure 4F below shows how the Peak & Continuous Wheel Torques change for an increasing final drive ratio.

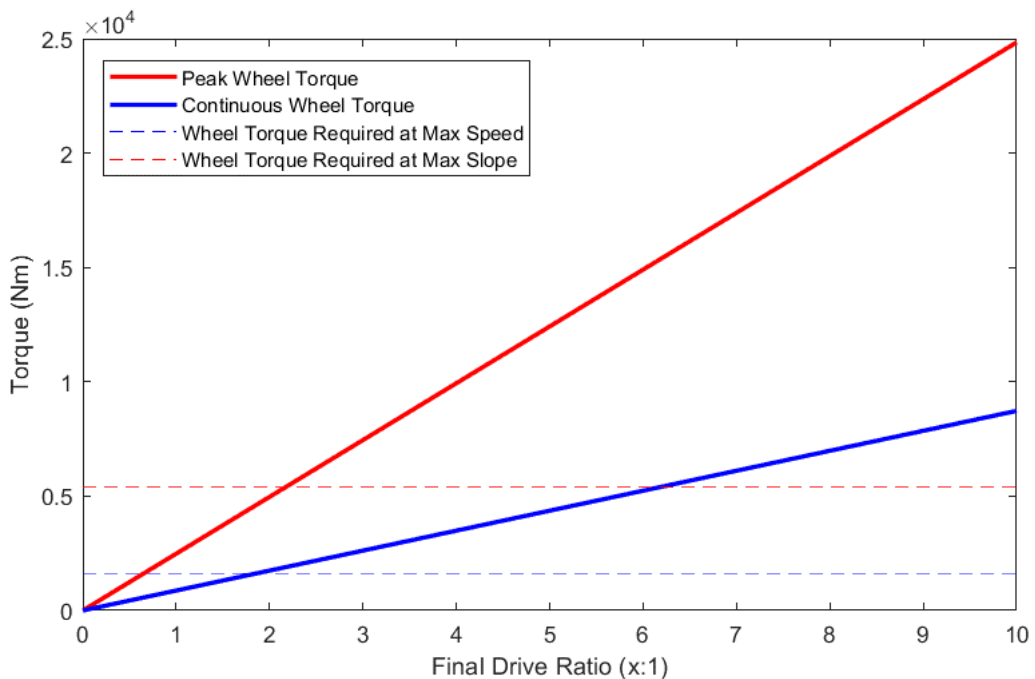


Figure 4F: A figure showing the CAD of the Fuel Cell System

To be suitable for use in the vehicle, final drive ratio must give values for Peak & Continuous Wheel Torque high than the Wheel torque requirements for maximum speed & slope (Equal to 1635Nm & 5388Nm respectively). To meet these requirements a final drive ratio of over 6.2:1 is needed, the best value for final drive ratio is one higher than this required number (to improve the vehicle's performance) but not too high as to dampen the powertrains efficiency. The value decided on was 8.1:1 as this perfectly fits the optimum value boundaries. Table 4K below shows the Peak & Continuous Wheel Torques for the vehicle using this value of Final Drive Ratio.

Table 4K: A table showing the Peak & Continuous Wheel Torques using an Fd=8.1:1

Parameter	Value
Peak Torque at Wheels (Nm)	20120
Continuous Torque at Wheels (Nm)	7071

4.3.4 Noise Reduction

An important topic to research into is how much the noise of the powertrain system is reduced by the usage of an alternate power type. Over 30% of the EU population is exposed to levels of noise that are unhealthy [9], which can lead to hearing loss and stress over time. This number can be reduced using electric/fuel cell technologies in bus powertrains. Table 4L below shows the noise (dB[A]) for various scenarios using a diesel bus and an electric bus.

Table 4L: A table showing the comparison of noise generated by a diesel bus and an electric bus [9]

Scenario	Diesel Bus Noise (dB[A])	Electric Bus Noise (dB[A])	Noise Reduction (dB[A])	% Noise Reduction
7m away from Bus Idling.	56	44	12	21
Sat inside Bus Idling.	63	53	10	16
Sat inside bus @ Constant 30mph.	70	64	6	9

The reduction in dB shown is positive, as a decrease in noise of 10dB is perceived as being the same as halving the noise being heard [10].

4.4 Battery Specification

4.4.1 System Overview

Table 4M below shows the final component choices for the battery section of the vehicle powertrain.

Table 4M: A table showing the final component choice for the Batteries

Component	Part Number	Component Choice
Battery Pack 1	AL003	26 Valence U27-12XP Batteries
Battery Pack 2	AL004	26 Valence U27-12XP Batteries

The batteries are run with 2 separate packs of 26 running in series with each other, and the 2 separate packs running in parallel with one another. The final specifications given to the battery pack from this system is shown below in table 4N.

Table 4N: A table showing the specifications of the Battery Pack [11]

Parameter	Concept Phase	Design Phase
Total Nominal Voltage (V)	332.8	332.8
Total Battery Capacity (kWh)	95.85	95.85
Total Dimensions – LxWxH (mm)	612x2236x450	612x2236x450
Total Mass (kg)	998.4	998.4

Figure 4G below shows the final CAD produced for the Batteries.

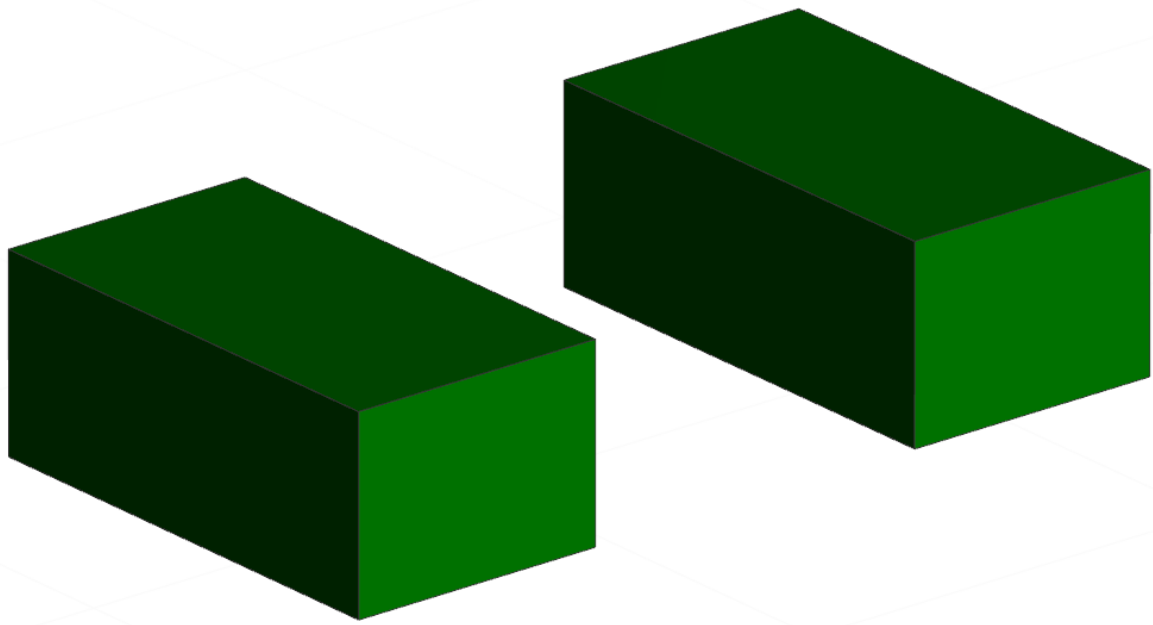


Figure 4G: A figure showing the CAD of the Batteries

Table 4O below shows the cost of each component of this powertrain section.

Table 4O: A table showing the cost of components

Component	Estimated Cost (£)
52 x Valence U27-12XP Batteries	52000
Charging System	250

4.4.2 Charging System

As stated in the Concept report, the vehicle will use 2 x 7.5kW Integrated on Board Chargers CHAdeMO DC Charging Protocol [12] giving a total time for charging of 6 hours and 24 minutes. Figure 4H below shows the cable diagram for the system using CHAdeMO DC Charging Protocol [12] to charge the batteries.



Figure 4H: A figure showing the system cable diagram

4.5 Fuel Cell Specification

4.5.1 System Overview

Before a system overview is given for the Fuel Cell System, the choices made for the Fuel Cell and Hydrogen Storage Tanks made in the concept report will be justified. Table 4P below shows the benchmarking completed for the PEM Fuel Cell system used in the vehicle.

Table 4P: A table showing the options for type of PEM Fuel Cell System available

Parameter	HyPM-HD30 [13]	PowerCell MS-30 [14]	FCveloCity-MD30 [15]	FCveloCity-HD100 [16]
Power (kW)	31	30	30	100
Weight (kg)	72	145	125	280
Power:Weight (W/kg)	430	207	240	357
Dimensions - LxWxH (mm)	719x406x261	415x641x656	900x480x375	1200x869x487
Volume (mm ³)	7.61x10 ⁷	1.74x10 ⁸	1.62x10 ⁸	5.07x10 ⁸

The clear choice from Table 4P above was the HyPM-HD30 Fuel Cell system. This is due to it having the greatest Power to Weight ratio of any of the benchmarked PEM Fuel Cells and the smallest Volume, meaning it can be packaged into the vehicle with ease.

Table 4Q below shows the benchmarking completed for the Hydrogen Storage Tanks used in the vehicle. The Dynatek Hydrogen Tanks in which were stated as the choice for the vehicle in the concept report do not feature in the Benchmarking. This is due to Dynatek being taken over by Luxfer in 2015, due to this the Luxfer Tanks will be benchmarked against competitors.

Table 4Q: A table showing the options for type of PEM Fuel Cell System available

Parameter	Luxfer G-Stor W100N [17]	Worthington ALT836U [18]	Mahytec H ₂ Tank [19]
H ₂ Capacity (kg)	2.41	2.10	9.5
Diameter (mm)	415	432	490
Length (mm)	1168	1003	3070
Water Volume (L)	100	90.2	300
Weight (Excluding H ₂) (kg)	51.5	59.4	260
H ₂ Weight:Tank Weight	0.047	0.035	0.037

The chosen tank for use in the vehicles powertrain system is the Luxfer G-Stor W100N. This reasoning is due to the tanks having the greatest ratio between the weight of Hydrogen which can be stored in the tanks and the actual weight of the tanks, which is useful for the vehicles powertrain as it reduces unnecessary weight on the bus.

Table 4R below shows the final component choices for the Fuel Cell System section of the vehicle powertrain.

Table 4R: A table showing the final component choice for the Fuel Cell System

Component	Part Number	Component Choice
Hydrogen Storage Tanks	AL001	1 to 9 Luxfer G-Stor W100N
Fuel Cell	AL002	4 HyPM-HD30

As previously stated in the Concept Report, the Fuel Cell System will use 1 to 9 Hydrogen Tanks (dependant on the customer requirements) and 4 Fuel Cell systems. Four FC systems and 1 H₂ are used to make sure enough power is outputted from the fuel cell to give the bus its desired 70:30 energy split between Battery and Hydrogen power. Section 1 of this report discusses the calculations behind the need for only 1 H₂ Tank to satisfy the Power requirements. Table 4S below shows the final specifications for the Fuel Cell.

Table 4S: A table showing the specifications of the Fuel Cell [13]

Parameter	Concept Phase	Design Phase
Continuous Power (kW)	124	124
Dimension – LxWxH (mm)	522x406x1438	522x406x1438
Mass (kg)	288	288
Operating Current (A)	0 to 500	0 to 500
Operating Voltage (V)	60 to 120	60 to 120
Expected Lifetime (h)	10000+	10000+

Table 4T below shows the final specifications for the Hydrogen Storage Tanks.

Table 4T: A table showing the specifications of the Hydrogen Tanks [17]

H ₂ Parameter	Concept Phase	Design Phase Min	Design Phase Max
No. of Tanks	9	1	9
H ₂ Capacity (kg)	-	2.41	21.69
Diameter (mm)	400	415	415
Length (mm)	1175	1168	1168
Water Volume (L)	-	100	900
Weight (Excluding H ₂) (kg)	864	51.5	463.5

Figure 4I below shows the final CAD produced for the Fuel Cell System.

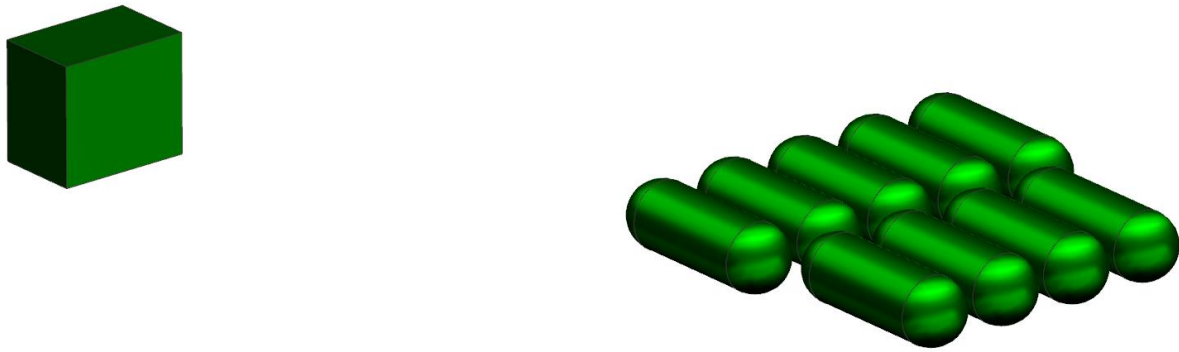


Figure 4I: A figure showing the CAD of the Fuel Cell System.

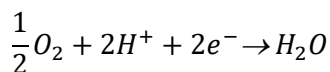
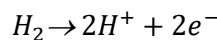
Table 4U below shows the cost of each component of this powertrain section.

Table 4U: A table showing the cost of Hydrogen System components

Component	Estimated Cost (£)
4 x HyPM-HD30 PEM Fuel Cells	50000
1 x Luxfer G-Stor W100N H ₂ Storage Cylinders	2000

4.5.2 Fuel Cell Chemistry

The main process behind the chemical work in a Proton Electrolyte Membrane Fuel Cell (PEMFC) is the basic hydrogen combustion reaction $H_2 + \frac{1}{2}O_2 \rightarrow H_2O$. This reaction is split into two electrochemical half reactions, shown below [20].



From the above chemical reactions, there are zero pollutants formed in the PEMFC process. Considering the zero pollutants formed in battery power process, the vehicle can be assumed to have an emissions value of 0g/km.

4.5.3 Hydrogen Refuelling System

The system in place to refuel the vehicle is explained in Table 4V below.

Table 4V: A table showing the stages involved in the Refilling process [21]

Stage	Explanation
Low Pressure Storage	H ₂ stored in Low Pressure Tanks (20-200 Bar). Pressure is too low to refuel vehicle.
Compressor	Compression is used to overcome the difference in pressure between storage and refuelling, increases to 1000 Bar.
High Pressure Storage	H ₂ stored in High Pressure tanks ready for refuelling.
Precooling	Precooling aims to stop hydrogen tanks heating above 85°C. Low temperature required is generated using compression refrigerating machine and heat exchanger.
Dispenser	Refuelling completed using a dispenser. Fuelling nozzle delivers compressed H ₂ into the vehicles pressure tank.

4.6 Design for Minimum Weight

4.6.1 Part Selection

The part selected to undergo a Design for Minimum Weight analysis in the vehicle's powertrain is the driveshaft. This part was chosen as it is an integral component of the vehicles powertrain and reducing its weight may improve the efficiency of the vehicle and hence increase its range.

Figure 4J below shows the original design of the Driveshaft.

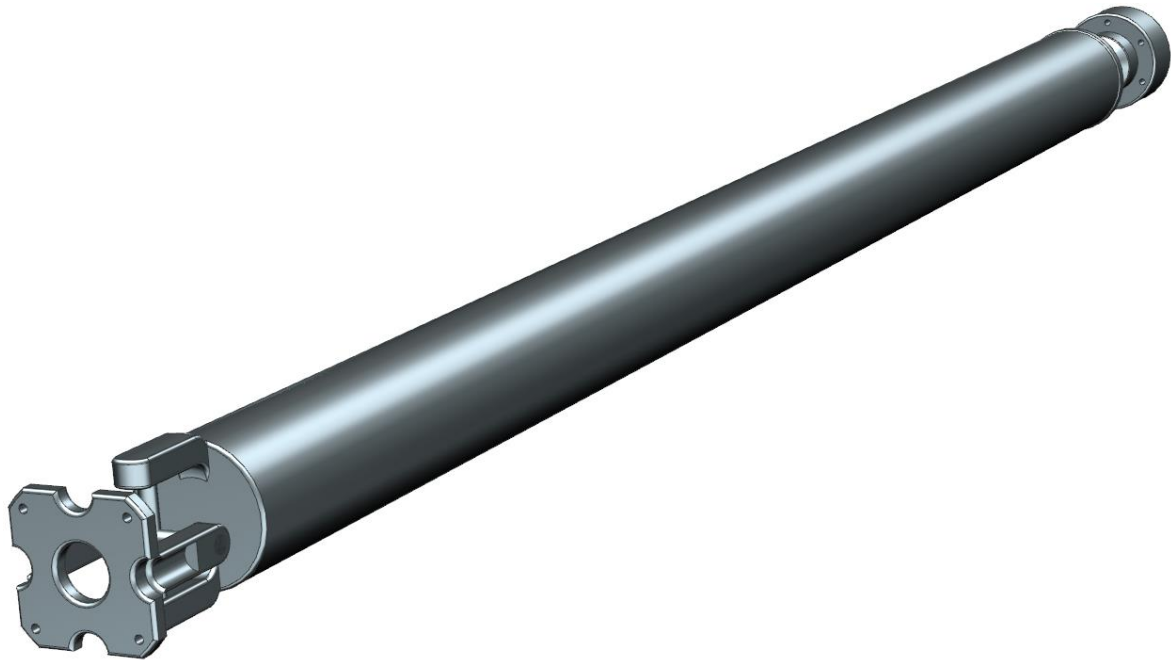


Figure 4J: A figure showing the original drive shaft design.

4.6.2 Assumptions & Load Cases

The Load Case to be analysed is one where the only loads acting on the shaft are due to the component weight and torque input from the motor. This Load Case is shown in the Free Body Diagram in Figure 4K below.

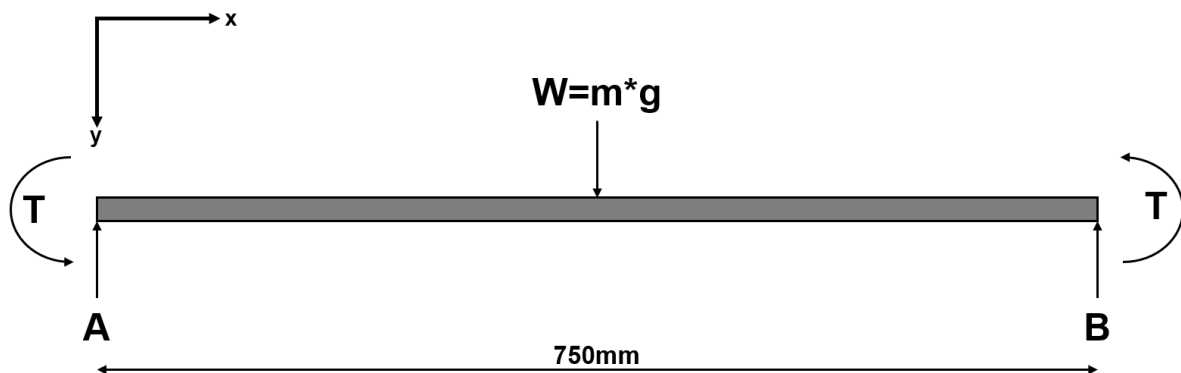


Figure 4K: A figure showing the Free Body Diagram for the Load Case

Table 4W below shows the assumptions made during the Design for Minimum Weight Analysis.

Table 4W: A table showing the assumptions made.

Assumptions
The shaft has a uniform circular cross section.
The shaft rotates at a constant (maximum) speed about its longitudinal axis.
The Centre of Gravity of the shaft is in the centre of the component.
A Safety Factor of 1.5 is used as it is deemed appropriate for this scenario. [23]
The component weight is negligible compared to the torsional forces caused by the motor torque output.
Loads are dynamic due to rotation of the shaft.

4.6.3 Material Selection

Table 4X below shows the material benchmarking work completed.

Table 4X: A table showing the options for driveshaft material [22]

Parameter	Low Carbon Steel	Aluminum Alloy	Carbon Fiber
Density (kg/m ³)	7800-7820	2640-2810	1500-1600
Elastic Modulus (GPa)	200-220	69-75	69-150
Tensile Strength (MPa)	379-532	186-510	550-1050
Yield Strength (MPa)	255-355	109-439	550-1050
Elongation (% Strain)	25-45	2.5-14	0.32-0.35
Melting Point (*C)	1480-1530	524-650	-
Price (£/kg)	0.57-0.59	1.89-2040	26.3-29.2

Table 4Y below shows the decision matrix used for material choice.

Table 4Y: A table showing the decision matrix for material choice

Parameter	Weighting	Low Carbon Steel	Aluminum Alloy	Carbon Fiber
Density (kg/m ³)	0.6	2 (1.2)	4 (2.4)	5 (3)
Elastic Modulus (GPa)	0.8	5 (4)	1 (0.8)	2 (1.6)
Tensile Strength (MPa)	0.9	4 (3.6)	2 (1.8)	5 (4.5)
Price (£/kg)	1	5 (5)	3 (3)	1 (1)
Total	-	13.8	8	10.1

From Table 4Y, the best option for material choice is Low Carbon Steel due to its cheap and strong properties.

4.6.4 Numerical Analysis

To reduce the weight of the driveshaft, the driveshaft will have a hollowed out cross section. The effect this hollowing has on the Shear Criteria is shown in the next section. All calculations can be found in Appendix 4B.

4.6.4.1 Maximum Shear Criteria

The maximum shear stress which can be achieved in the driveshaft is given by [24]:

$$\tau_{Max} = \frac{S_y}{N}$$

Where S_y is the Material Yield Strength and N is the Safety Factor. From this it can be determined that to avoid failure [24]:

$$\frac{S_y}{N} > \sqrt{\sigma_x^2 + 4\tau_{xy}^2}$$

$$\text{Where, } \sigma_x = \frac{32 * \text{Bending Moment}}{\pi * \text{Diameter}^3} \text{ and } \tau_{xy} = \frac{16 * \text{Output Torque}}{\pi * \text{Diameter}^3}$$

Due to the only loading on the driveshaft being dynamic, there is no Bending Moment in the system [24]. Due to this the following equations can be derived for Diameter requirements for a solid shaft and a hollowed shaft.

$$D > \sqrt[3]{\frac{32T}{\pi \frac{S_y}{N}}}$$

$$D_i < D_o - \sqrt[3]{\frac{32T}{\pi \frac{S_y}{N}}}$$

Table 4Z below shows the parameters used in the analysis and the resulting minimum diameter required for the shaft to not fail.

Table 4Z: A table showing the parameter values

Parameter	Value
Output Torque (Nm)	2760
Yield Strength (MPa)	305
Safety Factor	1.5
Minimum Diameter (mm)	51.71

It was decided that an Outer Diameter of 55mm will be used on the driveshaft. Using the above equation for hollowed shaft diameter requirements, the following maximum inner diameter was calculated.

$$D_i < D_o - \sqrt[3]{\frac{32T}{\pi \frac{S_y}{N}}} < 3.29mm$$

From the requirements, the inner shaft diameter has been chosen as 3mm. Table 4AA below shows the final Specifications for the driveshaft.

Table 4AA: A table showing the final driveshaft specs

Parameter	Value
Length (m)	0.75
Volume (m ³)	1.6x10 ⁻³
Density (kg/m ³)	7810
Mass (kg)	12.44
Mass reduction from hollowing out shaft	11%

4.6.5 Technical Drawing

Figure 4L shows the technical drawing for the driveshaft.

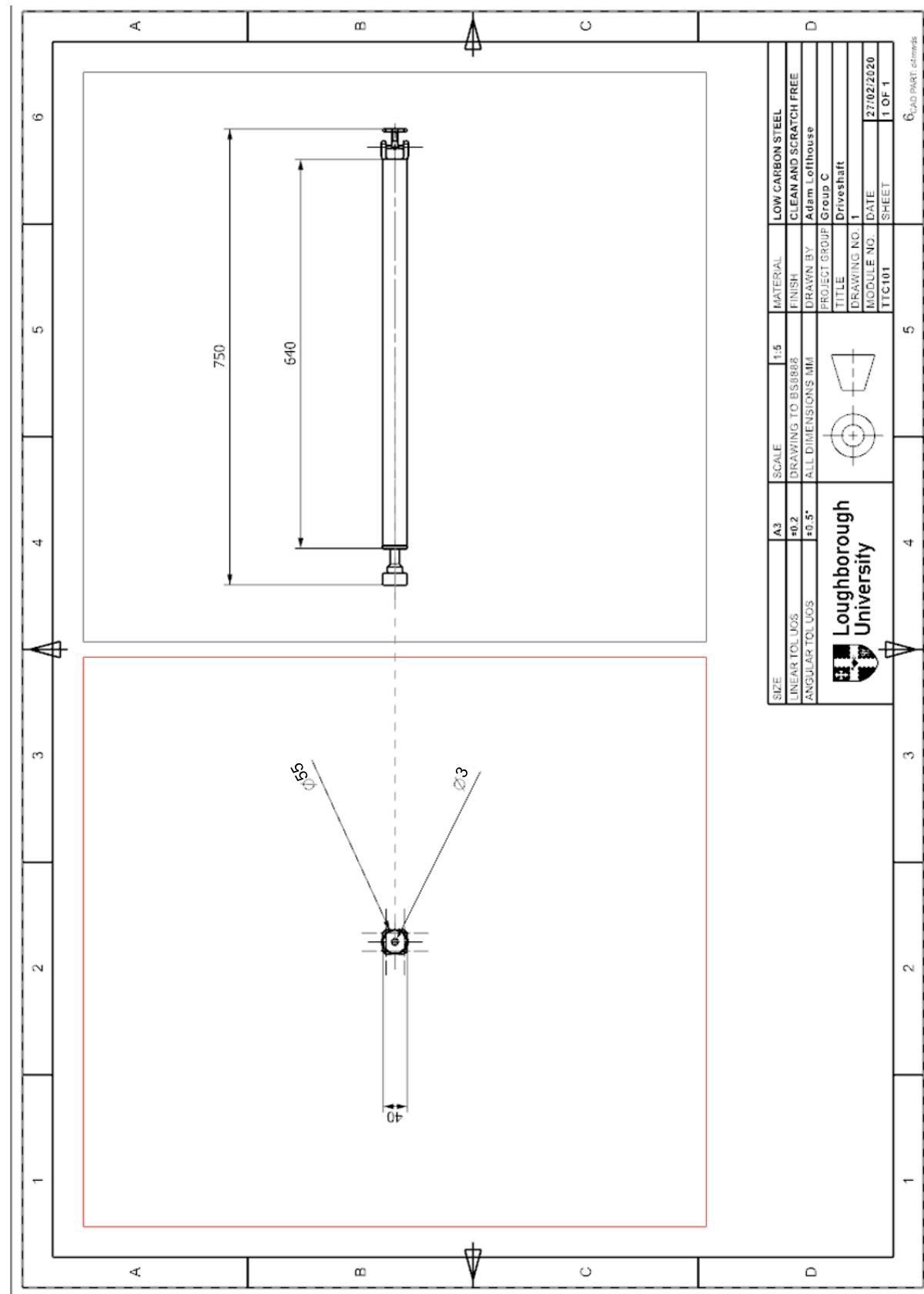


Figure 4L: A figure showing the Technical Drawing for the Driveshaft

Appendix

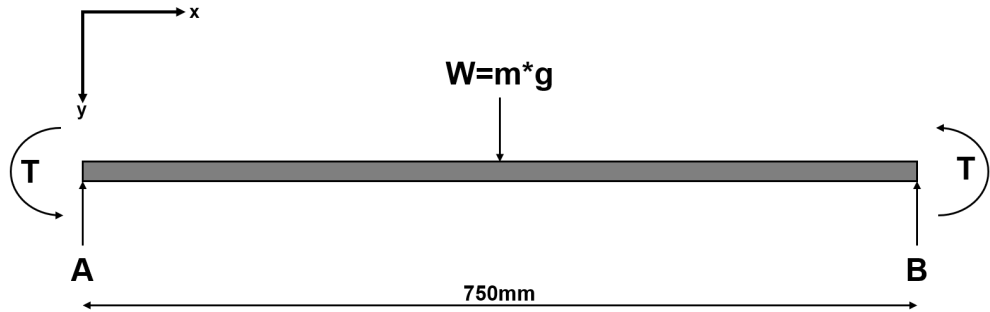
Appendix 4A

$$E_{ij} = \frac{d_{ij}}{3600} \left[mg(A_d \cos\theta_{ij} + \sin\theta_{ij}) + 0.00386(\rho C_d A v_{ij}^2) + m \left(\frac{dv}{dt} \right)_{ij} \right]$$

Where:

- E_{ij} = Mechanical energy required at the wheels to drive on a distance [kWh]
- m_{ij} = Total vehicle mass [kg]
- g = Gravitational acceleration $\left[\frac{m}{s^2}\right]$
- A_d = Vehicle coefficient of rolling resistance [-]
- θ = Road gradient angle [°]
- ρ = Air density $\left[\frac{kg}{m^3}\right]$
- C_d = Drag coefficient of the vehicle [-]
- A = Vehicle equivalent cross section [m^2]
- v_{ij} = Vehicle speed between the point and the point $\left[\frac{km}{h}\right]$
- d_{ij} = Distance driven from point to point [km]

Appendix 4B



The maximum shear stress is calculated as:

$$\tau_{Max} = \frac{S_y}{N} = 205MPa$$

Deriving Diameter Requirements Equations:

$$\frac{S_y}{N} > \sqrt{\sigma_x^2 + 4\tau_{xy}^2}$$

$$\sigma_x = 0 \text{ and } \tau_{xy} = \frac{16T}{\pi D^3}$$

$$\frac{S_y}{N} > \sqrt{4 \cdot \left(\frac{16T}{\pi D^3} \right)^2}$$

$$\frac{S_y}{N} > \frac{32T}{\pi D^3}$$

$$D > \sqrt[3]{\frac{32T}{\pi \frac{S_y}{N}}}$$

For hollowed out shafts:

$$D_o - D_i > \sqrt[3]{\frac{32T}{\pi \frac{S_y}{N}}}$$

$$D_i < D_o - \sqrt[3]{\frac{32T}{\pi \frac{S_y}{N}}}$$

Minimum Diameter Calculations:

$$D > \sqrt[3]{\frac{32T}{\pi \frac{S_y}{N}}} = \sqrt[3]{\frac{32(2760)}{\pi(205 \times 10^6)}} = 51.71mm$$

Maximum Inner Diameter Calculations:

$$D_i < D_o - \sqrt[3]{\frac{32T}{\pi \frac{S_y}{N}}} = (55 \times 10^{-3}) - \sqrt[3]{\frac{32(2760)}{\pi(205 \times 10^6)}} = 3.29 \text{ mm}$$

References

Final Powertrain System:

- [1] - <https://www.scribd.com/document/360801521/energies-08-08573> - Accessed 12/2/20
- [2] - <http://www.sankey-diagrams.com/electric-vehicle-with-energy-recuperation/> - Accessed 15/2/20
- [3] - <https://www.fueleconomy.gov/feg/atv-ev.shtml> - Accessed 15/2/20
- [4] - <http://www.sankey-diagrams.com/tag/bus/> - Accessed 15/2/20
- [5] - https://www.engineeringtoolbox.com/electrical-motor-heat-loss-d_898.html - Accessed 15/2/20

Motor System:

- [6] - https://www.danatm4.com/wp-content/uploads/2019/08/TM4-SUMO-MD_Dana-TM4_web.pdf - Accessed 23/10/19
- [7] -
http://www.farnell.com/datasheets/52020.pdf?fbclid=IwAR3kjKai_QFHjnfHc04KtrlfTKtiHZvNo-KivxmMcFKNZbetxnNQOaiPutQ - Accessed 21/2/20
- [8] - <https://www.fuelcellstore.com/blog-section/electrical-subsystem-fuel-cells> - Accessed 20/2/20
- [9] - http://www.bullernatverket.se/wp-content/uploads/2014/05/Electric-buses-and-noise_Volvo-Bus.pdf - Accessed 21/2/20
- [10] -
https://learn.lboro.ac.uk/pluginfile.php/1092011/mod_resource/content/1/Useful%20acoustic%20scales.pdf - Accessed 21/2/20

Battery System:

- [11] - <https://lithiumwerks.com/valence-batteries/standard-modules/xp-module/> - Accessed 1/11/19
- [12] - <https://www.chademo.com/>

Fuel Cell System:

- [13] - <http://www.hydrogenics.com/wp-content/uploads/HyPM-30-Spec-Sheet.pdf> - Accessed 3/2/20
- [14] - <https://www.powercell.se/wordpress/wp-content/uploads/2018/12/powercell-ms-30-datasheet-18-11-26.pdf> - Accessed 3/2/20
- [15] - https://www.ballard.com/docs/default-source/spec-sheets/fcvelocitymd.pdf?sfvrsn=ebc380_2 - Accessed 3/2/20
- [16] - https://www.ballard.com/docs/default-source/spec-sheets/fcvelocity-hd.pdf?sfvrsn=2debc380_2 - Accessed 3/2/20
- [17] - <http://www.luxfercylinders.com/products/g-stor-h2#tech-spec> - Accessed 3/2/20
- [18] - https://worthingtonindustries.com/getmedia/36f82710-5051-441d-9760-b7afe0aba690/Hydrogen-Type-III-Spec-sheet_7.pdf?ext=.pdf - Accessed 3/2/20

[19] - <https://www.mahytec.com/en/products/compressed-hydrogen-storage/> - Accessed 3/2/20

[20] - https://www.epj-conferences.org/articles/epjconf/pdf/2017/17/epjconf_eps-sif2017_00013.pdf - Accessed 4/2/20

[21] - <https://hydrogenezurope.eu/refueling-stations> - Accessed 1/3/20

Design for Minimum Weight:

[22] - CES Edupack - Accessed 1/2/20

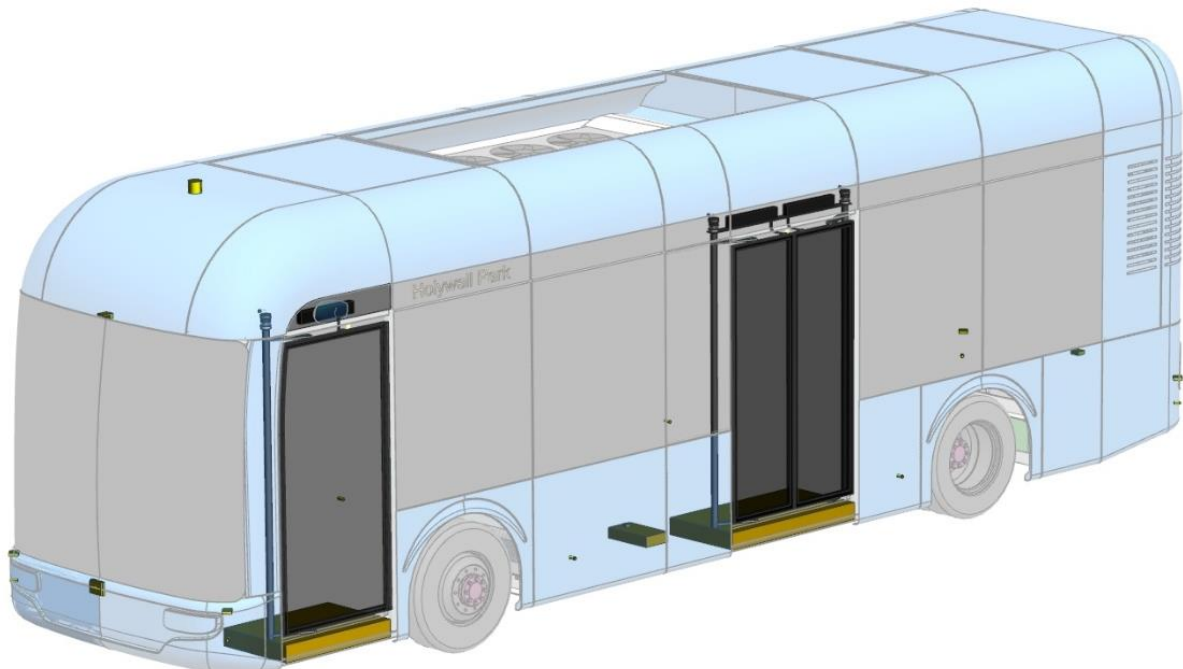
[23] -
https://learn.lboro.ac.uk/pluginfile.php/623708/mod_resource/content/3/TTB207_machine_elements_notes_DJO_L1_2.pdf - Accessed 14/2/20

[23] -
https://learn.lboro.ac.uk/pluginfile.php/623745/mod_resource/content/1/TTB207_machine_elements_notes_DJO_L4.pdf - Accessed 14/2/20

Vehicle Concept Definition and Design: Design Report

Section 5

Autonomy, Ramp and Door Systems



(s) Paul Theodosie - B716787

Number of Pages: 25
Number of Words: 1991

Contents

5.1 Introduction	103
5.2 Autonomous Driving.....	103
5.2.1 Requirements.....	103
5.2.2 Final Specification	104
5.2.3 System Description	105
Field of View and Positioning	105
System Diagrams	109
5.2.4 System Performance.....	110
5.3 Passengers Loading and Unloading	111
5.3.1 Requirements	111
5.3.2 System Description	111
Passengers Loading	111
Passengers Unloading	112
5.3.3 System Performance.....	113
5.4 Ramp System.....	113
5.4.1 Requirements	113
5.4.2 Final Specification	113
5.4.3 System Description	114
5.4.4 System Performance.....	114
5.5 Door System	115
5.5.1 Requirements	115
5.5.2 Final Specification	115
5.5.3 System Description	115
5.5.4 System Performance.....	117
5.6 Design for Minimum Weight.....	117
5.6.1 Initial Design.....	117
5.6.2 Materials.....	118
5.6.3 Analysis Assumptions	118
5.6.4 Load Cases	119
5.6.5 Results	120
5.6.6 Manufacture	120
5.6.7 Final Design	120
Appendix	122
Appendix A	122
Appendix B	123
References	125

5.1 Introduction

This section of the report outlines the final specifications of the autonomous system, along with the design of the door and ramp systems of the bus. Following the concept stage, the ramp system has been slightly optimized, while the bus-stop procedure has been revamped to be more efficient. A minimum weight analysis is also considered in this section on the door system brackets.

5.2 Autonomous Driving

5.2.1 Requirements

The concept stage requirements for the autonomous driving system are presented below in the system targets and objectives table.

Table 5A: Autonomous driving targets and objectives

Code	Targets	Achieved during concept stage?	Obtaining/ Refining method
T1	Level 4 SAE autonomy	Yes	Driver isn't required to intervene in the driving (see 5.2.3)
T2	No critical blind spots around the bus	Yes	Scaled sketches have been produced, using every sensor's horizontal and vertical field of view (see 5.2.3)
T3	Reaction time to be as quick as a human driver	Yes	The choice and performance of the control unit (see 5.2.4)
T4	Sensor field of view to reach 200 m in range, which would help with gaining time and preventing unexpected manoeuvres	Yes	The Velodyne VPL-32C Ultra Puck Lidar gives a 200 m 3D perspective imagery around the bus
T5	Average 1 minute saved every university campus bus cycle compared to non-autonomous driving	Not discussed	The automated driving of the bus saves an average of 1 minute per bus cycle (see 5.2.4)

5.2.2 Final Specification

Table 5B: Components specification details

Component	Size (mm)	Weight (kg)	Cost (£)	Power (W)	Description
Velodyne VPL-32C Ultra Puck Lidar [1]	100x100x87	0.925	3000-10000	10	<ul style="list-style-type: none"> Offers an accurate and 3D perspective image at range around the bus
Continental MFC500 Camera [2]	88x70x38	0.2x3	100x3	7x3	<ul style="list-style-type: none"> Detects traffic signs and lights. It is a mono camera, meaning that it captures a small part of the light spectrum with each filter, making room for more detail.
Continental ARS540 Long range radar (LRR) [3]	130x101x32	0.4	40	16	<ul style="list-style-type: none"> Gives accurate readings of a target's speed and position. Not affected by weather changing conditions.
Bosch MRR rear Medium range radar (MRR) [4]	70x82x30	0.19	35	8	<ul style="list-style-type: none"> Vision at the rear needs to be checked too, but it doesn't require the range used for the front. MRR doesn't have the range of the LRR, but it has a wider field of view, giving a better perspective at the rear.
Continental SRR520 Short range radar (SRR) [5]	83x69x22	0.17x4	35x4	4.5x4	<ul style="list-style-type: none"> Better than MRR or LRR for proximity detection in blind spots
Bosch Ultrasonics [6]	26x26x44	0.14x8	120x8	4x8	<ul style="list-style-type: none"> Helps with parking and manoeuvring in tight spaces because of its proximity detection
Garmin GPS16-HVS (GPS)	86x86x42	0.032	66	3	<ul style="list-style-type: none"> Crucial to have an existing pre-uploaded map of the University campus route
Inertial Labs IMU-P (Inertial measurement unit)	39x45x22	0.07	300	8	<ul style="list-style-type: none"> Locates the vehicle after knowing the initial position. Requires no information from the external world. Makes up for the often inaccuracies of the GPS.
NXP Bluebox Control Unit [7]	400x220x80	2.5	4631	192	<ul style="list-style-type: none"> It is the computer that does the sensor fusion and makes the necessary driving decisions
Total		6.517	9472-16472	308	

*the weight, cost and power consumption of every component was multiplied by the number of components of that type in the system.

The only change that has been made since the concept stage is the addition of 2 extra cameras positioned on top of the entry and exit doors with the purpose of monitoring the passenger flow during bus-stops. As it does not majorly influence the driving, but the loading of the passengers, this will be further discussed in section 5.3. This change added 0.4 kg to the weight, £200 to the cost and 14 W to the power consumption.

5.2.3 System Description

Field of View and Positioning

Table 5C: Field of view data

Sensor	Range (m)	Horizontal FOV (°)	Vertical FOV (°)
Lidar	200	360	-25 to +15
Camera	50	120	60
Long range radar	200	20	18
Medium range radar	80	90	10
Short range radar	30	140	6
Ultrasonic	5.5	160	4

To check for blind spots and achieve T2, the component data from Table 5C was used in the concept report to produce the horizontal (Figure 5A) and vertical (Figure 5B) sketches of the bus FOV. The figures only represent the field of view in the proximity of the bus, while the maximum ranges of the sensors are presented in the table above.

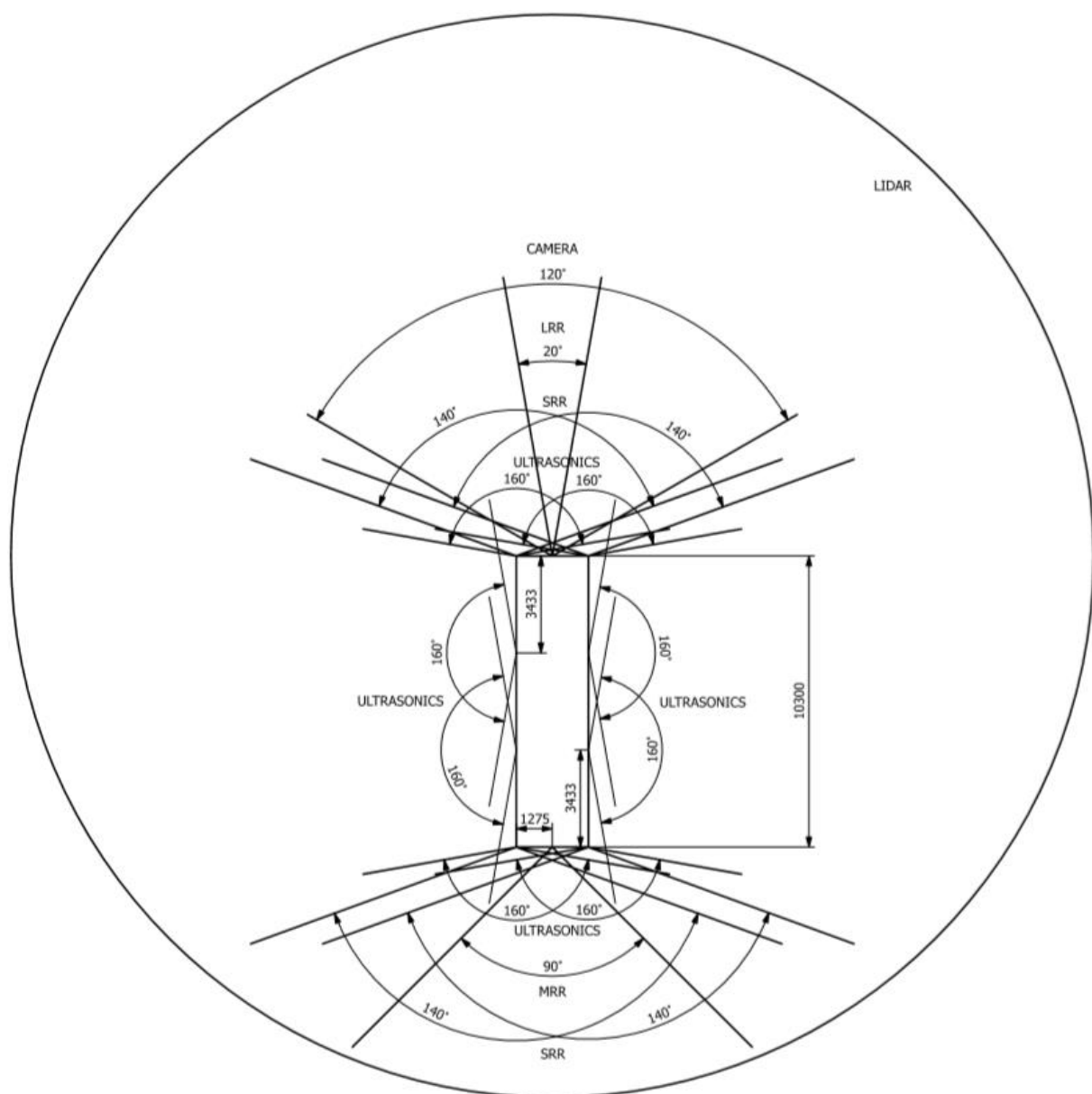


Figure 5A: Horizontal field of view

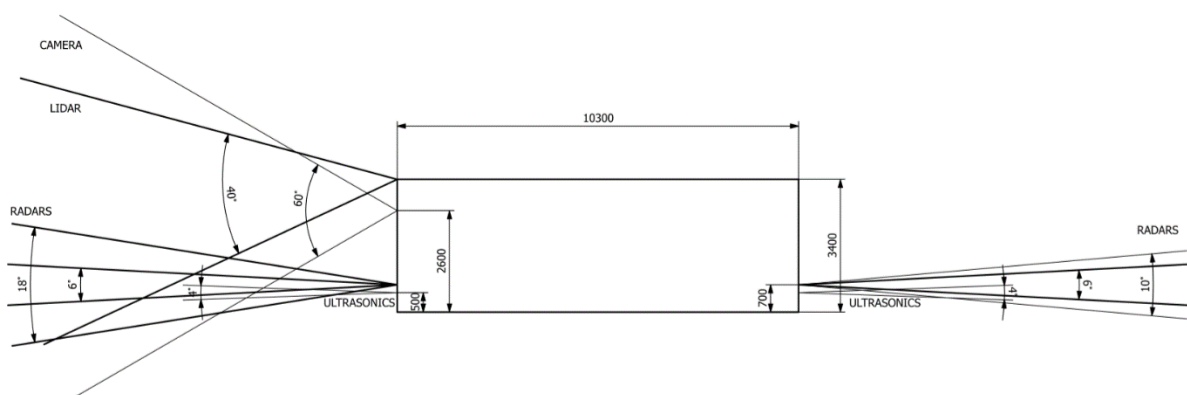


Figure 5B: Vertical field of view

Figures 5C, 5D and 5E show the positioning of the detection sensors on the bus.

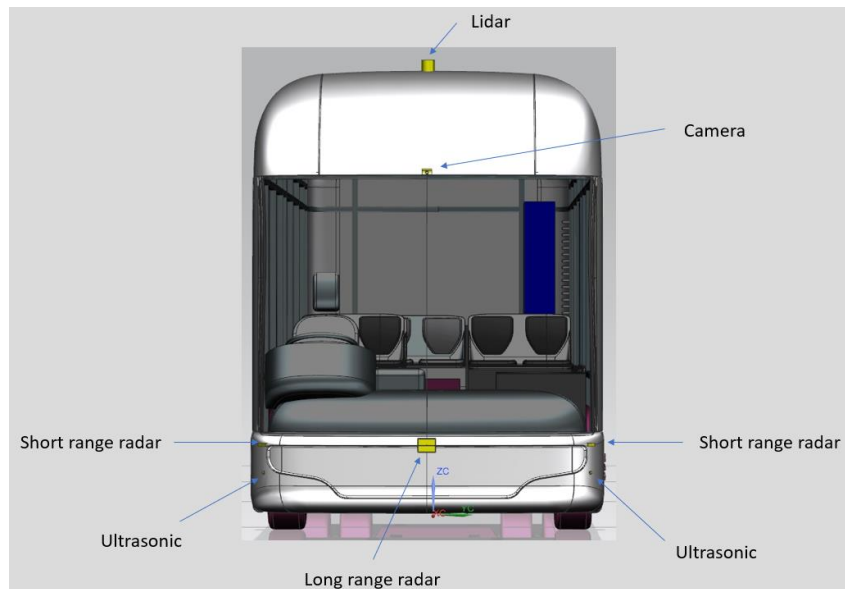


Figure 5C: Sensor placement at the front

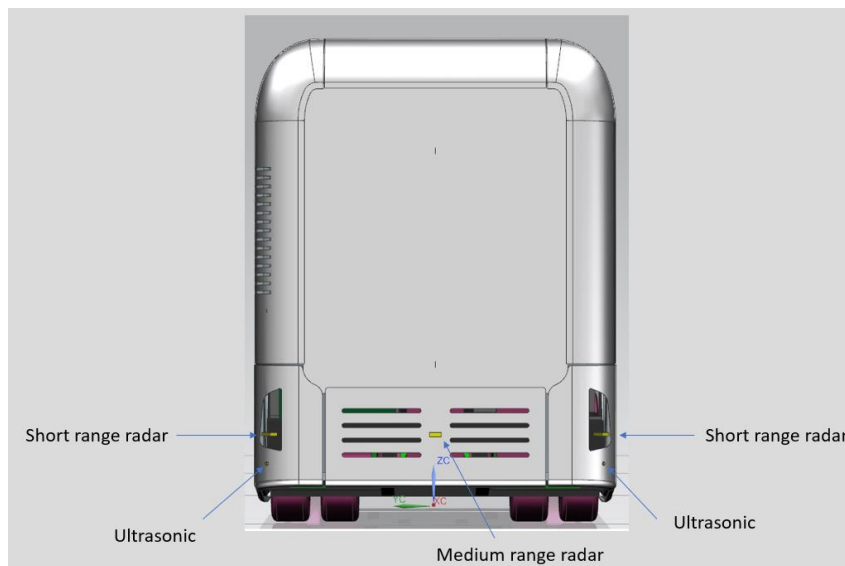


Figure 5D: Sensor placement at the rear

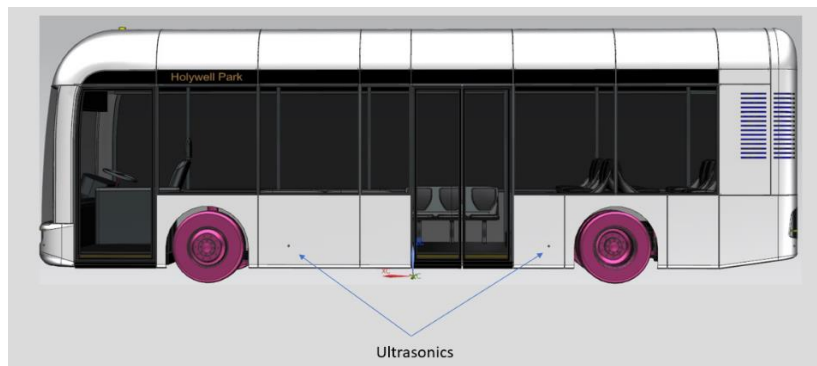


Figure 5E: Sensor placement on the side

Table 5D: Justification of sensor placement

Sensor	Placement reasoning
Lidar	<ul style="list-style-type: none"> Front of the rooftop offers the best vision at the front, which is being prioritised. It cannot use its vertical FOV for the portion under the rooftop at the rear. However, this is not needed because the radars can detect approaching or overtaking vehicles. Adding a Lidar at the back would've increased the cost exponentially.
Camera	<ul style="list-style-type: none"> 2600 mm off the ground is an ideal height for detecting traffic signs and lights
LRR	<ul style="list-style-type: none"> Important to have accurate readings in front of the bus at range
MRR	<ul style="list-style-type: none"> It has a wider FOV than LRR Range of LRR is not needed at the rear
SRR	<ul style="list-style-type: none"> Corners represent blind spots Better than MRR and LRR for proximity detection Rangier than ultrasonic sensors
Ultrasonic	<ul style="list-style-type: none"> Placed in corners and on the sides to help with parking and going into narrow spaces Better at proximity detection than SRR

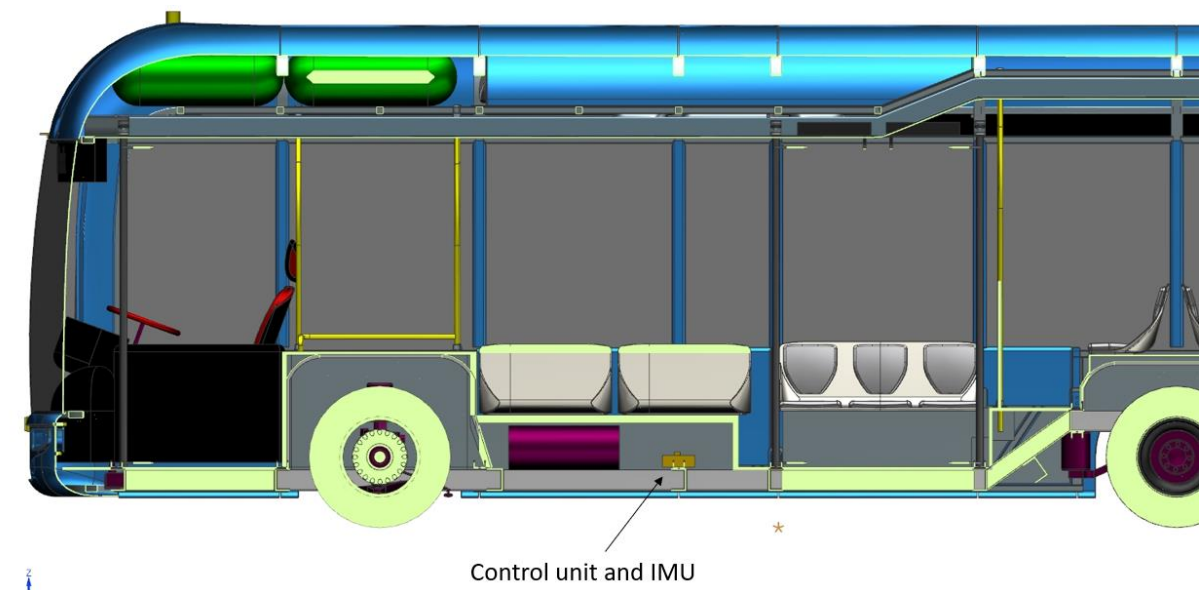


Figure 5F: Control unit and IMU

System Diagrams

The data collected by every set of sensors is transmitted via Ethernet to the control unit (Figure 5G), which proceeds then with the sensor fusion.

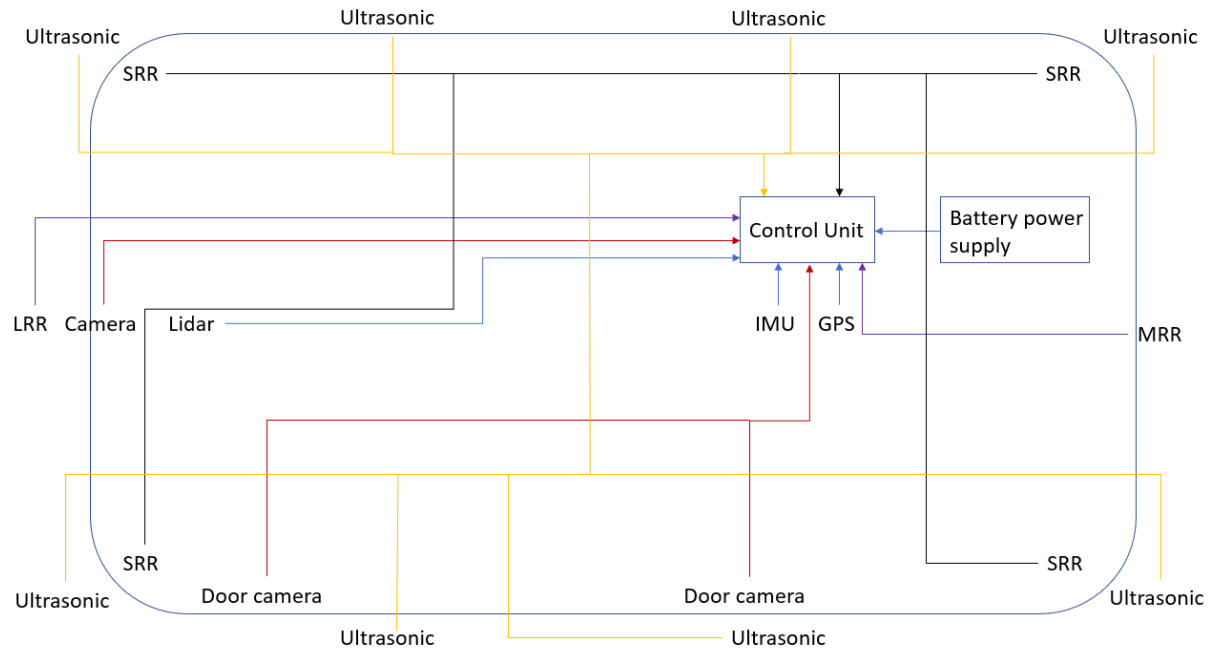


Figure 5G: Sending of information

After the fusion of the information is complete, the unit makes the necessary decision and sends electric signals to the domain actuators (Figure 5H). Being a level 4 autonomy system, it doesn't require the input of the driver, even though there always needs to be one present to take over in case of a catastrophic control unit failure. The NXP Bluebox is equipped with an emergency system that would be able to stop the vehicle before failure, which would be followed by a restart and normal takeover by the driver [4].

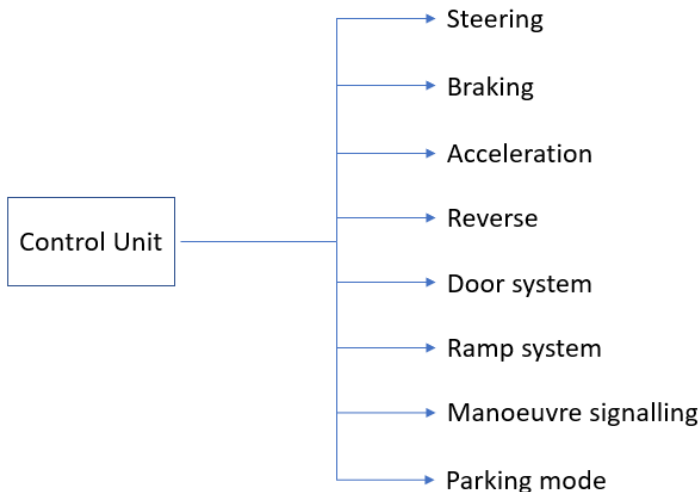


Figure 5H: Domain actuators

5.2.4 System Performance

From the market benchmarking [8], the set of sensors selected in this design generates an estimated 110.83 Mbps, which translates into 49.875 GB/hr. Therefore, the Bluebox that comes with a 256 GB SSD [7] can permanently store approximately 5 hours of driving data (23 bus cycles). After the SSD storage is full, the flash kicks in, which is easily rewritable. Since the bus follows the same route, the information already gathered could help save time on the next trip, for example: it would foresee a turn or an uphill gradient from further away, meaning it could prepare its speed sooner so there would be no sudden manoeuvres.

The average human reaction time is 0.25 seconds for visual stimulus. Since the NXP Bluebox is capable of processing 90000 million instructions per second [7], in a span of 0.25 secs the control unit would be able to process 22500 million. Assuming from studied data [9][10] that:

- Sensory part: 10000 neurons = 50 mil instructions
- Data processing part: 250000 neurons = 250 mil instructions
- Moving away: 500000 neurons coordinate and move muscles = 500 mil instructions

In total that would add to 800 mil instructions required in the 0.25 sec time span of a human reflex (less than the 22500 mil. of Bluebox). Even though the analysis is assuming and there should be a margin of error, it shows that the control unit is just as capable as a human driver at reacting (target T3).

Since a human driver has more blind spots and a FOV with a shorter range than an autonomous system, it could lead to inconsistencies in driving for e.g.: travelling at the wrong speed or lift off for an upcoming blind spot. Having a Lidar that can foresee these situations gives the control unit the opportunity to compute a more consistent trip. As a result, it is possible that the autonomous system could save a number like 5 seconds between each stop. Considering there are 13 stops in one cycle (Figure 5I), this would mean about 1 minute saved per bus cycle (T5).

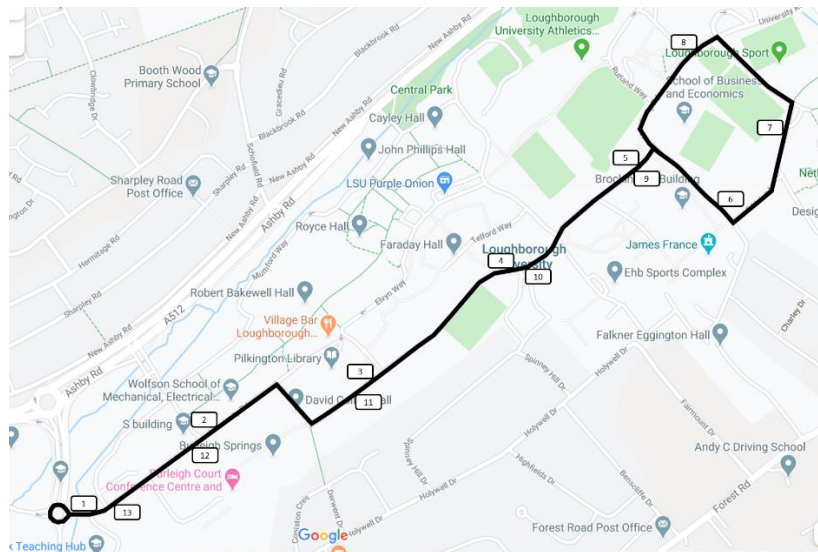


Figure 5I: Bus cycle figure (also present in Section 4)

5.3 Passengers Loading and Unloading

5.3.1 Requirements

Table 5E: Passenger loading targets

Code	Targets	Achieved at concept?	Obtaining method / Refining method
T6	Have an efficient fully autonomous passenger loading system	No	<ul style="list-style-type: none">• Extra cameras have been added to monitor the passengers flow.• A door closing timer has been added to avoid trapping people.
T7	Efficient contactless payment	Yes	<ul style="list-style-type: none">• A scanning device next to each door has been proposed
T8	Ability to be on time	Yes	<ul style="list-style-type: none">• Implementing autonomy helps with consistency.• Implementation of a phone app for live tracking.

5.3.2 System Description

The bus is pre-set by the control unit to stop in every marked bus-stop from Figure 5I. It will have to rely on the Lidar, IMU and front camera to pull in the stop more safely because of the inaccuracies of the GPS. The bus will open both doors in every stop and in case of the wheelchair ramp being used, it will be retracted after the doors have closed.

The utility of the mobile app is shown in Table 5F.

Table 5F: Smartphone app utility

Feature
<ul style="list-style-type: none">• Live tracking of the bus and accurate timekeeping capabilities• Map of all buses in function• Surveillance capabilities to prevent for e.g.: 2 buses ending up right after one another• Ability to request wheelchair ramp• Provide a virtual bus card that can be scanned via mobile phone when onboard

Passengers Loading

The camera placed above the door would be able to detect the people with intent of coming in (Figures 5J and 5K). Every person boarding should scan their university ID or bus card (from Table 5F) to let the bus know who is on board. In case the wheelchair was not requested on the app, the camera can detect it [2] and deploy the ramp. The closing of the entry door is pre-announced on a light panel with a 5 seconds timer in order to avoid trapping people. The entry door closing procedure is shown in Figure 5L.

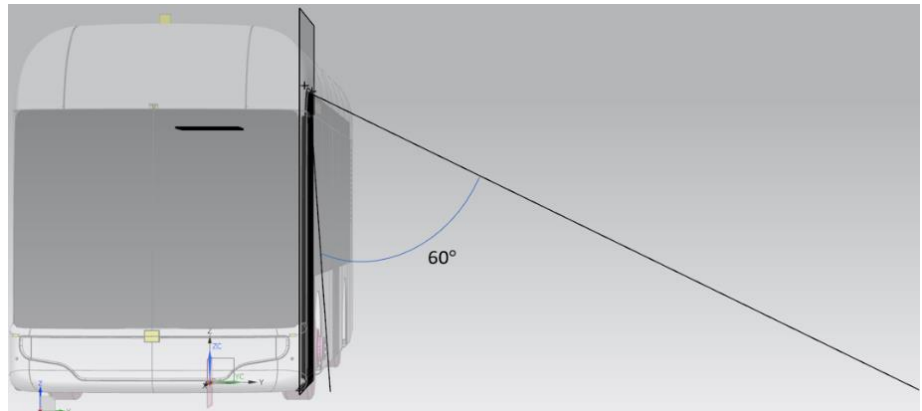


Figure 5J: Vertical FOV of camera

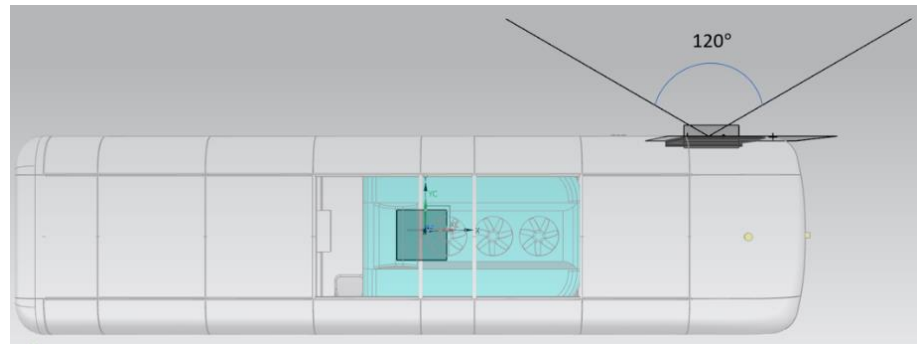


Figure 5K: Horizontal FOV of camera

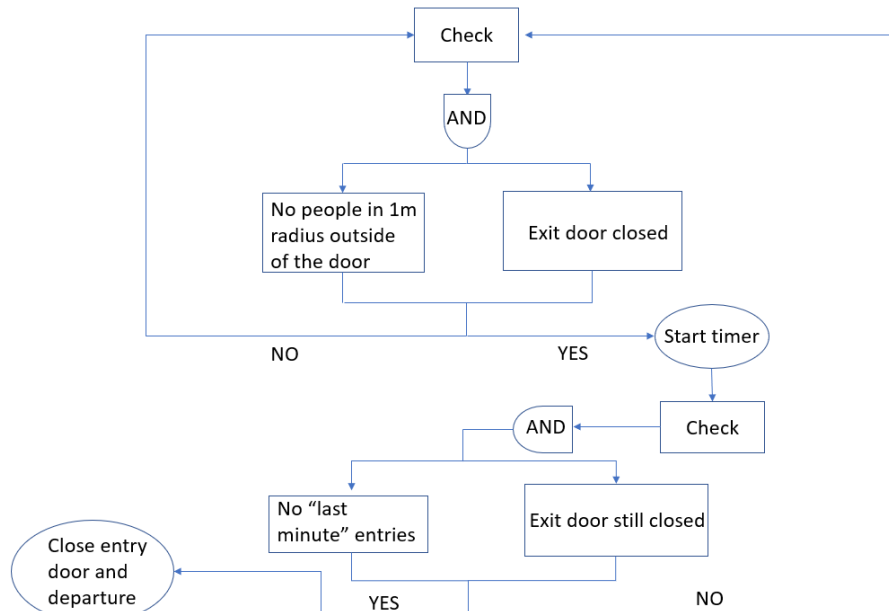


Figure 5L: Entry door closing procedure

Passengers Unloading

The ID or phone should be scanned before disembarking the bus as well. That way the computer will know the details of the journey and it would be able to withdraw credit like Oyster for example [11]. If a wheelchair ramp is required, there will be an interior button that can be pressed. The exit door closing timer would start after 5 seconds from the last ID scanning and if a person didn't manage to scan the card before the door closed, an emergency button could be pressed that would open it back.

5.3.3 System Performance

Assuming an average of 5 people embarking and disembarking per stop, it would mean 5 scans per door which can add up to about 10 seconds. Adding the two 5 second panel timers and considering the doors opening and closing times (see section 5.5.4), the total time would be 35 seconds. “Last minute” entries or exits that would momentarily disrupt the flow of the system were not considered in the calculation.

If the wheelchair is in use, the deployment and retracting time needs to be considered (see section 5.4.4) along with a safety time of an extra 5 seconds. The total estimate time in this case for a bus stop would be 50 seconds.

5.4 Ramp System

5.4.1 Requirements

Table 5G: Ramp system targets

Code	Targets	Achieved at Concept?	Obtaining method / Refining method
T9	Facilitate wheelchair users with accessible ramp system like the ones benchmarked [12]	Yes	<ul style="list-style-type: none"> Automated wheelchair that satisfies the legal requirements (>800 mm in width) Providing a convenient underfloor system.
T10	Ramp deployment and retracting time of 5 sec	Not discussed	<ul style="list-style-type: none"> Choosing a motor that would provide the necessary power (see 5.4.4)

5.4.2 Final Specification

Table 5H: Components specification details

Component	Size (mm)	Weight (kg)	Cost (£)	Power Consumption (W)
Front and Rear ramps	600x850x67	92.26 x 2	295.23 x 2	-
Electrotech-drives 63 frame 3 phase electric motor [13]	220x120x130	4.5 x 2	54 x 2	120 x 2
Total		193.52	698.46	240

Since the concept report, slight adjustments to the dimensions of the ramp have been made to satisfy the packaging. The changes have not affected its strength to support the required loads or the legal dimensioning requirements. The reduction saved 30 kg and £ 95 per ramp.

5.4.3 System Description

The material usually chosen in industry for ramp boards is Aluminium 6061 because of its excellent corrosion resistance, good machining and strength to weight ratio [14]. The ramps will have a rubbery material covering the aluminium board to provide a more suitable surface for the wheelchairs.

Table 5I: Material properties

Property	Specification
Tensile Yield Strength (MPa)	276
Shear Yield Strength (MPa)	207
Density (kg/m ³)	2700
Cost (£/kg)	3.2

The ramp is packaged in an underfloor cassette, from where is being deployed and retracted longitudinally, giving an advantage over the folding ramps in case of a fully packed bus [9].

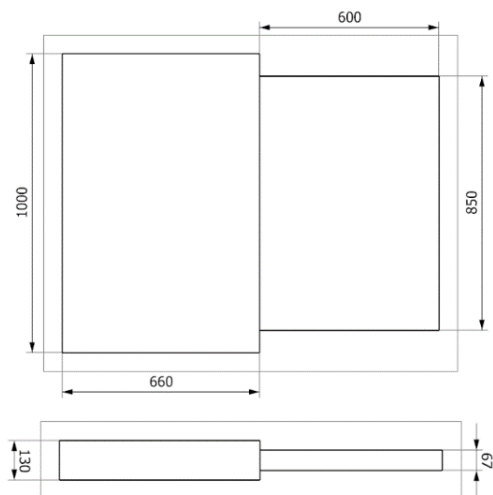


Figure 5M: Ramp and cassette dimensions

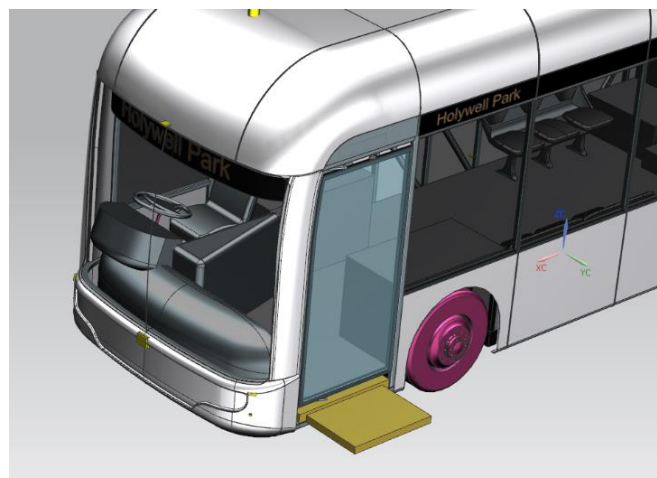


Figure 5N

5.4.4 System Performance

To satisfy T10, velocity of the ramp $v = \frac{0.6}{5} = 0.12 \text{ m/s}$.

From ramp weight \Rightarrow tractive force $F = 905 \text{ N} \Rightarrow P = F \times v = 108.6 \text{ W}$

After using a safety factor 1.1, the 0.12 kW motor is satisfactory.

An average human being along with a wheelchair weigh around 80 kg, which would give a distributed load of 784.8 N (see Figure 5O).

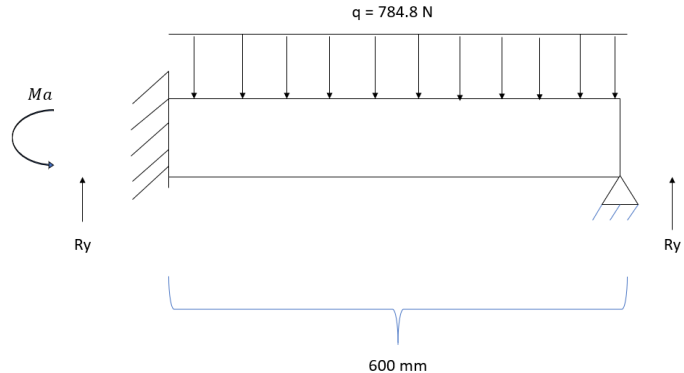


Figure 5O: Ramp FBD inclined to the ground

The deflection was found to be 0.0005 mm. The aluminium board could support loads that are up to 100 times bigger. However, this is assuming that the ramp acts as a cantilever beam when in fact, it doesn't have an infinitely strong and stiff support because it includes the axle and motor. All calculations, S.F and B.M diagrams can be found in Appendix A.

5.5 Door System

5.5.1 Requirements

Table 5J: Door system targets

Code	Targets	Achieved during concept stage?	Obtaining/ Refining Method
T11	Improve the efficiency of loading/unloading the passengers	Yes	A 2-door system is implemented to aid the flow of passengers
T12	Door opening and closing time of 5 seconds	Not discussed	Adding a reliable and efficient pneumatic system modelled after MAN [15]

5.5.2 Final Specification

Table 5K: Components specification details

Component	Size (mm)	Weight (kg)	Cost (£)
Front door	1000x50x2100	70	1050
Rear door	635x50x2100	45 x 2	840 x 2
Turning column	55x55x2240	42.73 x 3	193.5 x 3
Door bracket arm	328x55x12.5	1.67 x 6	7.56 x 6
Sliding system	500x20x100	4.5 x 3	13 x 3
Pneumatic system [12]	75x75x100	2 x 3	75 x 3
Total		317.71	3619.86

5.5.3 System Description

The door system functions pneumatically, which is more reliable, cost-effective and easier to install than a hydraulic one. Even though the hydraulic system is better at carrying heavier loads, the pneumatic system provides faster motion, which is ideal for bus doors.

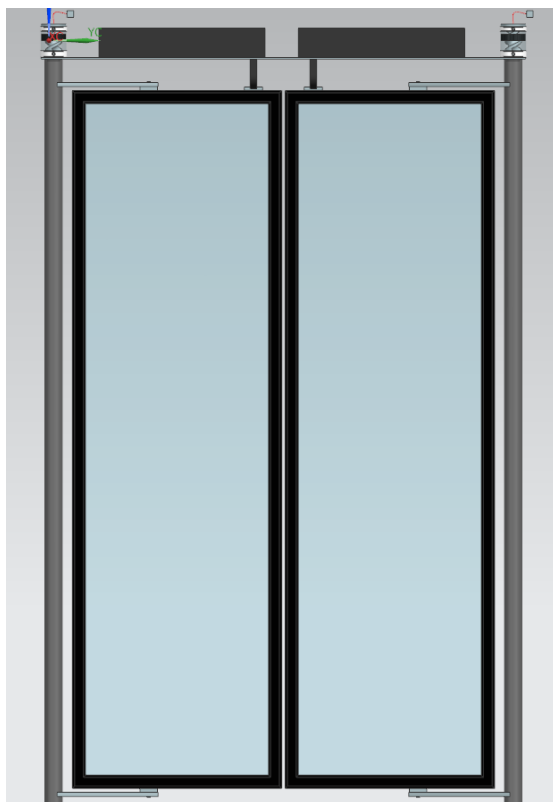


Figure 5P: Rear door

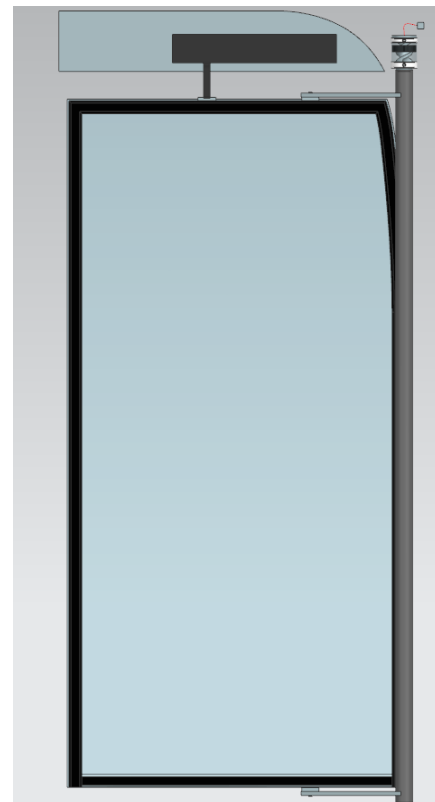


Figure 5Q: Front door

Referring to Figure 5R, the air compressors function when the actuator receives the signal from the control unit. The pressure difference from the compressed air moves the piston, enabling the rotation of the turning column.

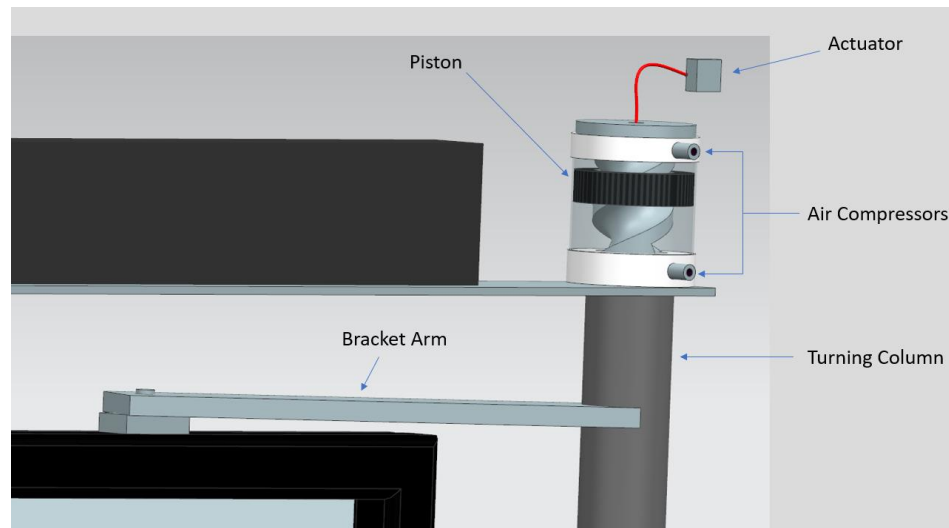


Figure 5R

The bracket arm is used to pull the door, as the turning column starts rotating. In order to have a safe and organised swing, the door's end needs to stay fixed. That is accomplished by having a sliding rail system (Figure 5S). One end of the door is pulled by the bracket arms, while the other stays fixed and slides towards the turning column.

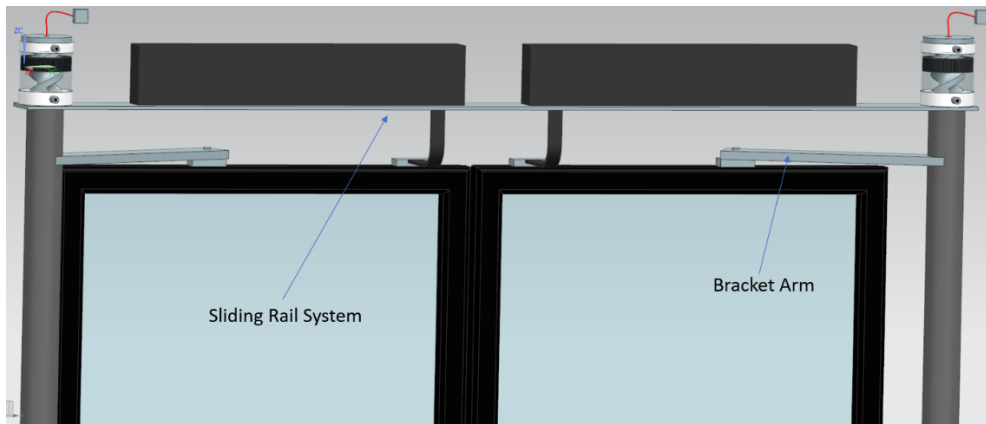


Figure 5S

5.5.4 System Performance

The constant angular velocity of the turning column required to achieve the 5 sec target (T12) was calculated:

$$\omega = \frac{\Delta\theta}{\Delta t} = \frac{\pi/2}{5} = 0.3 \text{ rad/s}$$

* ω = angular velocity (rad/s); $\Delta\theta$ = radial distance travelled (rad); Δt = time (s)

$$v = \omega * r = 0.3 * 0.0275 = 0.00825 \frac{m}{s} = 8.25 \text{ mm/s}$$

* v = linear velocity (m/s); r = radius of the turning column (m)

Considering the weight of the turning column, the rotational force to achieve this velocity is 420 N.

5.6 Design for Minimum Weight

The selected component is the bracket arm for the door system. One door is handled by 2 brackets: one at the top and the other at the bottom of the door (see Figure 5V). Each bracket will be welded to the turning column and will rotate with the help of a bearing on the other side.

5.6.1 Initial Design

The bracket is 328x55x20. It has a 12 mm fixing hole for the door and a 55 mm diameter cut in order to help welding it to the turning column.

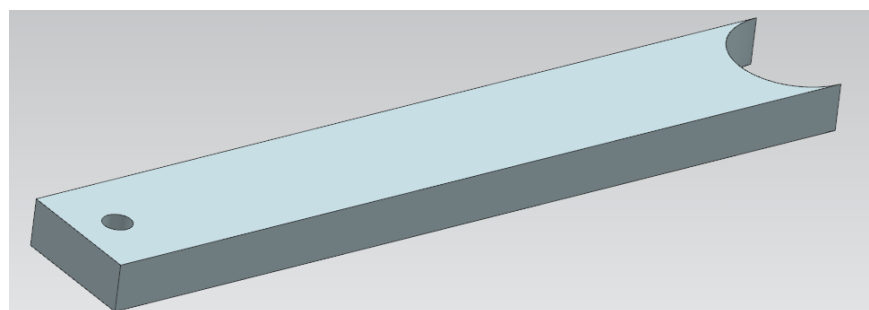


Figure 5T

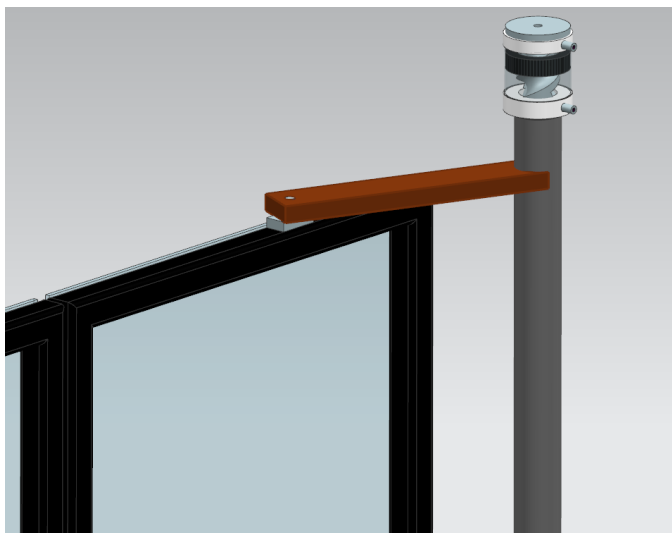


Figure 5U

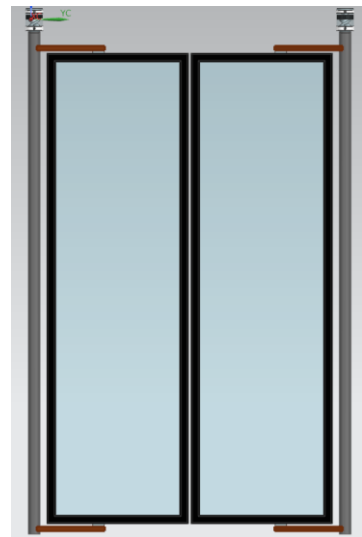


Figure 5V

5.6.2 Materials

The material chosen was stainless steel with the 316L specification, after using CES Edupack and [16]. It is a durable and cost-effective material that has great corrosion resistance, good strength and requires low maintenance. Stainless steel is generally an excellent material for welding and machining at low speeds. To improve the weldability and machining capabilities of the bracket, 316L steel was chosen instead of 316 because of the lower carbon content.

Table 5L: Material Properties

Property	Specification
Young's Modulus (GPa)	193
Tensile Yield Strength (MPa)	170
Ultimate Tensile Strength (MPa)	485
Shear Yield Strength (MPa)	102
Ultimate Shear Strength (MPa)	291
Density (kg/m ³)	8000
Cost (£/kg)	4.53

5.6.3 Analysis Assumptions

Table 5M: Analysis assumptions

Assumptions

- A safety factor of 1.25 is accounted for during the calculations.
- The turning column is infinitely strong and stiff.
- Only the front door is accounted for in calculations because it is heavier than one rear door. Assuming the bracket could support the front door, it would be able to support the rear one as well.
- Since there are 2 brackets supporting one door, it is assumed that one bracket needs to support half of the door weight.
- Bracket behaves like a cantilever beam.

5.6.4 Load Cases

All calculations, S.F and B.M diagrams can be found in the Appendix B.

Table 5N: Load cases

Load case	Description
Static Load	As stated in the assumptions, the bracket supports half of the mass of the door and behaves like a cantilever beam (Figure 5W). The chosen maximum deflection for this application is 2 mm.
Dynamic Load	The bracket needs to withstand the dynamics of opening and closing the door. The load is applied laterally (Figure 5X).
Longitudinal Acceleration	This is taken from the TL section (Figure 5Y)
Lateral Acceleration	The load from the TL section is distributed like in the Dynamic case (Figure 5X)
Crash Load	The crash load from the TL section is distributed both longitudinally and laterally
Abuse Load	The door system could be subject to abuse from passengers. Since this is a subjective load, the maximum amount of extra abuse before bending failure will be calculated instead. The abuse will be thought of as an extra load to the static case.

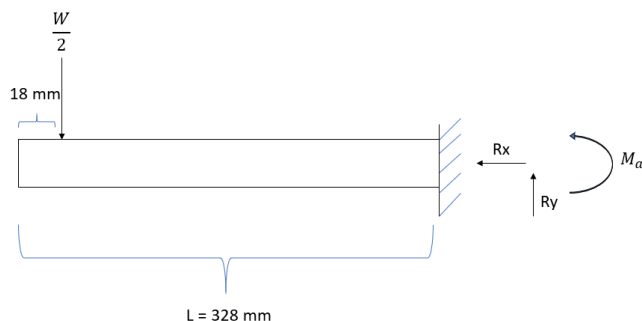


Figure 5W: Bracket cantilever FBD – static case



Figure 5X: Lateral distribution of load



Figure 5Y: Longitudinal distribution of load

5.6.5 Results

The DFMW analysis was done on the bracket's thickness. Table 5O shows the minimum required thickness of the bracket in order to withstand the load cases. The final design thickness was chosen to be 12.5 mm as 12.43 mm is highest value from the table below.

Table 5O: Bracket thickness results

Condition	Minimum thickness (mm)
Shear stress	0.09
Bending moment	8.26
Deflection	12.43
Dynamic - bearing failure	0.2
Dynamic – shear out	0.04
Longitudinal Acceleration – bearing failure	0.02
Longitudinal acceleration – shear out	0.004
Lateral acceleration – bearing failure	0.06
Lateral acceleration – shear out	0.01
Crash – bearing failure	2.1
Longitudinal Crash – shear out	0.4
Lateral Crash – shear out	0.34

Going with the selected bracket thickness, the maximum amount of abuse before a bending failure is an extra 442 N.

5.6.6 Manufacture

The manufacturing process for this component is simplistic. The bracket should be first cut at the required dimensions and have a hole of 12 mm drilled for the bearing. The bracket should then be TIG welded to the stainless-steel turning column. Lastly, the door should be mounted on the top and bottom brackets at the same time.

5.6.7 Final Design

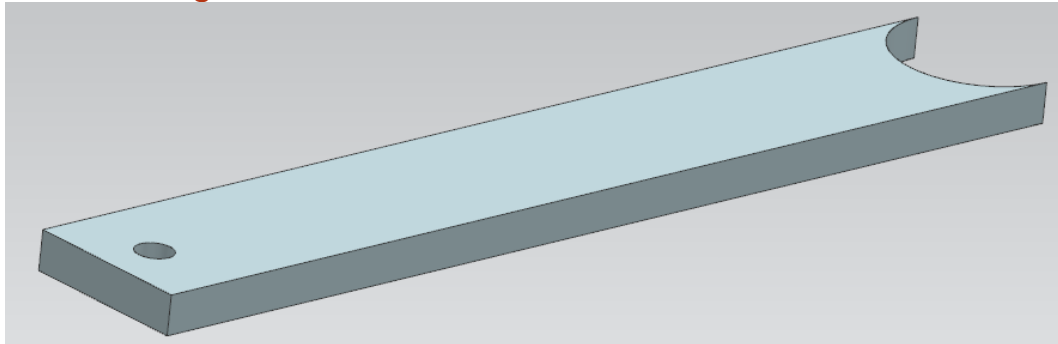


Figure 5Z

Table 5P shows the weight and cost saving per component.

Table 5P: Specifications per component

Design	Volume (mm ³)	Mass (kg)	Cost (£)
Initial	334779.76	2.68	12.14
Final	209237.35	1.67	7.56

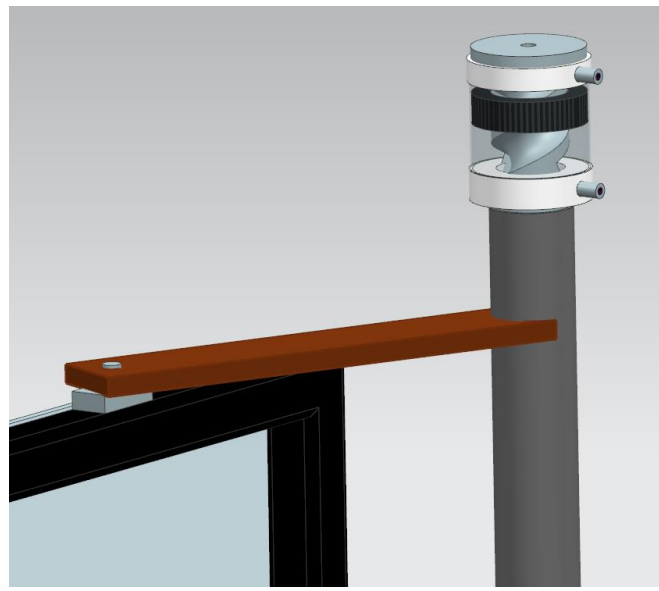


Figure 5AA

Since there are 6 components of this kind on the bus, the overall mass and cost of the final design would be 10.02 kg and £45.36. After the DFMW analysis, 6.06 kg and £27.48 have been saved.

The DFMW analysis only looked into elementary beam theory and dynamics. Even though the safety factor could cover loads that are not accounted for, there is a possibility that the results are not final. However, FEM analysis would be necessary to pursue further investigation.

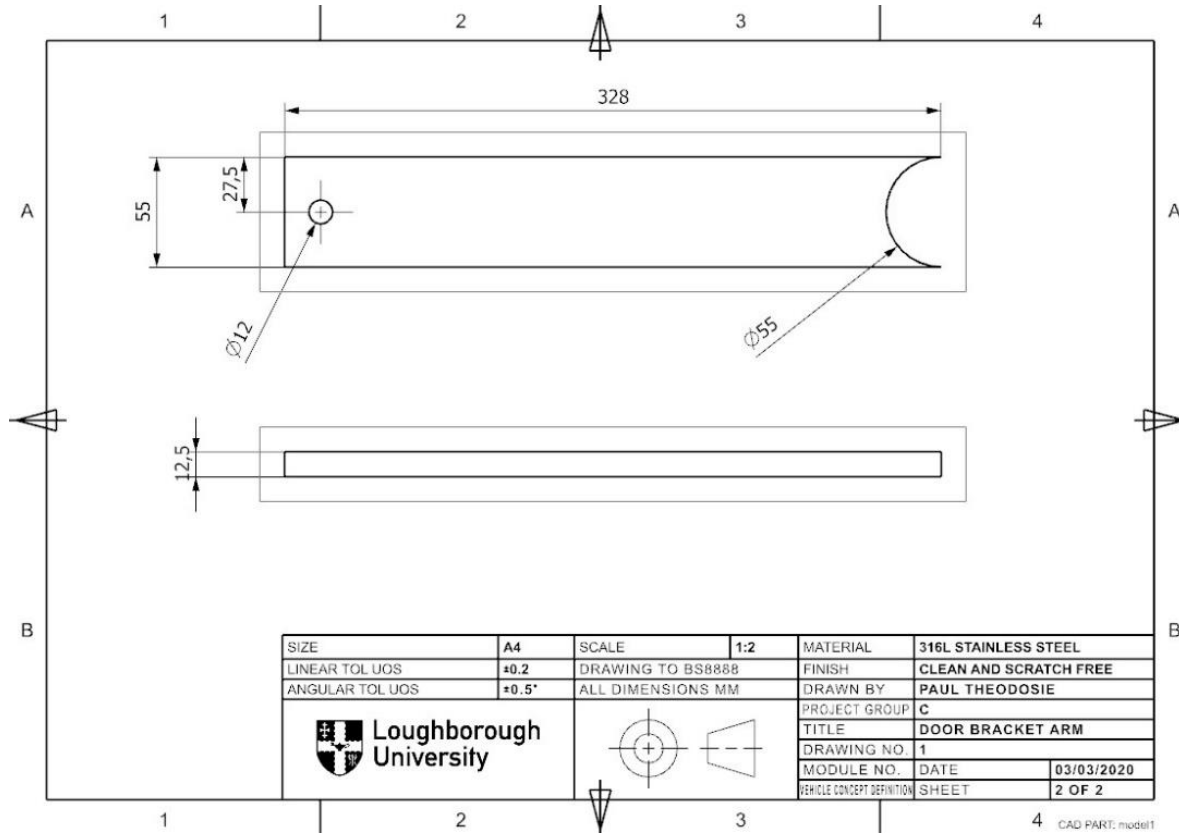


Figure 5BB: Bracket technical drawing

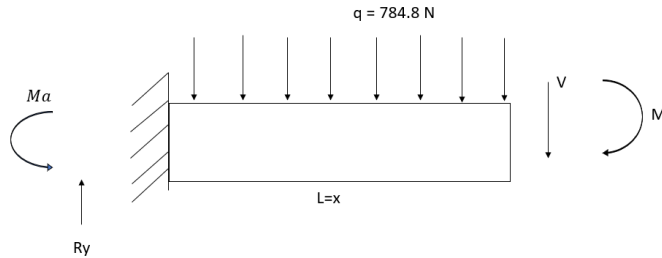
Appendix

Appendix A

Based on Figure 5O.

$$\sum P_y = 2R_y - q \times 0.6 = 0 \Rightarrow R_y = q \times 0.3$$

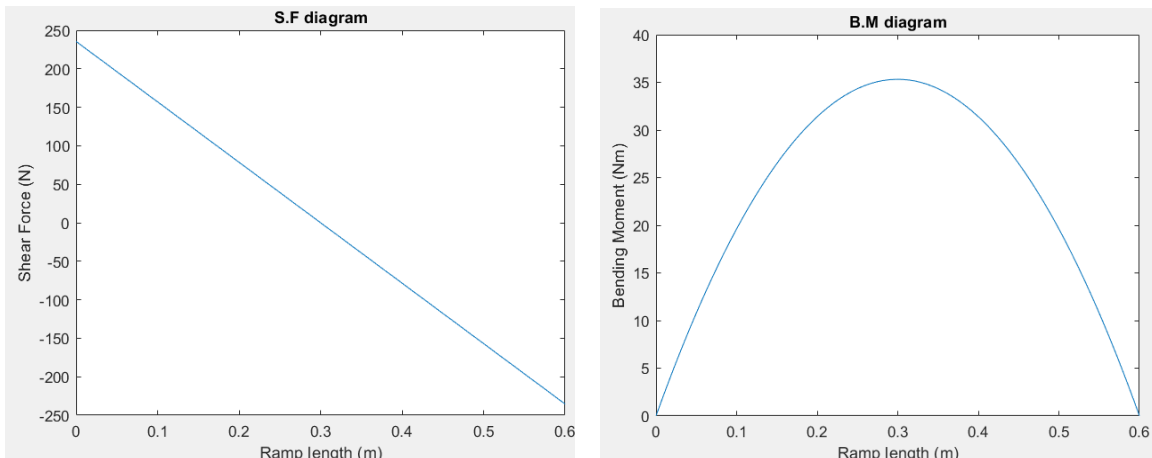
$$\sum M = M_a + q \times 0.6 \times \frac{0.6}{2} - R_y \times 0.6 = 0 \Rightarrow M_a = 0$$



For $0 < x < 0.6$

$$V = R_a - q \times x = q \times (0.3 - x)$$

$$M = R_a \times x + M_a - q \times \frac{x^2}{2} = q \times (0.3 \times x - 0.5 \times x^2)$$



$$EIv'' = -M$$

$$EIv' = -q \times 0.3 \times \frac{x^2}{2} + q \times 0.5 \times \frac{x^3}{3}, \quad EIv = -q \times 0.3 \times \frac{x^3}{6} + q \times 0.5 \times \frac{x^4}{12}$$

Integration constants C1 and C2 are equal to 0 because at $x = 0$; $v = v' = 0$

$$\text{At } x = 0.3 \Rightarrow EIv = -0.79$$

$$\text{With } E = 68.9 \text{ GPa and } I = \frac{b \times d^3}{12} \Rightarrow$$

$$v = \frac{0.79 \times 12}{E \times b \times d^3} = \frac{0.79 \times 12}{68.9 \times 10^9 \times 0.85 \times 0.067^3} = 5 \times 10^{-4} \text{ mm}$$

Appendix B

Static Load

$$\sum P_y = \frac{W}{2} - R_y = 0 \Rightarrow$$

$$R_y = \frac{70 \times 9.81}{2} = 343.35 N$$

$$\sum M = \frac{W}{2} \times 0.31 - M_a = 0 \Rightarrow$$

$$M_a = 106.4385 Nm$$



For $0 < x < 310$ mm

$$V = R_y = 343.35 N$$

$$M = M_a - R_y \times x$$

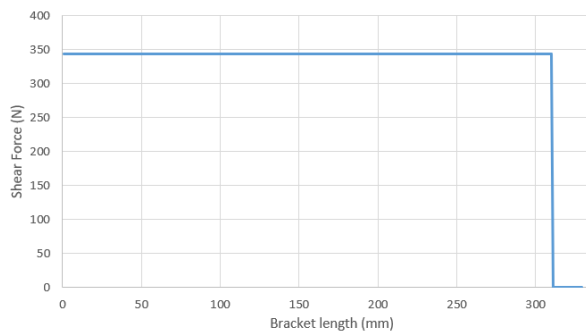


For $310 < x < 328$ mm

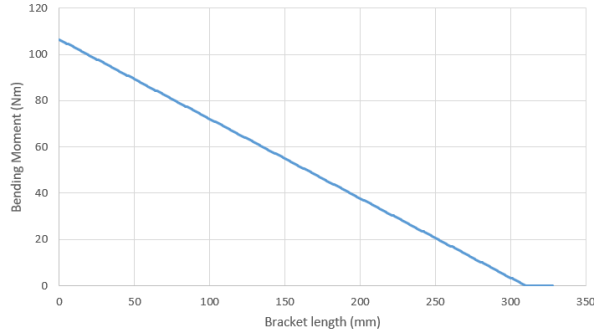
$$V = R_y - \frac{W}{2} = 0$$

$$M = M_a - R_y \times x + \frac{W}{2} \times (x - 0.31) = 0$$

S.F static case



B.M static case



With d = minimum thickness; τ = shear yield strength; σ = tensile yield strength; E = Young's modulus; v = maximum chosen deflection (2 mm)

$$\tau = \frac{3 \times V_{max}}{2 \times b \times d} \Rightarrow d = \frac{3 \times 343.35}{2 \times 0.055 \times 102 \times 10^6} = 0.09 mm$$

$$\sigma = \frac{M \times y}{I} = \frac{M \times \frac{d}{2}}{\frac{b \times d^3}{12}} \Rightarrow d = \sqrt{\frac{6 \times 106.4385}{0.055 \times 170 \times 10^6}} = 8.26 mm$$

For $0 < x < 310$ mm

$$EIv'' = -M = -M_a + R_y \times x, \quad EIv' = -M_a \times x + R_y \times \frac{x^2}{2}, \quad EIv = -M_a \times \frac{x^2}{2} + R_y \times \frac{x^3}{6}$$

Integration constants C1 and C2 are equal to 0 because at $x = 0$; $v = v' = 0$

$$\text{At } x = 310 \text{ mm} \Rightarrow EIv = E \times \frac{b \times d^3}{12} \times v = -3.4 \Rightarrow$$

$$d = \sqrt[3]{\frac{3.4 \times 12}{193 \times 10^9 \times 0.055 \times 0.002}} = 12.43 mm$$

Dynamic Load

$$P = \frac{W}{2} \times S.F = 343.35 \times 1.25 = 429 N$$

With t = plate thickness; d = hole diameter; a = distance from edge of plate; τ_{ult} = ultimate shear strength; σ = tensile yield strength

$$\text{Bearing failure} \Rightarrow \sigma = \frac{P}{t \times d} \Rightarrow t = \frac{429}{170 \times 10^6 \times 0.012} = 0.2 mm$$

$$\text{Shear out} \Rightarrow \tau_{ult} = \frac{P}{2 \times a \times t} \Rightarrow t = \frac{429}{2 \times 0.018 \times 291 \times 10^6} = 0.04 mm$$

Longitudinal Acceleration

$$P = m \times acc \times S.F = 35 \times 0.11 \times 9.81 \times 1.25 = 47.21 N$$

$$\text{Bearing failure} \Rightarrow t = \frac{47.21}{170 \times 10^6 \times 0.012} = 0.02 mm$$

$$\text{Shear out} \Rightarrow t = \frac{47.21}{2 \times 0.018 \times 291 \times 10^6} = 0.004 mm$$

Lateral Acceleration

$$P = 35 \times 0.3 \times 9.81 \times 1.25 = 128.75 N$$

$$\text{Bearing failure} \Rightarrow t = \frac{128.75}{170 \times 10^6 \times 0.012} = 0.06 mm$$

$$\text{Shear out} \Rightarrow t = \frac{128.75}{2 \times 0.0215 \times 291 \times 10^6} = 0.01 mm$$

Crash Load

$$P = 35 \times 10 \times 9.81 \times 1.25 = 4291.875 N$$

$$\text{Bearing failure} \Rightarrow t = \frac{4291.875}{170 \times 10^6 \times 0.012} = 2.1 mm$$

$$\text{Shear out} \Rightarrow \text{Lateral} \Rightarrow t = \frac{4291.875}{2 \times 0.0215 \times 291 \times 10^6} = 0.34 mm$$

$$\text{Longitudinal} \Rightarrow t = \frac{4291.875}{2 \times 0.0215 \times 291 \times 10^6} = 0.4 mm$$

Abuse Load

$$P = R_y + P_{\max abuse}$$

$$\text{From the bending moment equation} \Rightarrow M' = \frac{d^2 \times b \times \sigma}{6} = \frac{0.0125^2 \times 0.055 \times 170 \times 10^6}{6} = 243 Nm$$

$$M' = P \times 310 mm \Rightarrow P = 785.45 N \Rightarrow P_{\max abuse} = 442 N$$

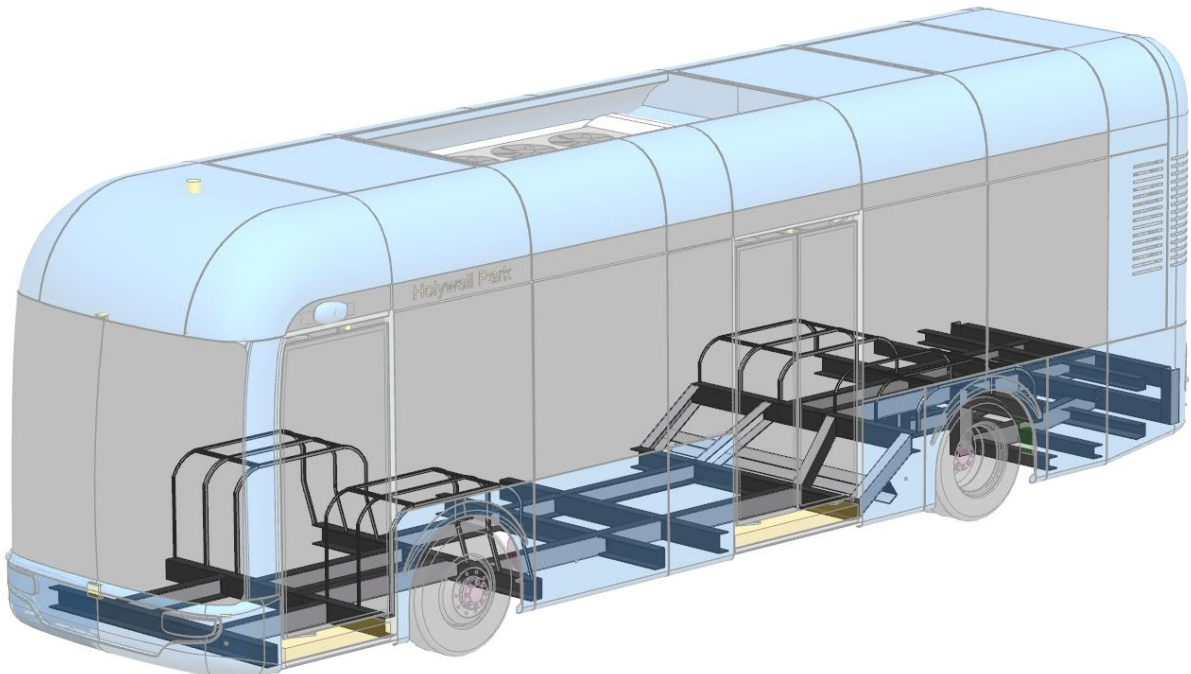
References

- [1] - Velodyne Lidar. (2020). *Ultra Puck™ | Velodyne Lidar*. [online] Available at: <https://velodynelidar.com/products/ultra-puck/> [Accessed 4 Mar. 2020].
- [2] - Continental-automotive.com. (2020). *Continental Automotive*. [online] Available at: <https://www.continental-automotive.com/en-gl/Passenger-Cars/Autonomous-Mobility/Enablers/Cameras/Mono-Camera> [Accessed 4 Mar. 2020].
- [3] - Continental-automotive.com. (2020). *Continental Automotive*. [online] Available at: <https://www.continental-automotive.com/en-gl/Passenger-Cars/Autonomous-Mobility/Enablers/Radars/Long-Range-Radar/ARS540> [Accessed 4 Mar. 2020].
- [4] - Bosch-mobility-solutions.com. (2020). *Mid-range radar sensor (MRR rear)*. [online] Available at: <https://www.bosch-mobility-solutions.com/en/products-and-services/passenger-cars-and-light-commercial-vehicles/driver-assistance-systems/lane-change-assist/mid-range-radar-sensor-mrrrear/> [Accessed 4 Mar. 2020].
- [5] - Continental-automotive.com. (2020). *Continental Automotive*. [online] Available at: <https://www.continental-automotive.com/en-gl/Passenger-Cars/Autonomous-Mobility/Enablers/Radars/Short-Range-Radar/SRR520> [Accessed 4 Mar. 2020].
- [6] - Bosch-mobility-solutions.com. (2020). *Ultrasonic sensor*. [online] Available at: <https://www.bosch-mobility-solutions.com/en/products-and-services/passenger-cars-and-light-commercial-vehicles/driver-assistance-systems/construction-zone-assist/ultrasonic-sensor/> [Accessed 4 Mar. 2020].
- [7] - Nxp.com. (2020). *NXP BlueBox Autonomous Driving | NXP*. [online] Available at: <https://www.nxp.com/design/development-boards/automotive-development-platforms/nxp-bluebox-autonomous-driving-development-platform:BLBX> [Accessed 4 Mar. 2020].
- [8] - Dmitriev, S. (2020). *Autonomous cars will generate more than 300 TB of data per year*. [online] Tuxera. Available at: <https://www.tuxera.com/blog/autonomous-cars-300-tb-of-data-per-year/> [Accessed 4 Mar. 2020].
- [9] - Frc.ri.cmu.edu. (2020). *Comparing the retina with computer vision*. [online] Available at: <https://frc.ri.cmu.edu/~hpm/book97/ch3/retina.comment.html> [Accessed 4 Mar. 2020].
- [10] - Core.ac.uk. (2020). [online] Available at: <https://core.ac.uk/download/pdf/81107023.pdf> [Accessed 4 Mar. 2020].
- [11] - En.wikipedia.org. (2020). *Oyster card*. [online] Available at: https://en.wikipedia.org/wiki/Oyster_card [Accessed 4 Mar. 2020].
- [12] - Ramp, L. (2020). *Low-Floor City Bus Powered 2 Stage Ramp*. [online] PSV Ramps. Available at: <https://psvramps.co.uk/products/psv-04-052-psv-two-stage-full-electric-fixed-floor-powered-access-ramp> [Accessed 4 Mar. 2020].
- [13] - Anon, (2020). [online] Available at: <https://www.electrotechdrives.co.uk/product/0-12kw-three-phase-electric-motor-0-16hp-6-pole-1500rpm-63-frame/> [Accessed 4 Mar. 2020].
- [14] - Metal Supermarkets (2020). *Aluminum 6061 | Metal Supermarkets* [online] Available at: <https://www.metalsupermarkets.com/metals/aluminum/aluminum-6061/> [Accessed 4 Mar. 2020].
- [15] - AG, M. (2020). *The new MAN Lion's City – The perfect city bus*. | MAN Bus Germany. [online] Bus.man.eu. Available at: <https://www.bus.man.eu/de/en/city-buses/lions-city-18/overview/overview-lions-city-18.html> [Accessed 4 Mar. 2020].
- [16] - AZoM.com. (2020). *Stainless Steel - Grade 316L - Properties, Fabrication and Applications (UNS S31603)*. [online] Available at: <https://www.azom.com/article.aspx?ArticleID=2382> [Accessed 4 Mar. 2020].
- [17] - Granta Design. (2020). *GRANTA EduPack | Granta Design*. [online] Available at: <https://grantadesign.com/education/ces-edupack/> [Accessed 4 Mar. 2020].

Vehicle Concept Definition and Design: Design Report

Section 6

Chassis, Crash Protection and Flooring



(s) Clayton Hunt – B724884

*Number of Pages: 22
Number of Words: 1985*

Contents

6.1 Chassis.....	128
6.1.1 Chassis Performance Targets	128
6.1.2 Main Ladder Structure Design to Minimum Weight	129
Main Beam Calculations	129
Loads on the Bus at Maximum Capacity	129
Material Analysis	131
The C-Section Being Used:.....	132
Maximum Bending Stress	132
Results of Analysis.....	133
Comparison of the Materials	134
Final Material Decision:.....	134
Torsional Strength Modifications to the Concept Design	135
6.1.3 Crash Protection	136
Crash Protection	136
Battery Protection.....	136
6.1.4 CAD of the Chassis.....	137
6.1.5 Manufacturing	139
6.1.6 Evaluation of the Chassis	139
Mass and COG Calculations vs Predicted.....	139
Final Product vs Targets	140
6.2 Flooring	141
6.2.1 Targets for Flooring.....	141
6.2.2 Wheel Arch Design	141
6.2.3 Flooring Specifications.....	143
6.2.4 Flooring Performance Against Targets	144
6.3 Costing	145
Appendix	146
References	147

6.1 Chassis

This section will cover the development of the chassis of the shuttle bus from the concept into an accurate finalised design. The two main chassis beams will be designed for minimum weight. This component was chosen as it would have greatest effect on the overall weight of the vehicle, improving efficiency and increasing the range of the bus to meet vehicle objectives PE2 and EI1.

6.1.1 Chassis Performance Targets

A list of targets has been produced which are specific to the design of the chassis. These include concept targets, Overall Vehicle Objectives as well as numerical targets specific to the chassis design and strength, these are shown in Table 6A

Table 6A: Chassis Targets

Target Code	Target Area	Target Description	Action Performed to Meet Target
C01	Dimensioning	The chassis must be of suitable size to mount the body and all components such as powertrains and ramps – 9.73m x 2.34m	Use dimensions determined in the concept as well as communication with group members to ensure the chassis is packaged well with the rest of the bus
C02	Overall Vehicle Environmental Impact	Design the main beams of the chassis to minimum weight in order to improve vehicle efficiency. Target a 1500kg maximum for the whole chassis based on the concept estimation of 1462kg. If weight can be optimised to be below this figure the design for minimum weight would be successful	Consider multiple materials and minimise the beams cross section in order to produce the most cost-effective light weight solution
C03	Overall Vehicle Manufacturing Objectives	Design to be easily manufactured by considering tooling costs and joining	Manufacturing and joining will be considered for all areas of the chassis to ensure the design is viable
C04	Durability	Use materials with proven durability in wet conditions which the chassis would regularly be exposed to	Consider corrosion resistance of materials used
C05	Dimensioning	Maintain the low floor height of 400mm in the front section of the bus as specified in the concept report	Keep the height of the chassis cross section 150mm to retain the low floor height established in the concept model
C06	Strength	A maximum deflection of 5mm on the main chassis beams under maximum passenger load to avoid chassis deflection interfering with moving parts in the powertrain. Ensure maximum bending stress does not exceed flexural yield stress of material.	Tune the thickness of the material in the cross section to ensure maximum deflection is below 5mm and ensure yield stress is not exceeded by maximum bending moments of the beam under the extreme load case considered
C07	Strength	Meet strength Requirements listed above with a safety factor of 1.25 to allow for passenger overloading and extreme circumstances	Apply a safety factor of 1.25 to each load in the load case to account for over loading and other more extreme load cases
C08	Crashworthiness	Increased protection around the batteries to avoid damage in the case of a crash and therefore reduce risk of a fire	

6.1.2 Main Ladder Structure Design to Minimum Weight

Main Beam Calculations

The material for the chassis will be reconsidered to include a wider range of materials in the strength calculations. This will allow the chassis to be designed to minimum weight more effectively with all options considered for the specific case of the chassis. Manufacturing, cost and durability will also be analysed to ensure the outcome is realistic for this project.

The beam will be modelled as a straight beam resting on two points (the front and rear axle) and analysed using a high load case as defined in the team leader section. The load case is A fully laden bus. A safety factor of 1.25 will be applied to the mass of the passengers and components to account for other extreme load cases.

Loads on the Bus at Maximum Capacity

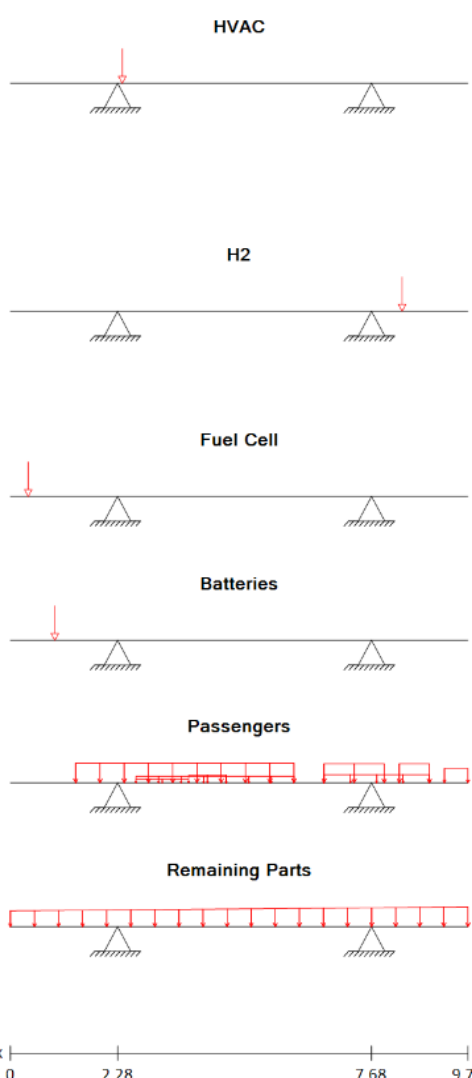
Figure 6A below shows the load of the passengers on the bus as well as the load from the buses sprung mass components. Passengers have been distributed similarly to the diagram shown in the team leader section. As there are two main beams the loads have been divided by two. This allows them to be analysed individually. Heavy components of the sprung mass have been modelled as point loads on the chassis. The body frame and panels are distributed along the length of the chassis similarly to the less significant masses. This is summarised in Table 6C. Assumptions made in these calculations are listed in Table 6B.

Table 6B: Loading Assumptions

Assumption	Explanation	Effect on Accuracy
The beams carry symmetrical weight	The loading on both sides of the chassis should be fairly similar at all times as the Centre of mass was measured from the parts list as only 25mm off centre in the y direction.	Very Minimal
Passengers at maximum capacity are distributed as stated in the team leader section	Due to the floorplan and seating the team leaders estimate of passenger weight distribution is sensible	Reasonable effect on accuracy which can be covered by the safety factor
The axles act as rigid supports in this load case	To simplify this model each axle is modelled to have one rigid connection to the chassis	Minimal
Small components and the body frame/windows/panels can be modelled as evenly distributed along the length of the chassis	Due to the body panels being similar along the length of the bus and the small components having a relatively small impact on the overall load on the chassis this is a sensible assumption	Minimal. Assumption is fairly accurate of actual positions

Table 6C: Summary of Loads

Component	Force on each beam with safety factor of 1.25 (1.25*mg/2) [N]	Centre of Gravity in x Direction From the rear of the chassis (mm)
HVAC System	1580	2380
H2 Cylinders	5293	8330
Fuel Cell	2070	380
Batteries	6115	945
Distribution of remaining parts (inc. body frame, windows and panels)	22246	Distributed evenly across the length of the chassis



Loads

Load Case	x [m]	Fz [kN]	M _y [kNm]
HVAC	2.38	1.58	0
H2	8.33	5.29	0
Fuel Cell	0.38	2.07	0
Batteries	0.94	6.12	0

Load Case	x ₁ [m]	x ₂ [m]	q ₁ [kN/m]	q ₂ [kN/m]
Passengers	1.39	6.03	6.03	6.03
Passengers	2.67	6.03	1.94	1.94
Passengers	2.67	3.79	1.05	1.05
Passengers	3.79	4.59	2.33	2.33
Passengers	6.67	8.91	2.5	2.5
Passengers	6.67	7.95	5.82	5.82
Passengers	8.27	8.91	5.82	5.82
Passengers	9.23	9.73	4.37	4.37
Remaining Parts	0	9.73	1.83	2.29

Figure 6A: Load Distribution Model

Material Analysis

The decision of the material for the chassis will be revisited to more effectively design the chassis to minimum weight. PolyBeam is used to determine maximum deflection of the beam for a specified section and material. This will be used by tuning the thickness of the C section to meet the targeted maximum deflection of 5mm (C06). The mass of the resulting section, material cost and manufacturing cost can then be calculated to determine the best compromise for the chassis

The materials selected for use in calculations are shown in Table 6D below. CES Edupack and online databases were used to explore manufacturing techniques and to approximate costs associated with each material.

Table 6D: Material Properties [1][2][3][4][5]

Material	Reason for Selection	Youngs Modulus (E) [GPa]	Flexural Strength (MPa)	Density (Kg/m^3)	Manufacturing Technique	Corrosion Resistance	Price (£/kg)
Austenitic stainless steel (EN 1.4310 AISI 301)	A study into Bus Chassis materials found this the best material for fatigue, impact toughness and corrosion	212	190	8030	Cold rolled into section shape	Very Good	£1.8
Aluminium 2014 Alloy	Aluminium alloys are a good lightweight alternative to steel. This alloy is high strength and used in aerospace structural applications.	73.1	400	2800	Machined from extruded bar	Poor – requires painting	£2
Carbon Fibre Reinforced Carbon Matrix	A more modern approach to lightweight structures. This alternative will be far more expensive, but the weight saving could justify the price	95	230	1700	HIPping	Very Good	£165

The selected materials' properties were then input into the PolyBeam material selection and the thickness of the C-Section tuned to allow for the targeted maximum deflection of 5mm. The height and width of the section have already been defined in order to properly package the bus and mount components so only the thickness, t, can be tuned.

The C-Section Being Used:

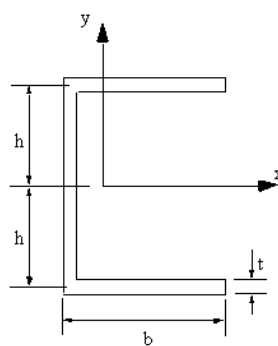


Table 6E: Symbol Key

Symbol	Value (mm)
h	75
b	100
t	To be defined for each material

Figure 6B: C-Section Diagram [6]

Equation 1: Moment of Intertia of C-Section

$$I_y = \frac{b(2h)^3}{3} - \frac{(b-t)(2h-t)^3}{3} = 112500000 - \frac{(100-t)(150-2t)^3}{3}$$

Maximum Bending Stress

PolyBeam calculated the bending moment along the beam under the loaded condition and plotted the maximum bending moment as shown in figure 3 below. This could then be used to determine the maximum bending stress for each section as shown in Equation 2.

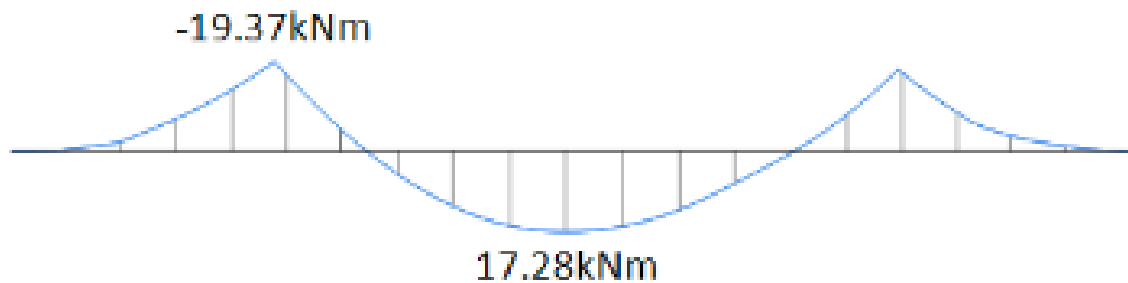


Figure 2: Bending Moment Distribution

M = Max Bending Moment = 19370Nm

Y = Distance from natural plane to surface of beam = 75mm

$$I = 2^{\text{nd}} \text{ Moment area (mm}^4\text{)} = 112500000 - \frac{(100-t)(150-2t)^3}{3}$$

Equation 2: Max Bending Stress

$$\sigma_{Max} = \frac{My}{I}$$

Results of Analysis

Stainless Steel AISI 301:

Table 2F: Results of AISI 301 Bending Analysis

Parameter	Value
Youngs Modulus	212GPa
Displacement set by PolyBeam to	5mm
Moment of Inertia	37,900,000mm^4
Calculated Minimum Thickness	7.8mm
Flexural Strength	190MPa
Calculated Max Bending Stress	38.33MPa

Aluminium 2014 Alloy

Table 6G: Results of Aluminium 2014 Alloy Bending Analysis

Parameter	Value
Youngs Modulus	73.1GPa
Displacement set by PolyBeam to	5mm
Moment of Inertia	109,900,000mm^4
Calculated Minimum Thickness	48.37mm
Flexural Strength	400MPa
Calculated Max Bending Stress	13.22MPa

Carbon Fibre Reinforced Carbon Matrix

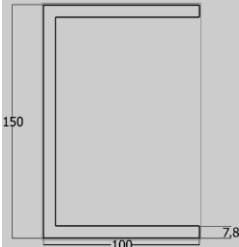
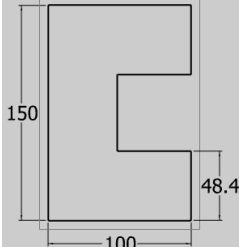
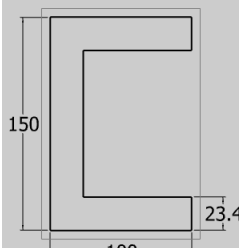
Table 6H: Results of CFRC Bending Analysis

Parameter	Value
Youngs Modulus	95GPa
Displacement set by PolyBeam to	5mm
Moment of Inertia	84,500,000mm^4
Calculated Minimum Thickness	23.43mm
Flexural Strength	230MPa
Calculated Max Bending Stress	17.19MPa

Comparison of the Materials

The mass and material cost can now be compared for the three materials with their minimum weight cross sections. The mass can be approximated by multiplying the section area by the length of the beams and the density of the materials. Table 6J below shows the comparison.

Table 6J: Section and Mass Analysis

Material	Thickness of C Channel (mm)	Section	Approximate Total Mass of One Beam (kg)	Max Bending Stress Supported? ($\sigma_{Max} < Flexural Strength$)	Material Cost (£)
Austenitic stainless steel (EN 1.4310 AISI 301)	7.80		196.25	Yes	353.25
Aluminium 2014 Alloy	48.37		321.52	Yes	643.04
Carbon Fibre Reinforced Carbon Matrix	23.43		113.01	Yes	18646.65

Final Material Decision:

Table 6J above concludes the Aluminium to be the least viable material. It's low Youngs' Modulus means the resulting cross section to meet the maximum displacement target is far too thick. This would make it difficult to manufacture and mount parts to as well as resulting in a greater weight and greater material cost.

The CFRC is the lowest weight solution at 113kg. However, due to very high material costs it cannot be selected as the cost for a 200-400kg weight saving would be approximately £50,000 which could not be justified in this project. Therefore, the selected material for the chassis will be the Austenitic stainless steel. Figure 6D shows the final section dimensions.

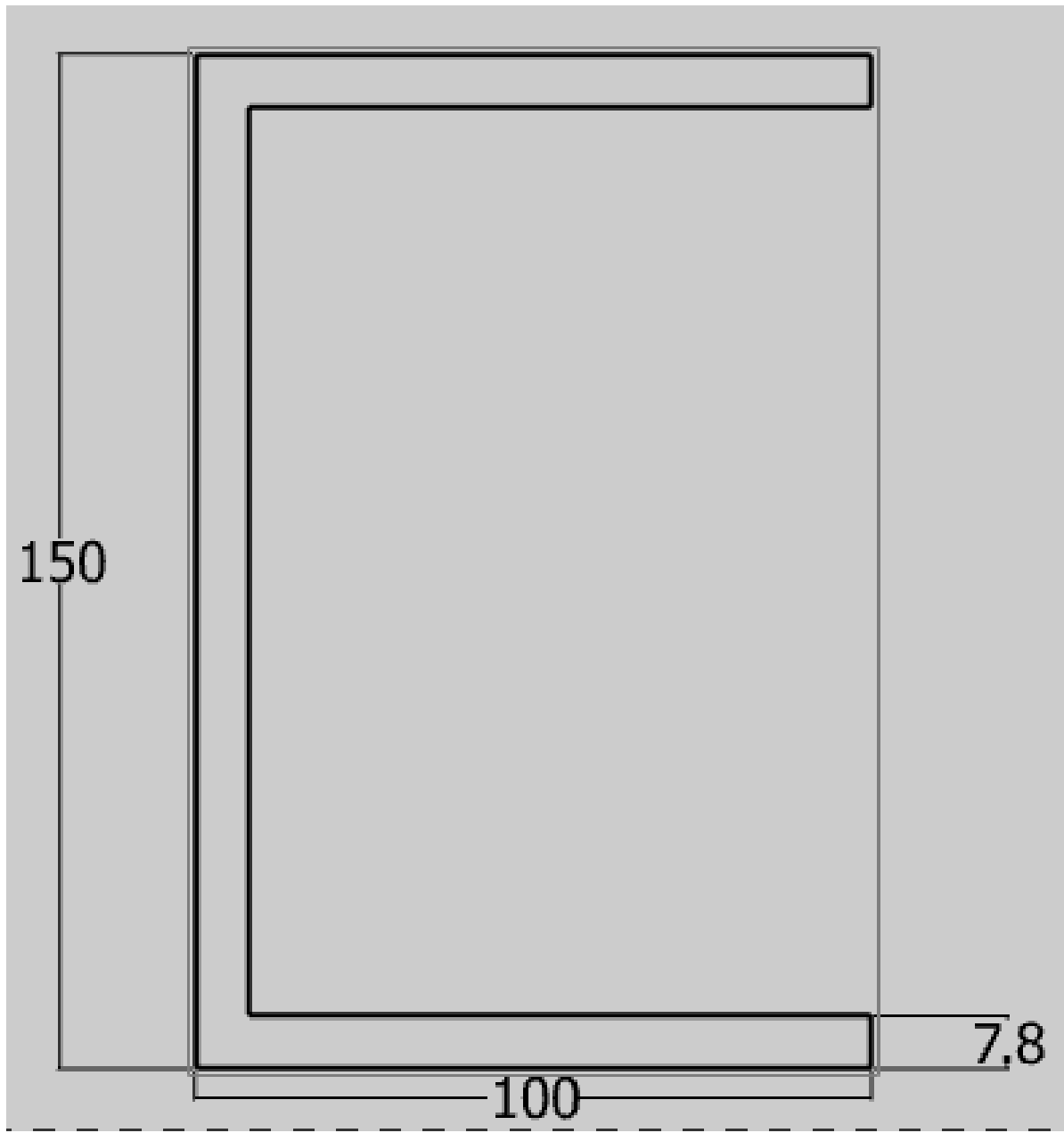


Figure 6D: C-Section Final Dimensions

Torsional Strength Modifications to the Concept Design

Adjustments were made to the initial ladder concept at the area where the floor raises, as a clear torsional weakness has been identified. The height change was adapted to allow the continuation of the ladder throughout the length of the bus. This is similar to chassis of existing low-floor electric powered buses such as the Mercedes Benz O 500 U 1726. [7]. Figure 6E below shows the concept design updated to include this modification.

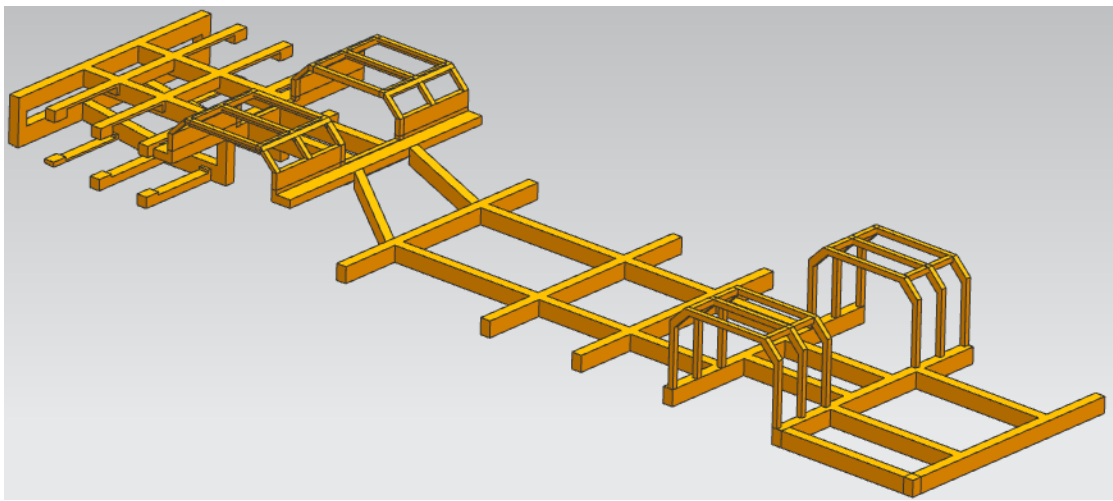


Figure 6E: Chassis Concept Modification

The area that has been modified is where the steps will be mounted. While producing the final CAD it was decided to add a further two members along the outside of the chassis at the height change to increase torsional stiffness of the whole chassis. A cross member was also mounted horizontally across the 4 members in order to meet the suspension hard points as defined in the suspension section of the report. The modification and addition of these members will eliminate the weakness in this area of the chassis. This can be seen in the CAD model shown in Section 6.1.4

6.1.3 Crash Protection

Crash Protection

Due to the low speed of buses and their large weight, few crash protection methods are required additional to the basic chassis and structure to protect the passengers [8]. However, due to the batteries being used and the hydrogen cylinders additional measures have been taken in the design of the chassis to ensure risk of fires and explosions are low. The chassis is reinforced around the battery as mentioned below and the hydrogen is stored on the roof of the bus as this is an area unlikely to be impacted in most crash scenarios.

Battery Protection

As covered in the concept report the “Kilovac K1K High Voltage Contactor” [9] will be installed on the bus to prevent fires caused by short circuits in the event of a crash or power surge. This will be included in the costing of the chassis and crash protection. It will be mounted on the chassis in close proximity to the batteries.

As can be seen in the final CAD of the chassis in figure 6 the rear of the bus has a substantial structure around it to protect the batteries and motor. This will reduce the risk of fire caused by the lithium batteries which are very reactive to physical damage.

6.1.4 CAD of the Chassis

With the material and section of the chassis now decided, A model was produced on NX11 to show the chassis as a C-Section. This model has been adapted from the concept to allow the chassis to meet suspension hardpoints and to line up with uprights from the body frame as well as adaptions to improve the strength at the height change. Additional members were used to ensure no risk of torsional weakness in the height change. The members used a similar cross section throughout the whole design of the chassis to reduce manufacturing tooling costs. Figure 6F shows the finalised CAD model of the chassis.

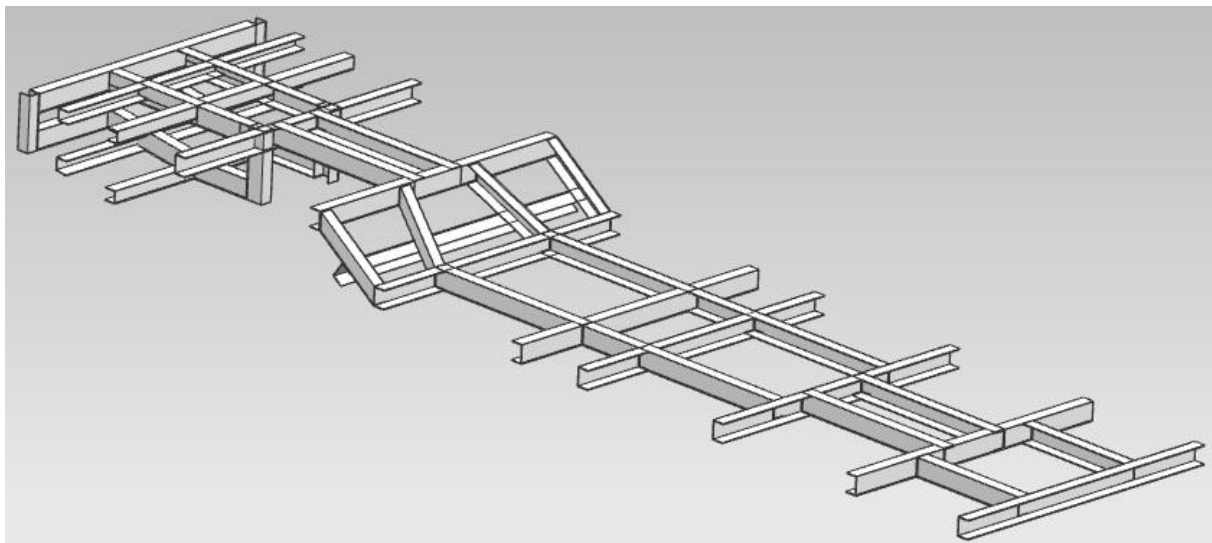


Figure 6F: Final CAD Model of Chassis

The chassis was constructed using the c-section defined as the minimum weight for the two main beams. The full dimensioning is shown in Figure 6G below:

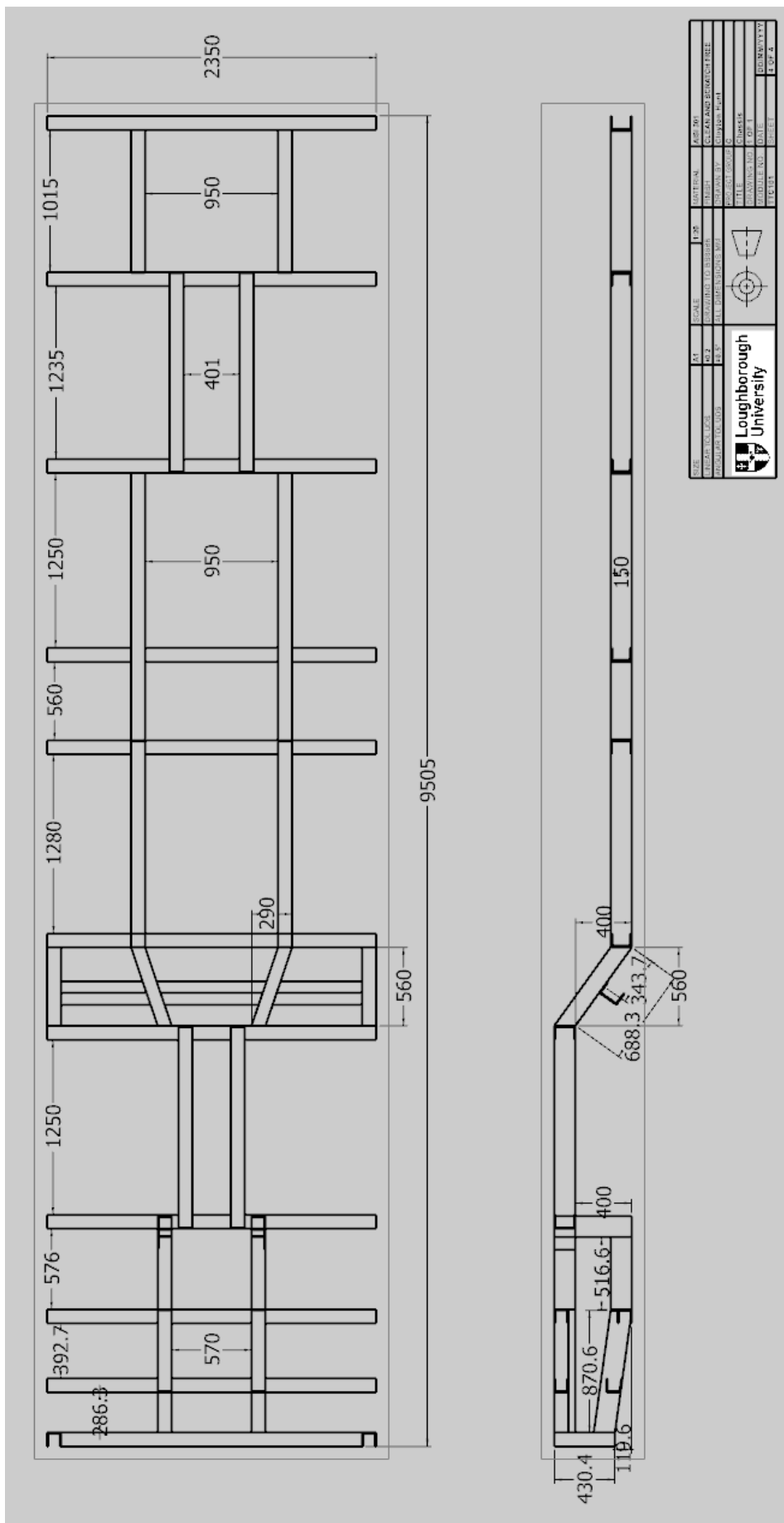


Figure 6G: Chassis Dimensions

6.1.5 Manufacturing

The consistent section used for the whole chassis will help to reduce the cost of manufacturing of the stainless steel. However, since the volume of production will be very low, it will not be high enough for hot rolling to be a viable option due to tooling costs for individual shapes being very high. Therefore, the best option to produce the C-section would be laser beam welding. This process is efficient even in small scale production and is flexible with length which is ideal for the production of the varied lengths of c-section. Laser beam welding does not reduce the strength of the section and produces tight tolerances. [10] The steel will therefore be able to meet its strength requirements at minimum weight.

The individual beams can be joined together using MIG welding. This method offers a strong joint between the beams which would be superior to spot welding which, while more economical, could reduce the overall strength of the chassis. TIG welding would be less suitable due to the thickness of the steel being used. After MIG welding the area around the weld would require minor treatment in the form of passivation to restore corrosion resistance that can be lost as a result of the heat of the welding [11]. This would be a relatively minor additional cost to the process but would significantly improve resistance to corrosion which the chassis would be very prone to.

6.1.6 Evaluation of the Chassis

Mass and COG Calculations vs Predicted

The mass and centre of gravity are displayed in Table 6K below as defined by assigning the material to the chassis in Nx11. From this mass the material cost can be estimated.

Table 6K: Mass, Cost and COG Results [5]

Property	Value
Total Mass (kg)	1192.8
Material Cost (£) (estimated)	2150
Centre of Mass from datum (centre of wheelbase on ground) (mm):	
X	-1319.4
Y	-0.8
Z	467.3

Final Product vs Targets

Table 6L: Chassis Performance Vs Targets

Target	Target Met?	Comments
The chassis must be of suitable size to mount the body and all components such as powertrains and ramps – 9.73m x 2.35m	Yes	The final chassis design is 9.73m x 2.35m and is dimensioned to allow the space required by powertrains and has gaps at each door to house the entry ramp
Design the main beams of the chassis to minimum weight in order to improve vehicle efficiency. Target a 1500kg maximum for the whole chassis based on the concept estimation of 1462kg. If weight can be optimised to be below this figure the design for minimum weight would be successful	Yes	The mass of the final chassis design is 1192.8kg, 307.2kg below the targeted mass. The main beams of the chassis were designed to a minimum thickness and therefore weight for a maximum displacement of 5mm. This cross section was then used for the cross members also to ensure strength across the width of the bus
Design to be easily manufactured by considering tooling costs and joining	Yes	The chassis section is consistent for the main beams and cross sections. This will reduce tooling costs for the laser beam welding of the sections. The beams can then simply be MIG welded together with the welds treated to reduce corrosion
Use materials with proven durability in wet conditions which the chassis would regularly be exposed to	Yes	Austenitic stainless steel has good corrosion resistance to water and salt water. MIG welding can reduce corrosion, but passivation will be used to replenish the materials corrosion resistance (see Edupack material properties in appendix) [5]
Maintain the low floor height of 400mm in the front section of the bus as specified in the concept report	Yes	The low floor height at the entry doors has been maintained to allow quick boarding of passengers and easy access for the disabled. The floor raises towards the rear to package powertrains and suspension components
A maximum deflection of 5mm on the main chassis beams under maximum passenger load. Ensure maximum bending stress does not exceed flexural yield stress of material.	Yes	The main chassis has been designed to minimum weight based on a maximum deflection of 4.99mm in high load conditions. This avoids large movements in mounted components of the chassis. The maximum bending stress was also calculated to ensure the flexural yield stress of the material is not exceeded and after any deflection the chassis will return to its original shape
Meet strength and Stiffness Requirements listed above with a safety factor of 1.25 to allow for passenger overloading and extreme circumstances	Yes	The load case considered had the safety factor applied by multiplying all calculated loads by 1.25. This accounts for extreme circumstances of loads greater than the load case considered
Increased protection around the batteries to avoid damage in the case of a crash and therefore reduce risk of a fire	Yes	There is a concentrated area of members surrounding the battery storage area at the rear. The rear of the bus also has two layers of the ladder running along towards the rear, doubling the resistance to buckling under impact.

6.2 Flooring

6.2.1 Targets for Flooring

Table 6M: Flooring Targets

Target Code	Target Area	Target Description
C09	Footfall	Use materials with a proven durability under the footfall of a shuttle bus
C10	Shape	Lay over the chassis covering wheel arches and the full area of the buses floor with all elements of the powertrains covered from view
C11	Aesthetics	Use a simple colour scheme which will not become quickly outdated
C12	Dimension	Fit within the 50mm allocated for flooring above the chassis to minimise floor height for quick and easy access on and off the bus.

The flooring will be laid on the chassis with a solid base laminated by a durable, grippy surface for the safety of passengers. The floor must lay over the wheel arches where seating will be mounted. Therefore, the wheel arches must be designed first and built onto the chassis. The section being used will be considered to ensure the strength to hold the weight of seats and passengers.

6.2.2 Wheel Arch Design

Due to the difficulty of joining other materials with steel it is sensible to use steel section for the wheel arches for ease of manufacture and to save cost. Steel section can be MIG welded to the chassis similarly to the manufacture of the chassis.

To decide on the section used some simple calculations were used to determine the maximum load on the wheel arches. The rear wheel arches mount 4 seats so these will be under the highest load. Table 6N below shows the maximum weight on the wheel arches with a safety factor applied.

Table 6N: Loads on Wheel Arch

Load	Weight	Quantity	Total
Double Seat	196	2	392
Passenger	666.4	4	2665.6
	Total		3057.6

With a total weight to carry of 3822N and the wheel arch consisting of 3 beams along the length of the bus, the beams must be rated to carry a minimum of 1019.2N. This produces a maximum bending moment of 98Nm per beam. A safety factor of 2 will be used for this load case for circumstances such as heavier than average passengers or bags adding to the weight. The section to be chosen must have a bending failure moment below 196Nm. The common section closest to this failure moment was chosen. It is shown in Table 6O below.

Table 6O: Selected Material/Section Summary [5]

Section	Material	Failure Moment
Equal Angle 25x25x5	AISI 301	248N

This section has a suitable failure moment and is a standard size to reduce manufacturing cost. This section was then added to the chassis CAD as shown in Figure 6H.

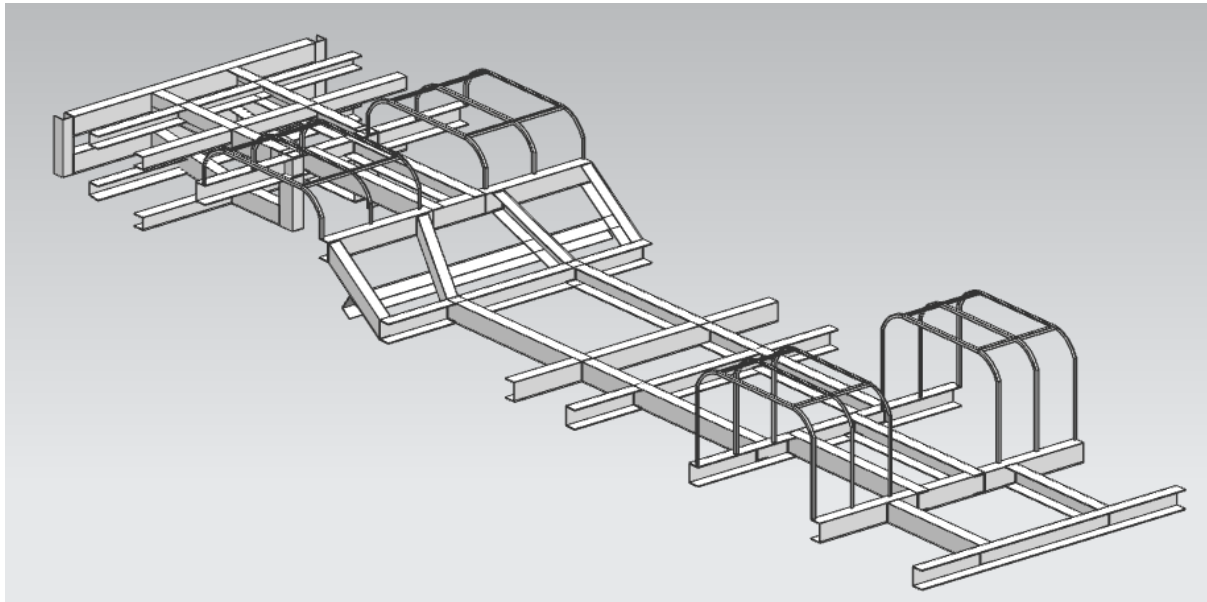


Figure 6H: Chassis with Wheel arches

The mass and centre of gravity of the wheel arches was then calculated as shown in Table 6P.

Table 6P: Wheel Arch Mass, COG and Cost

Property	Value
Total Mass (kg)	57.1
Material Cost (£) (estimated)	103
Centre of Mass from datum (centre of wheelbase on ground) (mm):	
X	416
Y	0
Z	1012

6.2.3 Flooring Specifications

The flooring was specified in the concept report as 10mm Birch Plywood laminated with a 2.2mm layer of Altro Transflor Chroma. This product has a range of colours to suit the style of the customer. It is lightweight and slip resistant which is ideal for this application and has a life expectancy of 15 years which is very reasonable.

Figure 6J shows the layout of the flooring to cover all components within the bus. The calculated mass and centre of gravity is shown in Table 6Q.

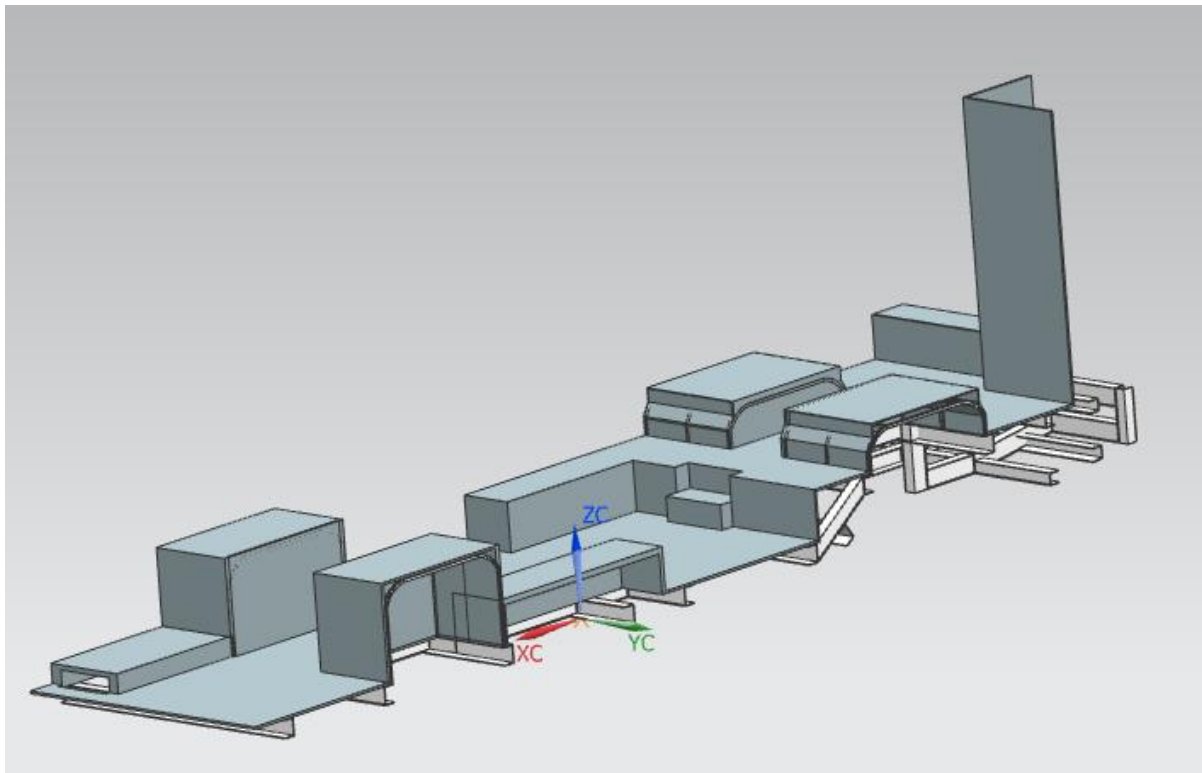


Figure 6J: Flooring Resting on Chassis CAD

Table 6Q: Flooring Mass, COG and Cost [5][12]

Property	Value
Total Mass (kg)	413
Estimated Material Cost (£) (Altro Transflor Chroma at £9 per m ² and Birch plywood at £5 per m ²) [6]	518
Centre of Mass from datum (centre of wheelbase on ground) (mm):	
X	117
Y	10
Z	396

6.2.4 Flooring Performance Against Targets

Table 6R shows the performance of the final flooring and wheel arch design against the targets set for it.

Table 6R: Flooring Evaluation Vs Targets

Target	Target Met?	Comments
Use materials with a proven durability under the footfall of a shuttle bus	Yes	Altro flooring is designed to last 15 years in applications such as buses and trains
Lay over the chassis covering wheel arches and the full area of the buses floor with all elements of the powertrains covered from view	Yes	The Birch Ply is laid over the entire chassis as well as protruding upwards to covered wheel arches and powertrains components
Use a simple colour scheme which will not become quickly outdated	Yes	There is a range of 18 colours which could be specified before manufacturer to meet customers' preferences
Fit within the 50mm allocated for flooring above the chassis to minimise floor height for quick and easy access on and off the bus.	Yes	The thickness of the flooring is 12.2mm

6.3 Costing

Each of the components designed/purchased for this section of the design report has been costed based on material and manufacturing cost per bus. Table 6S summarises this.

Table 6S: Summary of Costing Per Bus [5][13][14][15][16][17]

Component	Estimated Material Cost Per Bus	Estimated Manufacturing Cost Per Bus	Explanation of Costing
Fully Welded Chassis	£2150	£157	Material cost based on £1.80 per Kg as defined in [5]. Using a cost of £9 per 1000 inches the laser beam cost was estimated [10]. (Estimated length of welds required: 4613 inches). A cost calculator [11] was used to find the MIG welding costs with an estimated 1000 inches of MIG weld used per chassis.
Welded Wheel Arches	£103	£19	Cost of the section per kg of £0.27 used [5] and 38 inches of MIG weld used per bus [11]
Flooring	£518	\$130	Total material cost by mass of wood and area of flooring as defined by [5] and [6]. Installation cost estimated as 7 hours work [12]
Kilovac K1K High Voltage Contactor	£147	£0	The contactor is purchasable online and installation costs are assumed negligible [9]
Resettable Inertia Switch Crash Sensor	£40	£0	The sensor is purchasable online and installation costs are assumed negligible [8]
Total	£2958	£306	£3264

The approximate total cost of flooring chassis and wheel arches per bus is £3264. This accounts only for material costs and approximate labour costs. While tooling and equipment costs would also be significant, they would depend on the quantity produced and are not easily estimated but have been considered throughout the design to ensure they remain reasonable.

Appendix

AISI 301 Stainless steel properties [5]

Price

Price	(i)	* 1.71	-	1.9	GBP/kg
Price per unit volume	(i)	* 1.34e4	-	1.51e4	GBP/m^3

Physical properties

Density	(i)	7.88e3	-	7.96e3	kg/m^3
---------	-----	--------	---	--------	--------

Mechanical properties

Young's modulus	(i)	200	-	210	GPa
Specific stiffness	(i)	25.3	-	26.6	MN.m/kg
Yield strength (elastic limit)	(i)	200	-	240	MPa
Tensile strength	(i)	503	-	556	MPa
Specific strength	(i)	25.3	-	30.3	kN.m/kg
Elongation	(i)	30	-	40	% strain
Compressive strength	(i)	* 159	-	200	MPa
Flexural modulus	(i)	* 200	-	210	GPa
Flexural strength (modulus of rupture)	(i)	179	-	207	MPa
Shear modulus	(i)	77	-	80.9	GPa
Bulk modulus	(i)	145	-	152	GPa
Poisson's ratio	(i)	0.27	-	0.281	

Durability

Water (fresh)	(i)	Excellent
Water (salt)	(i)	Excellent
Weak acids	(i)	Excellent
Strong acids	(i)	Acceptable
Weak alkalis	(i)	Excellent
Strong alkalis	(i)	Excellent
Organic solvents	(i)	Excellent
Oxidation at 500C	(i)	Excellent
UV radiation (sunlight)	(i)	Excellent
Galling resistance (adhesive wear)	(i)	Limited use

Notes

Aluminum bronze is the most suitable mating material to minimize galling.

Flammability	(i)	Non-flammable
--------------	-----	---------------

References

6.1.2

[1] Kyröläinen, Antero & Vilpas, Martti & Hänninen, Hannu. (2000). Use of Stainless Steels in Bus Coach Structures. *Journal of Materials Engineering and Performance*. 9. pp. 669-678. 10.1361/105994900770345548.

[2]

<http://www.matweb.com/search/datasheet.aspx?matguid=0cf4755fe3094810963eaa74fe812895>

[3] <http://www.performance-composites.com/carbonfibre/structuralprofile.asp>

[4] <http://www.matweb.com>

[5] CES EduPack

[6] <http://www.aeromech.usyd.edu.au>

[7] https://www.mercedes-benz-bus.com/en_NG/models/o500-u1726.html

6.1.3

[8] <https://www.dalroad.com>

[9] <https://www.electricmotorsport.com/>

6.1.5

[10] <https://www.montanstahl.com>

[11] <https://www.atwf-inc.com/>

6.2.3

[12] <https://www.altro.co.uk/Altro-Transflor-Chroma>

6.3

[13] <https://www.electricmotorsport.com/ev-parts/contactors-relays/resettable-inertia-switch-crash-sensor.html>

[14] <https://cpc.farnell.com/te-connectivity-kilovac/ev200haana/>

[15] <https://www.thefabricator.com>

[16] <https://www.mtisystems.com/costmodels/Welding-Mig.php>

[17] <https://www.bidvine.com/flooring/price-guide>